Technische Universität München

II. Medizinische Klinik und Poliklinik des Klinikum rechts der Isar

Role of Bcl-3 in sterile inflammation

Liang Song

Vollständiger Abdruck der von der Fakultät für Medizin der Technischen Universität München zur Erlangung des akademischen Grades eines

Doktors der Naturwissenschaften (Dr. rer. nat.)

genehmigten Dissertation.

Vorsitzende(r): Univ.-Prof. Dr. Mathias Heikenwälder

Prüfer der Dissertation:

1. apl. Prof. Dr. Hana Algül
2. Univ.-Prof. Dr. Heiko Witt
3. Univ.-Prof. Dr. Jens Werner

Die Dissertation wurde am 22. 04. 2015 bei der Technischen Universität München eingereicht und durch die Fakultät für Medizin am 27. 04. 2016 angenommen.

Zusammenfassung

Mittelpunkt der vorliegenden Studie war es, den Beitrag von Bcl-3 in der Steuerung und Auflösung der sterilen Bauchspeichldrüsen- und Gallenwegsentzündung zu analysieren.

Während steriler Entzündung binden DAMPs (*damaged associated molecular patterns*; freigesetzt von nekrotischen Zellen) zu TLRs (*toll-like receptors*) und lösen eine Signalkaskade aus, welche am deutlichsten durch die Aktivierung des IKK / NF-κB Signalweges dargestellt werden kann. Als atypisches Mitglied der IκB-Familie spielt Bcl-3 eine wichtige Rolle bei der Modulation der NF-κB-Aktivität. Jedoch sind die Mechanismen mit denen Bcl-3 die Aktivität von NF-κB während steriler Entzündung steuert, bislang unerforscht geblieben. Um die Bedeutung von Bcl-3 in steriler Entzündung aufzuklären, wurden Bcl-3 komplett defiziente Mäuse anhand von Tiermodellen der akuten Pankreatitis (AP) und sterilen Cholangitis detailliert charakterisiert. Darüber hinaus wurde der murine Phänotyp mit humanen Bauchspeicheldrüsen- bzw. Leberproben mit AP bzw. primär sklerosierender Cholangitis (PSC) verglichen.

Bcl-3 wurde in der Bauchspeicheldrüse und im Gallensystem während steriler Entzündung bei Menschen und Mäusen hochreguliert. Genetische Inaktivierung von Bcl-3 führte zu schwereren Formen der AP und Cholangitis, begleitet durch eine erhöhte Infiltration von Immunzellen sowie Produktion von Zytokinen und Chemokinen. Außerdem, wurde die kanonische Aktivierung von NF-κB signifikant während steriler Entzündung in *Bcl-3*$^{-/-}$ Mäusen verlängert. Mittels diversen genetischen Modulationen, konnten wir zeigen, dass Bcl-3 die Ubiquitinierung und den Proteasom-vermittelten Abbau von p50-Homodimeren hemmt und so die prolongierte Bindung von NF-κB-Heterodimeren an die DNA blockiert. Mit Hilfe von Knochenmarkschimären konnten wir die zelluläre Quelle von Bcl-3 lokalisieren, welche sich in Epithelzellen, aber nicht in myeloiden Zellen befand. SNP Analyse der UBE2L3 Variante war jedoch nicht mit dem Schweregrad assoziiert.

Zusammenfassend befasst sich die vorliegende Studie mit der zentralen Rolle von Bcl-3 in der Kontrolle der sterilen Entzündung in verschiedenen Organen und Organismen. Die hierin gewonnen Erkenntnisse eröffnen damit einen neuen Weg für die gezielte Therapie steriler Entzündungen im Gastrointestinaltrakt.

Part of this thesis was published:

1) **Song L,** Wörmann S, Ai J, Neuhöfer P, Lesina M, Diakopoulos KN, Ruess D, Treiber M, Witt H, Bassermann F, Halangk W, Steiner JM, Esposito I, Rosendahl J, Schmid RM, Riemann M, Algül H. Bcl-3 reduces the sterile inflammatory response in pancreatic and biliary tissues. Gastroenterology, 2016 Feb; 150(2):499-512.e20.

Additional publications not related to this thesis include:

2) Wörmann SM, **Song L,** Ai J, Diakopoulos KN, Kurkowski MU, Görgülü K, Ruess D, Campbell A, Doglioni C, Jodrell D, Neesse A, Demir IE, Karpathaki AP, Barenboim M, Hagemann T, Rose-John S, Sansom O, Schmid RM, Protti MP, Lesina M, Algül H. Loss of P53 Function Activates JAK2-STAT3 Signaling to Promote Pancreatic Tumor Growth, Stroma Modification, and Gemcitabine Resistance in Mice and Is Associated With Patient Survival. Gastroenterology. 2016 Jul; 151(1):180-193.e12.
3) Diakopoulos KN, Lesina M, Wörmann S, **Song L,** Aichler M, Schild L, Artati A, Römisch-Margl W, Wartmann T, Fischer R, Kabiri Y, Zischka H, Halangk W, Demir IE, Pilsak C, Walch A, Mantzoros CS, Steiner JM, Erkan M, Schmid RM, Witt H, Adamski J, Algül H. Impaired Autophagy Induces Chronic Atrophic Pancreatitis in Mice via Sex- and Nutrition-Dependent Processes. Gastroenterology. 2015 Mar; 148(3):626-638.e17.
4) Lesina M, Wörmann S, Neuhöfer P, **Song L,** Algül H . Interleukin-6 in inflammatory and malignant diseases of the pancreas. Semin Immunol. 2014; 26(1):80-87.
5) Zhang H, Neuhöfer P, **Song L,** Rabe B, Lesina M, Kurkowski MU, Treiber M, Wartmann T, Regnér S, Thorlacius H, Saur D, Weirich G, Yoshimura A, Halangk W, Mizgerd JP, Schmid RM, Rose-John S, Algül H. IL-6 trans-signaling promotes pancreatitis- associated lung injury and lethality. J Clin Invest. 2013 Mar 1; 123(3):1019-1031.
6) Neuhöfer P, **Song L**, Einwächter H, Schwerdtfeger C, Wartmann T, Treiber M, Zhang H, Schulz HU, Dlubatz K, Lesina M, Diakopoulos KN, Wörmann S, Halangk W, Witt H, Schmid RM, Algül H. Deletion of IκBα activates RelA to reduce acute pancreatitis in mice through up-regulation of Spi2A. Gastroenterology 2013 Jan; 144(1):192-201.
7) Treiber M, Neuhöfer P, Anetsberger E, Einwächter H, Lesina M, Rickmann M, **Song L**, Kehl T, Nakhai H, Schmid RM, Algül H. Myeloid, but not pancreatic, RelA/p65 is required for fibrosis in a mouse model of chronic pancreatitis. Gastroenterology 2011 Oct; 141(4):1473-1485.
8) Zhang H, Cai CZ, Zhang XQ, Li T, Jia XY, Li BL, **Song L**, Ma XJ. Breviscapine attenuates acute pancreatitis by inhibiting expression of PKCα and NF-kB in pancreas. World J Gastroenterol. 2011 Apr 14; 17(14):1825-1830.

Parts of this thesis were presented at the following scientific meetings:

1) “Bcl-3 protects acute pancreatitis by stabilizing p50 homodimers”, scientific presentation.

   Liang Song, Patrick Neuhöfer, Jiaoyu Ai, Marina Lesina, Matthias Treiber, Nina Diakopoulos, Karen Dlubatz, Marc Riemann, Sonja Wörmann, Roland M. Schmid and Hana Algül. (Jahrestagung der Deutschen Gesellschaft für Verdauungs- und Stoffwechselkrankheiten, September 11th-14th 2013, Nuremberg, Germany)

2) “Bcl-3 protects acute pancreatitis by stabilizing p50 homodimers”, scientific presentation.

   Liang Song, Patrick Neuhöfer, Jiaoyu Ai, Marina Lesina, Matthias Treiber, Nina Diakopoulos, Karen Dlubatz, Marc Riemann, Sonja Wörmann, Roland M. Schmid and Hana Algül. (Jahrestagung des Deutschen Pankreasclubs, January 23rd-25th 2014, Mannheim, Germany)

3) “Key contribution of Bcl-3 dependent stabilization of p50 homodimers to resolution of sterile inflammation in the pancreas and biliary system”, scientific presentation.

   Liang Song, Patrick Neuhöfer, Jiaoyu Ai, Marina Lesina, Matthias Treiber, Nina Diakopoulos, Karen Dlubatz, Sonja Wörmann, Marc Riemann, Florian Bassermann, Heiko Witt , Jonas Rosendahl, Roland M. Schmid and Hana Algül. (Jahrestagung des Deutschen Pankreasclubs, January 22nd-24th 2015, Rostock, Germany)

Table of contents

1 Introduction

1.1 Sterile inflammation

The inflammatory response plays a vital role in host defense against invasive pathogens. It is one of the first lines of defense recruited to combat a potential threat. One of the major triggers of inflammation is infection, with the inciting stimulus being certain proinflammatory molecules of the invading microbe.[1,2] In response to an infection, a cascade of signals leads to the recruitment of inflammatory cells, particularly innate immune cells such as neutrophils and macrophages. These cells, in turn, phagocytose infectious agents and produce additional cytokines and chemokines that lead to the activation of lymphocytes and adaptive *immune* responses. Similar to the eradication of pathogens, the inflammatory response is also crucial for tissue and wound repair.[2]

Inflammation as a result of ischemic, toxic or autodigestive damage to the heart, lung, liver, brain, kidney and pancreas,[3] typically occurs in the absence of any microorganisms and has therefore been termed 'sterile inflammation'. Similar to microbe-induced inflammation, sterile inflammation have all the clinical features of redness, swelling, heat, pain and loss of function. It is marked by the recruitment of neutrophils and macrophages and the production of proinflammatory cytokines and chemokines, notably tumor necrosis factor (TNF) and interleukin-1 (IL-1). These inflammatory responses, particularly the infiltration of tissues with neutrophils, can increase the amount of tissue injury because depleting neutrophils with antibodies[4,5] or blocking the signals that lead to their recruitment[6,7] reduces the amount of tissue injury. And yet, how a cell that is not inflammatory when alive becomes proinflammatory after death is incompletely understood.

1.1.1 Damage associated molecular patterns

The best understood initiator of sterile inflammation is necrotic cell death with the release of a large and diverse number of proinflammatory molecules which are termed damage associated molecular patterns (DAMPs). A common feature of DAMPs is that they are endogenous factors that are normally sequestered intracellularly and are therefore hidden from recognition by the immune system under normal physiological conditions. However, under conditions of extreme damage (for example, ischaemia or trauma) when necrosis occur, the loss of plasma membrane integrity thereby allows escape of intracellular material from the cell.[8,9] Prototypical DAMPs derived from necrotic cells including the chromatin-associated protein high-mobility group box 1 (HMGB1),[10] heat shock proteins (HSPs),[11] and purine metabolites, such as ATP[12] and uric acid[13] (Table 1-1). In addition to DAMPs from an intracellular source, there are also extracellularly located DAMPs. These are typically released by extracellular matrix (ECM) molecules that are upregulated upon injury or degraded following tissue damage.[14] ECM fragments, such as hyaluronan, heparan sulphate

and biglycan, are generated as a result of proteolysis by enzymes released from dying cells or by proteases activated to promote tissue repair and remodeling.[15]

Table 1-1: Sterile stimuli. Adapted from (Grace Y. Chen and Gabriel Nuñez, Nat Rev Immunol, 2010).

Sterile inflammatory signal	Putative sensor	Associated pathology	Refs*
Endogenous			
HMGB1	TLR2, TLR4, TLR9, RAGE and CD24	Cellular injury and necrosis	26,93,98,106
HSPs	TLR2, TLR4, CD91, CD24, CD14 and CD40	Cellular injury and necrosis	11,25,106,122
S100 proteins	RAGE	Cellular injury and necrosis	19
SAP130	CLEC4E	Cellular injury and necrosis	72
RNA	TLR3	Cellular injury and necrosis	39,123
DNA	TLR9 and AIM2	Cellular injury and necrosis	40,48–50
Uric acid and MSU crystals	NLRP3	Gout	13,55
ATP	NLRP3	Cellular injury and necrosis	20,60
Hyaluronan	TLR2, TLR4 and CD44	Cellular injury and necrosis	31,32,103
Biglycan	TLR2 and TLR4	Cellular injury and necrosis	14,33
Versican	TLR2	Cellular injury and necrosis	34
Heparan sulphate	TLR4	Cellular injury and necrosis	124
Formyl peptides (mitochondrial)	FPR1	Cellular injury and necrosis	125
DNA (mitochondrial)	TLR9	Cellular injury and necrosis	125
CPPD crystals	NLRP3	Pseudogout	55
β-amyloid	NLRP3, CD36 and RAGE	Alzheimer's disease	56,94,105
Cholesterol crystals	NLRP3 and CD36	Atherosclerosis	59,105
IL-1α	IL-1R	Cellular injury and necrosis	15,22,41
IL-33	ST2	Cellular injury and necrosis	16,86
Exogenous			
Silica	NLRP3	Silicosis and pulmonary interstitial fibrosis	44,57,58
Asbestos	NLRP3	Asbestosis and pulmonary interstitial fibrosis	57

Abbreviations: AIM2, absent in melanoma 2; CLEC4E, C-type lectin 4E; CPPD, calcium pyrophosphate dihydrate; DAMP, damage-associated molecular pattern; FPR1, formyl peptide receptor 1; HMGB1, high-mobility group box 1; HSP, heat shock protein; IL, interleukin; MSU, monosodium urate; IL-1R, IL-1 receptor; NLRP3, NOD-, LRR- and pyrin domain-containing 3; RAGE, receptor for advanced glycation end products; SAP130, spliceosome-associated protein 130; TLR, Toll-like receptor.

1.1.2 Mechanisms of sterile inflammation

Inflammatory responses induced by sterile stimuli are very similar to responses during infection. This suggests that both infectious and sterile stimuli may function through common receptors and pathways. Mechanisms by which sterile endogenous stimuli trigger inflammation include: activation of pattern recognition receptors (PRRs) by mechanisms similar to those used by microorganisms and pathogen-associated molecular patterns (PAMPs); release of intracellular cytokines and chemokines, such as IL-1α, that activate common pathways downstream of PRRs; and direct activation by receptors that are not typically associated with microbial recognition.

1.1.2.1 Activation of PRRs

To date five classes of PRRs have been identified: Toll-like receptors (TLRs), which are transmembrane proteins located at the cell surface or in endosomes; NOD-like receptors

(NLRs), which are located in the cytoplasm; RIG-I-like receptors (RLRs), which are also located intracellularly and are primarily involved in antiviral responses; C-type lectin receptors (CLRs), which are transmembrane receptors that are characterized by the presence of a carbohydrate-binding domain; and absence in melanoma 2 (AIM2)-like receptors, which are characterized by the presence of a pyrin domain and a DNA-binding HIN domain involved in the detection of intracellular microbial DNA.[16]

1) Recognition of endogenous DAMPs by TLRs: There is mounting evidence that TLRs sense endogenous molecules among those PRRs. DAMP activation of TLRs induces inflammatory gene expression to mediate tissue repair. All TLRs except for TLR3 signal through the adaptor protein MyD88 (myeloid differentiation primary response gene 88). Ligand binding to TLRs results in the recruitment of MyD88 and TIR domain-containing adaptor-inducing IFNβ (TRIF), which then triggers a signaling cascade, such as IκB kinase (IKK)/nuclear factor κB (NF-κB), mitogen-activated protein kinase (MAPK) and type I interferon pathways, thereby resulting in the upregulation of proinflammatory cytokines and chemokines that are important in inflammatory response. Among which the activation of NF-κB pathway is the most prominent one.[17,18]

2) Generation of IL-1β by inflammasomes: IL-1β is a potent proinflammatory cytokine that is produced mainly by macrophages and has many biological functions that are important in sterile inflammation.[19] The secretion of IL-1β by inflammatory cells is largely dependent on a multi-protein complex termed the inflammasome, of which the hallmark activity is the activation of caspase-1. Following activation, caspase-1 proteolytically cleaves IL-1β into its biologically active form. There are several inflammasomes that have been described to date, and each is named after the specific PRR contained in it. Of these inflammasomes, two have been described that can sense non-microbial molecules: the NLRP3 (NOD-, LRR- and pyrin domain-containing 3) inflammasome[20,21] and the AIM2 inflammasome.[22,23]

1.1.2.2 Release of intracellular cytokines

The passive release of biologically active cytokines during sterile injury-associated cell death is an important mechanism to alert the immune system of tissue damage and to initiate the healing response. Two cytokines of the IL-1 family, IL-1α and IL-33, are particularly relevant. Unlike its related family members IL-1β and IL-18, IL-1α is synthesized as a biologically active cytokine in its full-length precursor form and does not require processing for signaling through IL-1R.[24,25] When cells die by necrosis, such as during injury, this precursor form of IL-1α is released, leading to activation of its cognate receptor and rapid recruitment of inflammatory cells into the surrounding injured tissue. This is in contrast with apoptotic cells, in which IL-1α is sequestered intracellularly,[25] or with intact cells, in which the secretion of mature IL-1α is partially dependent on caspase-1 activity.[26] Similar to IL-1α, IL-33 is active as a precursor protein. Although it was initially thought that the IL-33 precursor was processed by caspase-1 to produce biologically active IL-33, it is now clear that its processing by the executioner caspases (caspase 3 and caspase 7) during apoptosis inactivates IL-33.[27,28] Thus, IL-33, which is expressed at high levels by endothelial cells and some epithelial cells, is expected to

be active when it is released during necrosis, but not apoptosis, which is associated with executioner caspase activation.

1.1.2.3 Non-PRR-mediated recognition of DAMPs

In addition to PRRs, DAMPs are recognized by DAMP-specific receptors, among which receptor for detecting advanced glycation end-products (AGes) is the prototypical one.[29,30] This receptor for AGes (RAGe) also recognizes HMGB1[31] and the S100 family members[32] apart from AGes, which are released during cellular stress and necrotic cell death. Activation of RAGe by its ligands results in the upregulation of several inflammatory signaling pathways, including, but not limited to, NF-κB, phosphoinositide 3-kinase (PI3K), Janus kinase (JAK)-signal transducer and activator of transcription (STAT), and MAPK signaling pathways, which lead to induction of proinflammatory cytokines such as TNF.[33] The mechanism by which RAGe activates these proinflammatory signaling pathways is unclear. It has also been shown that DAMP-specific receptors can negatively regulate inflammatory responses. Specifically, CD24, which can bind to both HMGB1 and HSPs, negatively regulates sterile inflammatory responses.[34]

1.2 Acute pancreatitis

Pancreatitis is a sterile inflammation of the pancreas. It may be acute (beginning suddenly and lasting a few days) or chronic (occurring over many years). The most common symptoms of pancreatitis are severe upper abdominal burning pain radiating to the back, nausea, and vomiting that is worsened with eating. Eighty percent of cases of pancreatitis are caused by alcohol and gallstones. Gallstones are the single most common etiology of acute pancreatitis (AP). Alcohol is the single most common etiology of chronic pancreatitis (CP).

1.2.1 Anatomy and function of pancreas

The normal pancreas constitutes about 0.1% of adult body weight in humans, and is of similar relative size in many domestic animals. It lies in the epigastrium and left hypochondrium areas of the abdomen, extends from the duodenum to the hilum of the spleen.

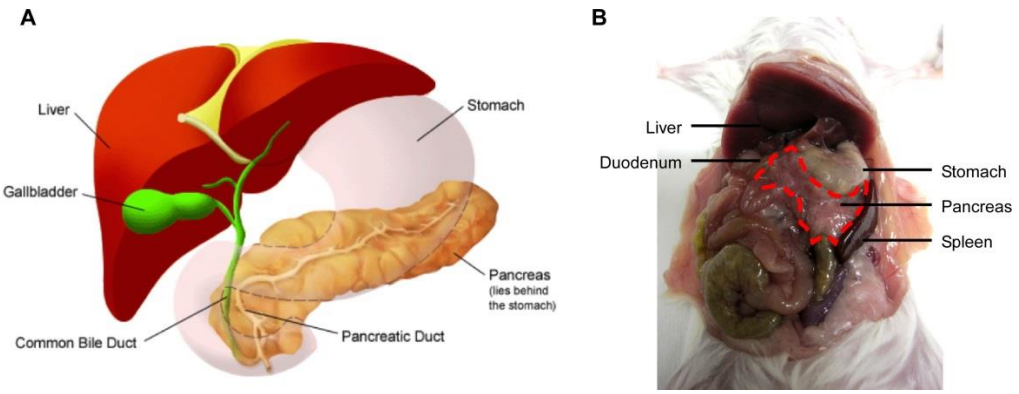

Figure 1-1: Anatomy of pancreas and liver (**A**) human (**B**) mouse.

The configuration of the pancreas varies with species and, to a lesser extent, within individuals of a species. The organ is compact and elongate in the human, whereas it is less compact in several rodent species. In the rat and mouse, for example, the tail (splenic portion) is relatively compact, whereas the head is dispersed within the mesentery of the duodenal loop. The central portion of the gland, between head and tail, is designated as body. These general topographical regions (head, body and tail) are useful for descriptive reference. However, the body and the tail are not divided by distinct anatomical landmarks (Figure 1-1).

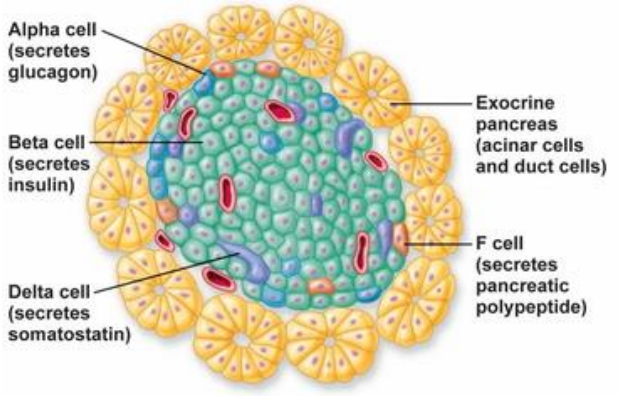

Figure 1-2: Function of the cells in pancreas.

The pancreas is a dual-function glandular organ in the digestive system and endocrine system of vertebrates. Both the exocrine and endocrine portions of it are highly specialized to synthesize and secrete a wide variety of specific proteins. More than 80% of gland consists of exocrine pancreatic acinar cells, which help out the digestive system. These cells secrete pancreatic juice containing digestive enzymes into the small intestine through the pancreatic duct system. These enzymes assist digestion and absorption of nutrients by breaking down the carbohydrates, proteins, and lipids in the chyme. The part of the pancreas with endocrine function is made up of approximately a million cell clusters called islets of Langerhans. Four main cell types exist in the islets. They are relatively difficult to distinguish using standard staining techniques, but they can be classified by their secretion: α (alpha) cells secrete glucagon (increase glucose in blood), β (beta) cells secrete insulin (decrease glucose in blood), Δ (delta) cells secrete somatostatin (regulates/stops α and β cells) and PP cells (secrete pancreatic polypeptide) (Figure 1-2).

1.2.2 Pathophysiology of AP

AP, a sudden inflammation of the pancreas, defined as the acute nonbacterial inflammatory condition of the pancreas, is initiated in the pancreas and characterized by local inflammation with recruitment of leukocytes. Acute and constant pain in the epigastric area or the right upper quadrant is the most common symptom.[35] Pain might last for several days, radiate to the back, and be associated with nausea and vomiting. In 80% of patients, AP is mild and

self-limiting, which resolves without serious morbidity, but in up to 20% of patients, develop a severe disease with local and extrapancreatic complications characterized by early development and persistent of hypovolaemia, as well as multiple organ failure, accompanied by substantial morbidity and mortality.[36] The main causes of AP are pancreatic hyperstimulation (mainly seen in experimental models), gallstone obstruction and alcohol abuse. In gallstone-induced pancreatitis, obstruction is localized in the bile duct, the pancreatic duct, or both. Duct obstruction promotes pancreatitis by increasing ductal pressure with subsequent upregulated activation of digestive enzymes. While the correlation between alcohol and pancreatitis is not completely understood. It showed that ethanol directly sensitizes acinar cells to cholecystokinin stimulation.[37]

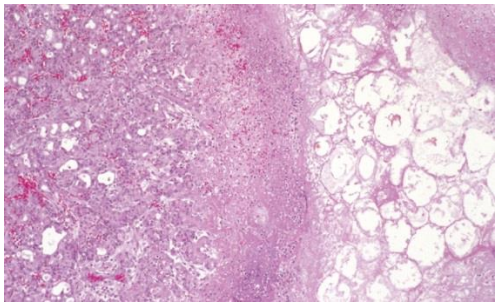

Figure 1-3: The microscopic field shows a region of fat necrosis (right) and focal pancreatic parenchymal necrosis (center).

The basic alterations of morphology in AP are: 1) microvascular leakage causing edema; 2) necrosis of fat by lipases; 3) an acute inflammatory reaction; 4) proteolytic destruction of pancreatic parenchyma; and 5) destruction of blood vessels leading to interstitial hemorrhage. In milder forms, histologic alterations include interstitial edema and focal areas of fat necrosis in the pancreatic substance and peripancreatic fat. Fat necrosis results from enzymatic destruction of fat cells; the released fatty acids combine with calcium to form insoluble salts that precipitate in situ (Figure 1-3). In more severe forms, such as acute necrotizing pancreatitis, necrosis of pancreatic tissue affects acinar and ductal tissues as well as the islets of Langerhans; vascular damage causes hemorrhage into the parenchyma of the pancreas. Macroscopically, the pancreas exhibits red-black hemorrhagic areas interspersed with foci of yellow-white, chalky fat necrosis. Fat necrosis also can occur in extrapancreatic fat, including the omentum and bowel mesentery, and even outside the abdominal cavity (e.g., in subcutaneous fat). In most cases the peritoneum contains a serous, slightly turbid, brown-tinged fluid with globules of fat (derived from enzymatically digested adipose tissue). In the most severe form, hemorrhagic pancreatitis, extensive parenchymal necrosis is accompanied by diffuse hemorrhage within the substance of the gland.

Although the molecular mechanisms of the pathophysiology are not completely understood, most investigators believe that AP is caused by the unregulated activation of trypsin within pancreatic acinar cells (Figure 1-4). Enzyme activation within the pancreas leads to the

autodigestion of the gland and local inflammation. AP arises when intracellular protective mechanisms for preventing trypsinogen activation or reducing trypsin activity are overwhelmed. These protective mechanisms include the synthesis of trypsin as inactive enzyme trypsinogen, autolysis of activated trypsin, synthesis of specific trypsin inhibitors such as serine protease inhibitor Kazal type 1 (SPINK1), and low intracellular Ca^{2+} concentrations. After activation of trypsinogen into active trypsin within acinar cells, several enzymes, such as elastase and phospholipase A2, and the complement and kinin pathways are activated.[38] Additionally, the release of proinflammatory mediators such as TNF-α, IL-6, IL-1β, IL-10, intercellular adhesion molecule-1 (ICAM-1), et al. by acinar cells in the pancreas and the recruitment of immune cells are crucial events in influencing the ultimate severity of the disease.[39,40] In addition to these events, activation of endothelial cells enables the transendothelial migration of leucocytes, which release other harmful enzymes. Decreased oxygen delivery to the organ and generation of oxygen-derived free radicals also contribute to injury.

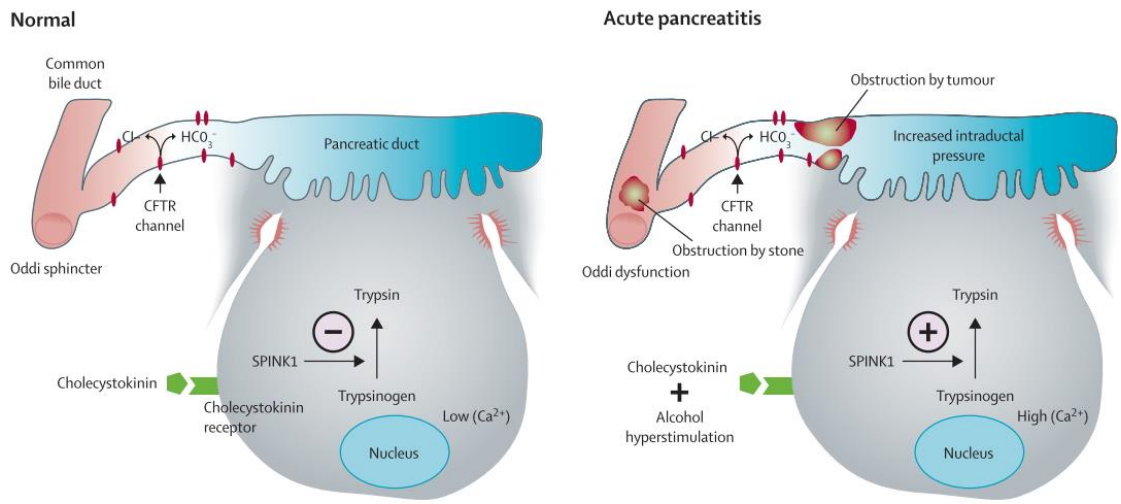

Figure 1-4: Pathophysiology of AP. Adapted from (J. Frossard et al. Lancet, 2008).

Thus, irrespective of the initial factor that triggers the disease, severity of pancreatic damage is related to injury of acinar cells and to activation of inflammatory and endothelial cells. Then, local complications (acinar cell necrosis, pseudocyst formation, and abscess) might develop, and injury in remote organs (i.e., lung) might follow the release of several mediators from the pancreas or from extra pancreatic organs such as the liver.

1.2.3 Experimental models of AP

Several experimental models of AP have been developed to investigate initiation, progression and possible treatment of AP. These models may be arbitrarily divided into invasive and non-invasive varieties according to the method of induction of AP. Among them, cholecystokinin-induced and L-arginine-induced AP is considered to be non-invasive models. Sodium

taurocholate-induced and pancreatic duct ligation-induced AP is the two best established invasive models.

1.2.3.1 Cholecystokinin-induced AP

Cholecystokinin (CCK) is a gastrointestinal hormone which plays a major role in normal pancreatic secretion. However, when administered at supramaximal concentrations, it inhibits pancreatic secretion and instigates a cascade of events which lead to acinar cell injury and AP. Cerulein, a cholecystokinin analogue, has been used to successfully cause AP in rats, mice, and dogs[41–43] by intravenous, subcutaneous or intraperitoneal injection routes. This model was frequently used to study the cell biology and pathophysiological events in AP, and known as a most common model so far. The underlying mechanisms are probable that cerulein upregulates ICAM-1 proteins in pancreatic acinar cells through intracellular upregulation of NF-κB. Surface ICAM-1 in turn promotes neutrophil adhesion onto acinar cells enhancing pancreatic inflammation.[44] In addition to promoting the inflammatory cell reaction to acinar cells, cerulein induces pancreatitis through dysregulation of digestive enzyme production and cytoplasmic vacuolization, leading to acinar cell death and pancreatic edema (Figure 1-5). Cerulein also activates NADPH oxidase, a source of reactive oxygen species contributing to inflammation, as well as the JAK signal transducer, another inflammation inducer.[45] In addition, cerulein-induced AP is also useful for studying systemic disease manifestation. It has been shown to be particularly effective for investigating the pathogenesis of pancreatitis-related pulmonary pathology.[46,47] The appearance of pulmonary injury in rats using this model resembles the early stages of the adult respiratory distress syndrome in humans.

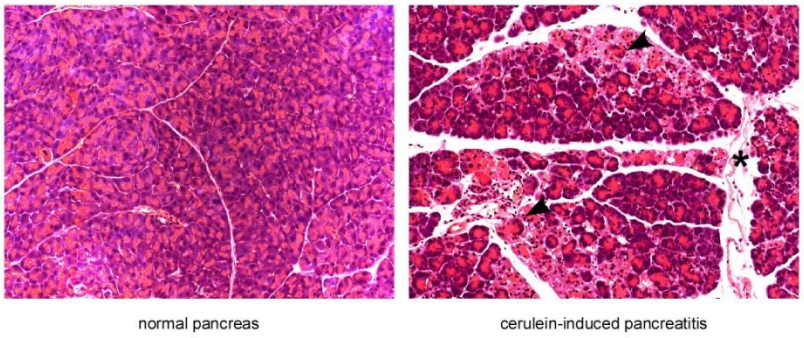

Figure 1-5: Histologic features of cerulein-induced pancreatitis. Note the appearance of focal necrosis (arrowheads) and edema (asterisk).

However, this model also has its disadvantages. The clinical relevance of this model is open to question because human pancreatitis is not generally triggered by supramaximal secretagogue stimulation. Additionally, cerulein treatment only develops mild AP, with negligible mortality. The course and severity of the underlying AP are highly variable and thus relatively unsuitable for controlled studies.[48]

1.2.3.2 L-arginine-induced AP

Mizinuma et al. were the first who studied the effect of an excessive dose of L-arginine (Arg) on different tissues in rats.[49] When male rats were given single i.p. injection of 500 mg of Arg

per 100 g body weight, the pancreatic acinar cells were destroyed selectively, without any morphological change of Langerhans' islets. After this first observation, researchers investigating Arg-induced pancreatitis usually modified the method of pancreatitis induction. Most of the authors, who studied the pathomechanisms of this kind of pancreatitis used 250mg/100 g body weight of Arg twice at an interval of one hour.

Furthermore, not only is this non-invasive model a good model to study the pathomechanisms of acute necrotizing pancreatitis, but it is also excellent to observe and influence the time course changes of the disease. The dose- and time-dependency of the effects of Arg gives an excellent opportunity to study the different phases of pancreatitis. A higher dose of Arg is suggested to study the pathomechanism of AP, while a smaller dose of Arg seems more suitable to characterize the regenerative processes. Long-term administration of Arg is suggested to study chronic pancreatitis. The mechanism by which Arg causes pancreatitis is not fully known. Accumulating evidence suggests that oxygen free radicals, nitric oxide (NO), inflammatory mediators all have a key role in the development of the disease.[50]

1.2.3.3 Sodium taurocholate-induced AP

Passage of a biliary tract stone into or through the terminal biliopancreatic duct is believed to be the most frequent triggering event in AP, Theoretically, stone impaction in the terminal duct could trigger pancreatitis simply by obstructing pancreatic juice outflow and, thus, causing ductal hypertension or, alternatively, it could trigger pancreatitis by establishing a common upstream channel through which bile might reflux retrogradely into the pancreatic duct. Accordingly, experimental AP elicited by the injection of sodium taurocholate (a bile salt) into the bilopancreatic duct of mice, rats, or larger animals is a seemingly clinically relevant model of pancreatitis. This pancreatitis, which is severe and necrotizing but non-lethal, is characterized by the very early, but transient, intrapancreatic activation of trypsinogen, hyperamylasemia, pancreatic edema, sequestration of inflammatory leukocytes within the pancreas, pancreatic acinar cell injury/necrosis, and intrapancreatic generation of the proinflammatory cytokine IL-6. Its severity is dependent upon the concentration of sodium taurocholate infused as well as the volume of the infusate and the time that has elapsed after infusion.[51]

1.2.3.4 Pancreatic duct ligation-induced AP

Surgical ligation of the pancreatic duct alone has not been successful in inducing AP. Most laboratory animals developed chronic lesions in the pancreas characterized by atrophy and apoptosis of acinar and ductal tissue, but not significant necrosis or inflammation. While the study combining pancreatic duct ligation with the secretory stimulation produced a greater degree of severe AP. The advantage of the duct ligation model is that it avoids artificial drug usage which may produce unwanted systemic effects, as well as the theory relating to clinical acute biliary AP with biliary pancreatic reflux.[52] However, the complexity, technical difficulty, high cost, limited reproducibility and the analogy to chronic pancreatitis, have made this model infrequently used for investigating AP.[48]

1.3 Primary sclerosing cholangitis

Primary sclerosing cholangitis (PSC), first described in the mid-1850s, is a complex liver disease that is heterogeneous in its presentation. PSC is characterized by chronic cholestasis associated with chronic inflammation of the biliary epithelium, resulting in multifocal bile duct strictures that can affect the entire biliary tree. Chronic inflammation leads to fibrosis involving the hepatic parenchyma and biliary tree, which can lead to cirrhosis and malignancy. This type of cholangitis is frequently associated with an inflammatory bowel disease (IBD), especially ulcerative colitis but also in Crohn`s disease patients.[53]

1.3.1 Pathophysiology of PSC

PSC usually appears as a cholestatic alteration of liver biochemistry, with an elevation of the alanine aminotransferase (ALT), alkaline phosphatase (ALP) and appearance of nonspecific serum antibodies such as atypical anti-neutrophil-cytoplasmatic-antibodies (ANCA). The typical histological features which can be found in human PSC are ductopenia of the medium and large ducts, onion-skin fibrosis, septal fibrosis, bridging necrosis and finally biliary cirrhosis. Although a relative high number of the patients are asymptomatic (15-55%), symptoms like fatigue, pruritus, jaundice, abdominal pain, weight loss, fever and hyperpigmentation are commonly reported at the time of diagnosis. The pathogenic mechanisms of PSC are incompletely understood, but the process is likely multifactorial. PSC likely occurs in genetically susceptible individuals, perhaps after exposure to environmental triggers. These could initiate a series of events that involve complex interactions between the innate and adaptive immune systems, ultimately leading to lymphocyte migration, cholangiocyte damage, and progressive fibrosis.[53]

Normally, biliary epithelial cells are exposed to common intestinal PAMPs such as lipopolysaccharide (LPS) and lipoteichoic acid (LTA). However, exposure to LPS may disrupt tight junctions in colonic and biliary epithelial cells through TLR4-dependent mechanisms.[54,55] Alteration of such barriers could expose cholangiocytes to a variety of substances, such as bile acids, that could promote injury and inflammation. Disruption of cholangiocyte tight junctions is an important step in the development of PSC in animal models.[56] For example, mice with altered cholangiocyte tight junctions leak bile acid into the portal tract. This leads to an inflammatory response that involves CD8+ and CD4+ T cells and upregulation of TNF-α, transforming growth factor β1 (TGF-β1), and IL-1β. This inflammatory infiltrate causes myofibroblast activation and fibrosis.[56]

Despite exposure to such common PAMPs, the innate immune system of patients without PSC does not appear to be as upregulated by these endotoxins.[57,58] For example, in liver explants from patients with PSC, biliary epithelial cells express higher levels of TLR, nucleotide-binding oligomerization domain, the MyD88/IRAK complex, TNF-α, interferon-γ (IFN-γ), and IL-8 than cells from those without PSC. Early-stage PSC samples express lower levels of IL-8, TNF-α, and TLR than late-stage samples. After repeated exposure to endotoxins, biliary epithelial cells from patients with PSC continued to secrete high levels of

IL-8, indicating a lack of tolerance to repeated endotoxin exposure. This hyper-responsiveness could be mediated by increases in levels of IFN-γ and TNF-α, which stimulate TLR4-mediated intake of endotoxin by biliary epithelial cells and ongoing TLR4 signaling in patients with PSC.[57] In addition, pathogens could stimulate TLR5 or TLR7 to induce T-helper-17 cells, which produce IL-17 in patients with PSC.[59]

Furthermore, the interaction between adhesion molecules and lymphocyte recruitment to the liver is emerging as an important step in the pathogenesis of PSC. Inflammatory mediators appear to upregulate a variety of adhesion molecules during development of PSC, including ICAMs, vascular cell adhesion molecule 1 (VCAM-1), and mucosal addressin cellular adhesion molecule 1 (MAdCAM-1).[60] Typically, MAdCAM-1 is expressed in the mucosal vessels of the intestine. However, under conditions of inflammation, it can be expressed by hepatic endothelium.[61] The observation that PSC can still develop after colectomy and IBD can still develop after liver transplantation suggesting that aberrant homing of lymphocytes between the intestine and liver could be involved in the pathogenesis of PSC. In this hypothesis, activated intestinal lymphocytes undergo enterohepatic circulation and persist as memory cells that cause hepatic inflammation. Chemokines and adhesion molecules that are shared by the intestine and liver could contribute to binding of immune cells at both sites.[62]

1.3.2 *Mdr2*$^{-/-}$ mice as a model of sclerosing cholangitis

Like several other ATP-binding cassette (ABC) transporters, ABCB4 (ATP-binding cassette, subfamily B, member 4, also named multidrug resistance protein 3, MDR3) is a floppase for phosphatidylcholine (PC). It translocates PC from the inner to the outer leaflet of the canalicular membrane of the hepatocyte.[63] Translocation of PC makes the phospholipid available for extraction into the canalicular lumen by bile salts. The primary function of biliary phospholipid excretion is to protect the membranes of cells facing the biliary tree against these bile salts: the uptake of PC in bile salt micelles reduces the detergent activity of these micelles.[64] Defects in ABCB4 have been associated with several adult cholestatic syndromes in addition to drug-induced cholestasis.[65]

In diverse animal models of PSC, Mdr2 (multidrug resistance protein 2, the rodent analogue to MDR3, also named Abcb4) knockout (*Mdr2*$^{-/-}$) mice spontaneously develop sclerosing cholangitis, biliary fibrosis and hepatocellular carcinomas that appears to be caused by the complete inability of the liver to secrete phospholipid into the bile.[56,66] The complete absence of phospholipids in *Mdr2*$^{-/-}$ mice leads to a hepatic disease, which becomes manifest shortly after birth and shows progression to an end stage in the course of 3 months.[67] In detail, livers of *Mdr2*$^{-/-}$ mice killed 1 day after birth showed a dense neutrophil-granulocytic infiltrate as well as proliferating fibroblasts and a ductular reaction in larger portal tracts. In livers of 2-week-old *Mdr2*$^{-/-}$ mice, medium-sized to larger bile ducts showed periductal fibroblast proliferation leading to periductal fibrosis, occasionally of the onionskin type. These bile ducts were also surrounded by neutrophils, and their epithelium was irregular with occasional mitoses. These changes were even more pronounced in 3- and 4-week-old *Mdr2*$^{-/-}$ mice, and ongoing fibro-

obliteration of small interlobular bile ducts was observed. Livers of mice aged 2, 3, 4, and 6 months showed identical morphology with complete and incomplete porto-portal septa, biliary type of fibrosis, periductal fibrosis of large, medium-sized but also small interlobular bile ducts, mostly of onionskin type, and fibro-obliteration of smaller ducts leading to fibrous scar formation (Figure 1-6). At these stages, the morphology closely resembled PSC in humans.[68]

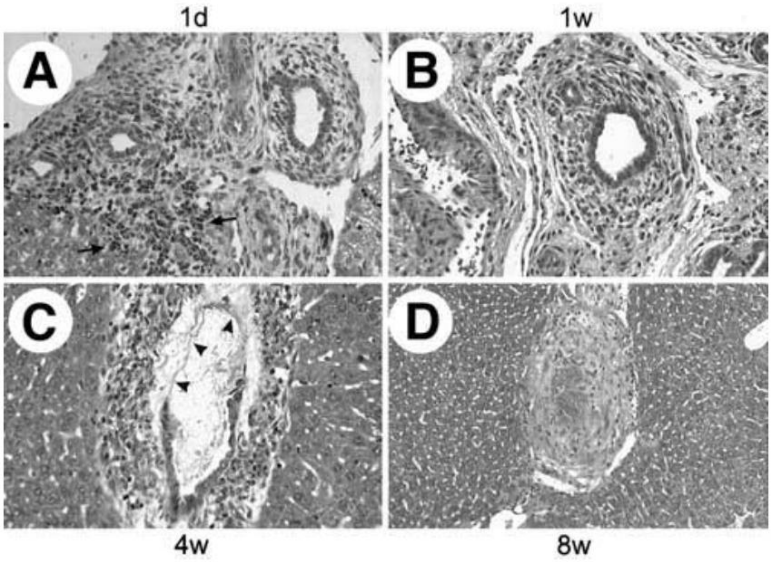

Figure 1-6: Development of bile duct lesions in *Mdr2*$^{-/-}$ mice. Adapted from (P Fickert et al. Gastroenterology, 2002).

The liver pathology of this model is that of a nonsuppurative inflammatory cholangitis with portal inflammation and ductular proliferation, consistent with toxic injury of the biliary system from bile salts unaccompanied by phospholipids. Thus, the *Mdr2*$^{-/-}$ mice represent a suitable animal model to mimick PSC in mice for studying mechanisms and potential interventions in nonsuppurative inflammatory cholangitis (in a generic sense) in human disease, be it congenital or acquired.[67]

1.4 NF-κB signaling pathway in sterile inflammation

1.4.1 NF-κB pathway

Nuclear factor κB is a ubiquitous inducible transcription factor responsible for mediating the expression of a large number of genes involved in inflammation, embryonic development, tissue injury, and repair.[69] NF-κB transcription factor family is composed of five factors: p65 (RelA), RelB, c-Rel, NF-κB1/p50 (processed from its precursor p105) and NF-κB2/p52 (processed from its precursor p100).[70] The different NF-κB family members can form heterodimers or homodimers to produce 15 possible NF-κB transcription factor complexes. These complexes, which are the downstream mediators of the ubiquitous NF-κB signaling

pathway, reside in the cytoplasm where they are sequestered by inhibitor of κB (IκB) proteins. There are seven IκB family members: IκBα, IκBβ, Bcl-3 (B cell leukemia 3), IκBε, IκBγ, and the precursor proteins p100 and p105, of which the most important are IκBα and IκBβ. IκBs are characterized by the presence of five to seven ankyrin repeats that assemble into elongated cylinders that bind the dimerization domain of NF-κB dimers.[71] Binding to IκB prevents the NF-κB:IκB complex from translocating into the nucleus, thereby maintaining NF-κB in an inactive state. When cells are stimulated by cytokines, LPS, or reactive oxygen species (ROS), IκBs are rapidly phosphorylated at specific serine residues by IκB kinase (IKK), and subsequently polyubiquinated and then degraded by the 26S proteasome. The IKK activity in cells can be purified as a 700-900 kDa complex, and has been shown to contain two kinase subunits, IKKα (IKK1) and IKKβ (IKK2), as well as a regulatory subunit, NEMO (NF-κB essential modifier) or IKKγ. Once IκBs degrade, nuclear translocation signals (NLS) of NF-κB are unmasked, leads to NF-κB dimers translocate into the nucleus where they bind directly to specific DNA sequences, called NF-κB binding sites, of target genes and modulate gene transcription.

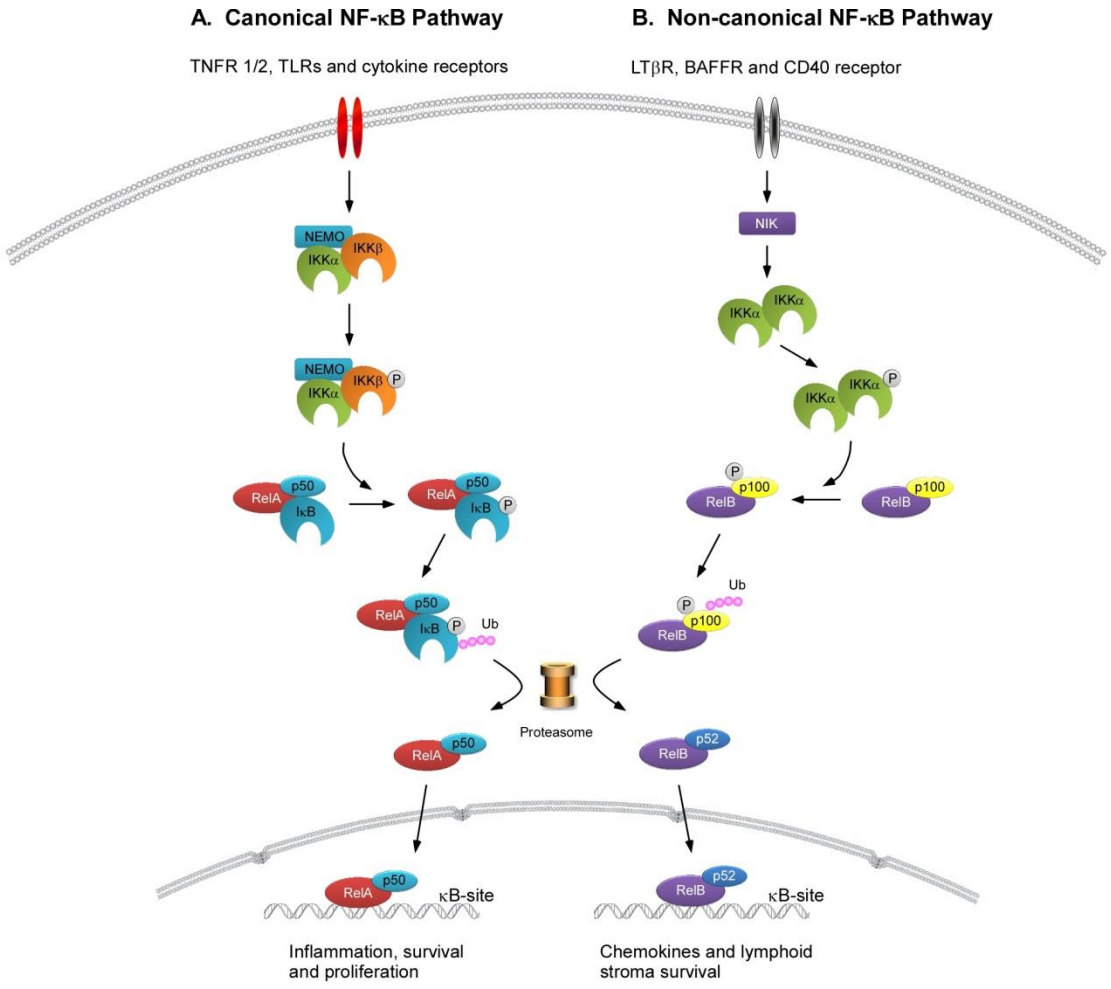

Figure 1-7: Classical (canonical) and alternative (non-canonical) pathways of NF-κB activation.

NF-κB signaling is generally considered to occur through either the canonical or non-canonical pathway (Figure 1-7). The canonical pathway mediates by IKKα and IKKβ and induces phosphorylation of IκB, leading to the transcription genes that regulate inflammation and cell survival. Inputs for the canonical pathway include tumor necrosis factor receptor 1/2 (TNFR 1/2), TLR, and many others. The non-canonical pathway involves NF-κB inducing kinase (NIK) activation of IKKα and leads to the phosphorylation and processing of p100, generating p52:RelB heterodimers. Input signals for the alternative pathway follow ligation of lymphotoxin-β receptor (LTβR), B-cell activating factor receptor (BAFFR), and CD40 receptor.[72] These canonical pathway stimuli also activate the non-canonical pathway.

1.4.2 NF-κB signaling in AP

NF-κB is activated very early in animal models of AP, information which is not available from patients, because it is too difficult to access the organ and obtain biopsy specimens. The first study demonstrating activation of NF-κB in AP was undertaken in the cerulein model of AP. In recent years, NF-κB family was strongly argued for the central factor in the regulation of inflammatory processes during AP.[73–77] However, the role of NF-κB activation in the pathogenesis of AP remains unclear so far.

One way to analyze the function of NF-κB during pancreatitis is to compare the course of pancreatitis with and without blocking its activation. Pharmacologic inhibition of NF-κB resulted in contradictory effects. Some reports showed that inhibition of NF-κB activation using non-specific chemicals, natural compounds, peptides or viral recombinant inhibitors revealed attenuation of severity or even improved survival in different experimental models of AP.[75] However, one other study suggested a protective mechanism mediated by NF-κB.[73] In this study two different non-specific inhibitors inhibited nuclear translocation of NF-κB during the course of pancreatitis which enhanced tissue injury and inflammation, demonstrating that NF-κB mediated induction of genes prevented a higher degree of damage of pancreatic tissue. The difficulty with all of these studies is the use of inhibitors which are not totally specific.

Another experimental approach is activation or inactivation of NF-κB in acinar cells via transgenic technique to determine whether NF-κB activation results in deterioration of the course of pancreatitis or even can induce pancreatitis per se. Our group previously used two mouse models with genetically inactivated IκBα or RelA/p65 in the pancreas respectively, to analyze the role of NF-κB. In our model, the effective protein RelA/p65 was shown to attenuate the severity of pancreatic damage through up-regulation of the serine protease inhibitor 2A (Spi2A)[78] and induction of pancreatitis-associated protein 1 (PAP1), a pancreas-specific acute phase protein[79] during AP. In contrast, two other mouse models with transgenic activation or inactivation of the IKK2, which is a upstream kinase of NF-κB pathway, was sufficient to activate NF-κB in the pancreas and induce pancreatitis[80] or attenuate response

towards pancreatitis.[81] Furthermore, the level of NF-κB activation correlates with the severity of AP in mice by expressing transgenic p65 or IKK2 in pancreatic acinar cells of mice.[82]

Several differences in the strategy of NF-κB activation or inactivation make it difficult to compare both models: 1) IKK2 (in)activation was achieved using a transgenic construct, whereas RelA/p65 inactivation was mediated by a knockin allele; 2) IKK2 was (in)activated constitutively under the control of a transgene promoter, leading to supraphysiologic and patchy expression of the mutated allele; and 3) NF-κB was (in)activated at 2 different stages - in the IKK2 models, the kinase activity was engineered, whereas, in the RelA/p65 model, the transcription factor was truncated. The loss-of-function approach of our model allowed us to investigate the function of endogenous, rather than transgenic, nuclear RelA/p65 in the pancreas. This approach mimics the natural events of NF-κB activation observed after stimulation more closely than transgenic overexpression of NF-κB.[83]

1.5 Molecular functions of Bcl-3

NF-κB activity is fine-regulated in the nucleus by a variety of mechanisms, including post translational modifications of Rel proteins, for example, sumoylation, phosphorylation, acetylation and ubiquitination.[84] Besides, some nuclear IκB proteins, which consist of Bcl-3, $I\kappa B_{NS}$, IκBζ and IκBη, can dramatically alter NF-κB-mediated effects via the regulation of dimer exchange, the recruitment of histone modifying enzymes or the stabilization of NF-κB dimers on the DNA. Although, these proteins formally belong to the IκBs due to the presence of ankyrin repeats in their structure, they do not act exclusively as repressors of NF-κB-mediated transcription, but more as NF-κB modulators which are involved in regulating nuclear NF-κB activities.[85] Those atypical IκBs show entirely different subcellular localizations, activation kinetics and an unexpected functional diversity. First of all, their interaction with NF-κB transcription factors takes place in the nucleus in contrast to classical IκBs, whose binding to NF-κB predominantly occurs in the cytoplasm. Secondly, atypical IκBs are strongly induced after NF-κB activation, for example by LPS and IL-1β stimulation or triggering of B cell and T cell antigen receptors, but are not degraded in the first place like their conventional relatives. Finally, the interaction of atypical IκBs with DNA-associated NF-κB transcription factors can further enhance or diminish their transcriptional activity. The capacity to modulate NF-κB transcription either positively or negatively, represents their most important and unique mechanistic difference to classical IκBs.[85]

Bcl-3 was the first identified atypical nuclear IκB protein. It consists of an amino-terminal transactivation domain (TAD) followed by 7 ankyrin repeats and a second carboxy terminal TAD, displaying an overall length of 448 amino acids. Bcl-3 was first described as a proto-oncogene expressed in patients, which suffered from B-cell chronic lymphocytic leukemia displaying the translocation t (14:19).[86]

There has been a great deal of conflicting results about the functional outcome of the interaction between Bcl-3 and NF-κB.

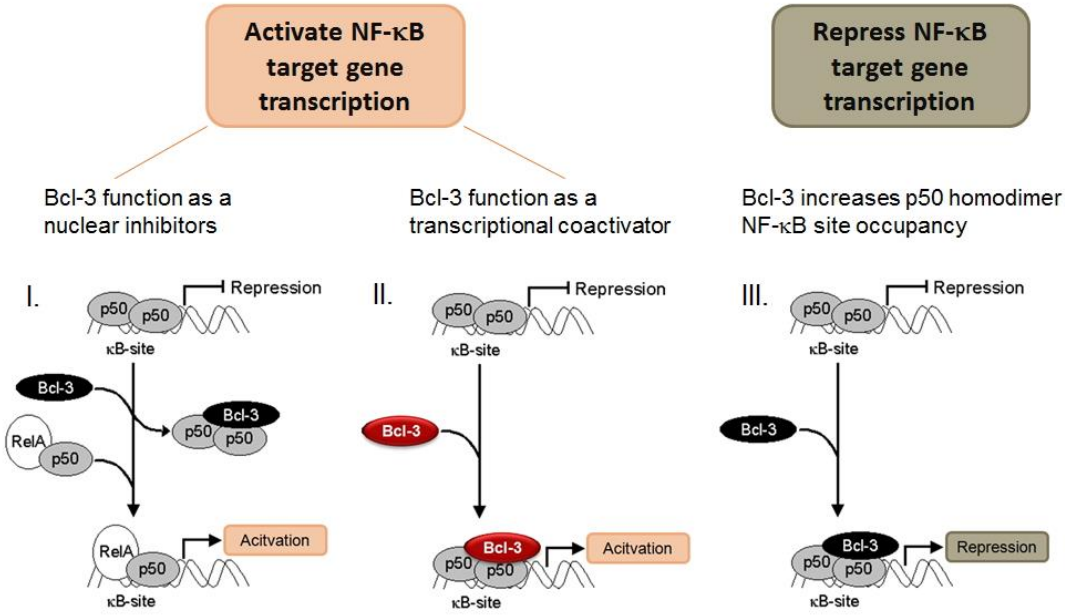

Figure 1-8: Schematic graph showing the function and interaction between Bcl-3 and p50 dimers.

In early reports, Bcl-3 was shown to inhibit DNA binding of the NF-κB subunit, p50. Some reports indicate that Bcl-3 could inhibit the DNA binding of p50:p65 heterodimer and p50 homodimer complexes to NF-κB sites.[87,88] However, reports by several other groups disputed the heterodimer claim, arguing that the inhibition of DNA binding by Bcl-3 was specifically limited to p50 and p52 homodimers.[89,90] These reports suggested that Bcl-3 facilitates NF-κB transactivation of NF-κB target genes by removing inhibitory p50 homodimers from the promoters of its target genes, thereby allowing the binding of activating p50/p65 or comparable heterodimers and indirectly forces transcriptional activation.[91] In contrast to these reports, it was found that Bcl-3 interact with p50 homodimers without dissociating the dimer from DNA.[92] Subsequent studies revealed that Bcl-3 can function as a coactivator capable of driving gene expression via its association with p50 and p52 homodimers.[93] Bcl-3 has also been shown to increase p50 homodimer binding to NF-κB sites in the regulatory elements of genes without causing coactivation.[94,95] The resulting effect is that Bcl-3 increases p50 homodimer NF-κB site occupancy, thereby indirectly repressing NF-κB target gene transcription. Furthermore, the increase in p50 homodimer binding caused by Bcl-3 is not due to an increase in the binding affinity of p50 homodimers but altering p50 turnover. Bcl-3 promotes p50 homodimer occupancy on the promoters of NF-κB target genes by delaying the K48 ubiquitination and subsequent degradation of DNA-bound p50 homodimers.[96] Thus, Bcl-3 seems to have two completely different functions (Figure 1-8). In one role, it delays the turnover of DNA-bound repressive p50 homodimers, creating a stable DNA-bound complex

thereby repressing transcription. In the other role, Bcl-3 binds to p50 and p52 homodimers, directly transactivating NF-κB-dependent transcription through domains in its N-terminal and C-terminal regions.

Bcl-3 itself is critically regulated via post-translational modifications, especially by phosphorylation and ubiquitination. It was shown that phosphorylation of Bcl-3 via GSK3 regulated Bcl-3 degradation and oncogenicity.[97] However, its proteasomal degradation in the cytoplasm is regulated by an E3-ligase complex containing TBLR1, which appears to be independently of GSK3.[98] In all known pathways, NF-κB activity is regulated by several upstream ubiquitination events through the balance between ubiquitin ligases and deubiquitinases. CYLD, a K63-deubiquitinase inhibits NF-κB activation in TRAF2-mediated NF-κB signaling pathways. Remarkably, Bcl-3 also becomes deubiquitinated by CYLD in the nucleus, upon UV-irradiation. This causes the rapid export of Bcl-3 from the nucleus and its inactivation.[99]

1.6 Aim of study

The central aim of the present study was to elucidate the function of specific subunits of NF-κB pathway in sterile inflammation. Animal models of AP and sterile cholangitis in *Bcl-3*$^{-/-}$ mice were used to evaluate sterile inflammation in the pancreas and biliary system. Bone marrow transplantation experiment between wild-type and *Bcl-3*$^{-/-}$ mice was performed to assess the effective cells of Bcl-3 during sterile inflammation. Moreover, the importance of p50 in Bcl-3-dependent inflammation was analyzed by using *p50*$^{-/-}$ mice.

2 Materials and methods

2.1 Animals and animal models

2.1.1 Mice

Mice used for the studies were maintained in a pathogen-free facility of the Zentrum für Präklinische Forschung at the Technical University of Munich (Bavaria, Germany). *Bcl-3*$^{-/-}$ mice have previously been described.[100] *Mdr2*$^{-/-}$ mice were acquired from Fabian Geisler at Technical University of Munich. *NF-κB1/p50*$^{-/-}$ mice were a gift by Marc Riemann at Leibniz-Institut für Altersforschung - Fritz-Lipmann-Institut. *Bcl-3*$^{-/-}$ and *Mdr2*$^{-/-}$ strains were interbred to obtain compound mutant *Bcl-3*$^{-/-}$/*Mdr2*$^{-/-}$ mice. C57BL/6 mice, purchased from The Jackson Laboratory (Bar Harbor, ME), were used as wild-type controls. All experiments were conducted on age- and sex-matched littermates. Mice were handled according to protocols approved by the Zentrum für Präklinische Forschung of the Technical University of Munich, which follows the federal German guidelines for ethical animal treatment.

2.1.2 Models of AP

8- to 10-week-old age- and sex-matched littermate mice were fasted for 18 h but provided with water ad libitum.

2.1.2.1 Cerulein-induced pancreatitis

Mice received 8 hourly intraperitoneal injections of 50 µg/kg body weight cerulein (Sigma-Aldrich) in 0.9% saline. The mice were sacrificed at different time points (1/2h, 1h, 4h, 8h, 24h and 72h) up to 72 h after the first injection of cerulein.

2.1.2.2 Severe acute pancreatitis (SAP)

Mice received 8 hourly intraperitoneal injections of 50 µg/kg body weight cerulein (Sigma-Aldrich) in 0.9% saline per day for 5 consecutive days. Mice were sacrificed according to the severity of pancreatitis in 5 days, and the rest of mice were sacrificed at 120 hours after the first injection of cerulein (Figure 2-1).

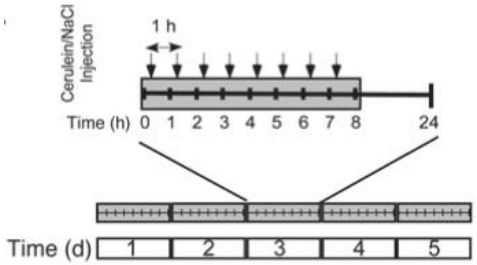

Figure 2-1: Schematic graph showing the induction of severe acute pancreatitis (SAP) via cerulein injection i.p. Adapted from (H. Zhang et al. JCI, 2013).

2.1.2.3 Sodium taurocholate-induced pancreatitis

Anesthesia of 8- to 10-week-old age- and sex-matched littermate mice was achieved with a ketamine/xylazine cocktail (70 mg/kg and 10 mg/kg, respectively). After a midline laparotomy was performed, 50 µl 2% sodium taurocholate (Sigma-Aldrich) in 0.9% saline was retrogradely infused into bile-pancreatic duct via papilla of Vater. Methylene blue (Sigma-Aldrich) was routinely included in the infusion solution to permit the identification and exclusion of animals in which the infusion had extravasated from the duct (Figure 2-2). Mice were killed 24 hours after the operation.

Figure 2-2: Operation of sodium taurocholate-induced AP. Adapted from (J. Laukkarinen. Gut, 2007).

2.2 Histological analyses

2.2.1 Hematoxylin and eosin (H&E) staining

H&E staining was performed by deparaffinizing embedded paraffin sections (1.5-3 µm) in xylene (X-TRA Solv, Medite GmbH) twice for 5 min. The sections were rehydrated in ethanol with decreasing concentration (100%, 96% and 70%) twice of each for 3 min. The slides were stained in hematoxylin solution (Merck Millipore) for 7 min and washed with flowed tap water for 10 min. Afterwards, the slides were stained in eosin solution (Waldeck GmbH) for 5 min, dehydrated in 96% ethanol and isopropanol for 25 sec of each, transparentized in xylene twice for 2 min sequentially. Finally, the slides were covered with mounting medium (pertex, Medite GmbH) and coverslips. Histologic images were taken with the Axiovert Imager (Zeiss).

2.2.2 Sirius red staining

The following solutions and buffers were prepared in advance:

Picro-sirius Red Solution: 0.5 g Sirius Red (Sigma-Aldrich), 500 ml saturated aqueous solution of picric acid (Sigma-Aldrich) (Keeps for at least 3 years and can be used many times)

Acidified Water: Add 5 ml acetic acid (glacial) (Sigma-Aldrich) to 1 L of water (tap or distilled)

Weigert's haematoxylin (Sigma-Aldrich)

Slides were deparaffinized and rehydrated as described (2.2.1). Next, the slides were stained with Weigert's haematoxylin for 8 min, washed with running tap water for 10 min. Afterwards,

the slides were stained in picro-sirius red solution for 1 hour (This gives near-equilibrium staining, which does not increase with long times. Short times should not be used, even if the colors look OK.), washed in 2 changes of acidified water. After removing physically most of the water from the slides by vigorous shaking, the slides were dehydrated in 3 changes of 100% ethanol. Finally, the slides were covered with mounting resinous medium (pertex, Medite GmbH) and coverslips. Histologic images were taken with the Axiovert Imager (Zeiss).

2.2.3 Immunohistochemistry (IHC)

Slides were deparaffinized and rehydrated as described (2.2.1). For antigen retrieval, slides were boiled in either 10 mM citrate acid buffer (pH 6.0) or 1 mM EDTA (pH 8.0) and sub-boiled for 15 min. Slides were cooled down at room temperature for 20-30 min and washed with water twice for 5 min. To quench endogenous peroxidase activity, sections were incubated with 3% H_2O_2 away from light for 15 min. Subsequently, slides were washed twice with TBS-T (or PBS-T) for 5 min. To block unspecific antibody binding, slides were incubated in TBS-T (or PBS-T) with avidin and 5% secondary antibody specific serum (e.g. goat serum for Bcl-3) for 1 h. After washing with TBS-T (or PBS-T) twice for 5 min, slides were incubated with primary antibody in TBS-T (or PBS-T) with biotin and 5% secondary antibody specific serum overnight at 4 °C (or room temperature) (Table 2-1).

After washing with TBS-T (or PBS-T) twice for 5 min in the following day, slides were incubated with secondary antibody (Vector laboratories) in TBS-T (or PBS-T) for 1 h at room temperature. Signal detection was performed with the ABC solution kit (Vector laboratories) and DAB kit (Vector laboratories) according to the manufacturer's instruction.

Table 2-1: Primary antibodies for immunohistochemistry

Antibody	Dilution	Source	Company	Product number
Bcl-3	1:250	rabbit	Santa Cruz	sc-185
F4/80	1:100	rat	Invitrogen	MF-48000
Phospho-IκBα	1:1200	mouse	Cell Signaling	# 9246
Phospho-RelA	1:200	rabbit	Cell Signaling	# 3037
Phospho-STAT3^{Y705}	1:400	rabbit	Cell Signaling	# 9145
p50	1:200	goat	Santa Cruz	sc-1190
CK19	1:250	rat	DSHB	TROMA-III
Ki67	1:2500	rabbit	Abcam	Ab15580
CD45	1:20	rat	BD Pharmingen	550539

Subsequently, slides were counterstained with hematoxylin solution (Merck Millipore) for 2-3 sec. After washing with flowed tap water for 10 min, slides were dehydrated in ethanol with increasing concentration (70%, 96% and 100%) twice of each for 10 sec, transparentized in

xylene twice for 2 min sequentially. Finally, the slides were covered with mounting medium (pertex, Medite GmbH) and coverslips. Histologic images were taken with the Axiovert Imager (Zeiss).

2.2.4 Morphometric quantification of necrosis and edema

Pancreatic tissue sections were stained with H&E. Necrotic cells with swollen cytoplasm, loss of plasma membrane integrity, and leakage of organelles into the interstitium were counted by 2 researchers in a blinded manner and analyzed using Axiovision software (version 4.8.; Zeiss). Necrosis was expressed as the percentage of examined pancreatic parenchyma. Edema was calculated as interlobular and intraacinar fluid accumulation within the total pancreatic area and analyzed using Axiovision software (version 4.8.; Zeiss). Morphometric quantification was performed with the assistance of Patrick Tomas Neuhöfer.

2.3 RNA/DNA analyses

2.3.1 DNA isolation from mouse tail tips for genotyping

Table 2-2: Genotyping PCR protocol

Type of mice	Step		Temperature	Time	
***Bcl-3*$^{-/-}$**	Pre-incubation		94 °C	10 min	
	Amplification	Denaturation	94 °C	1 min	32 cycles
		Annealing	60 °C	1 min	
		Extension	72 °C	2 min	
	Final extension		72 °C	10 min	
	Cooling		4 °C	∞	
***p50*$^{-/-}$**	Pre-incubation		94°C	4 min	
	Amplification		94°C	1 min	33 cycles
			66°C	2 min	
	Cooling		4 °C	∞	
***Mdr2*$^{-/-}$**	Pre-incubation		95 °C	5 min	
	Amplification	Denaturation	94 °C	45 sec	38 cycles
		Annealing	53 °C	30 sec	
		Extension	72 °C	1 min	
	Final extension		72 °C	10 min	
	Cooling		4 °C	∞	

Tail tips were lysed in 95 µl Lysis Buffer (100 mM Tris/HCl (Sigma-Aldrich) pH 8.5; 200 mM NaCl (Sigma-Aldrich); 5 mM EDTA (Sigma-Aldrich) pH 8.0; 0.2% SDS (Sigma-Aldrich)) with 5 µl Proteinase K (20 mg/ml, Roche) at 60 °C for 2-12 h (tissue was completely digested only fur was remained). After the incubation, samples were vortexed and heated at 95 °C for 10 min to inactivate the proteinase K. 900 µl dH_2O was added to dilute the DNA. Samples were centrifuged at 4 °C for 10 min full speed. 2-3 µl DNA (supernatant) was used as template for genotyping polymerase chain reaction (PCR).

2.3.2 Genotyping PCR

All genotyping PCRs were performed using the RedTaq Ready Mix (Sigma) with 1-2 µl DNA templates (2.3.1) with PCR protocol (Table 2-2) and all primers (Table 2-3) at a final concentration of 10 pM. Mice were genotyped with the assistance of Karen Dlubatz, Chantal Geisert and Viktoria Mayr.

Table 2-3: Genotyping primer

Type of mice		Primer sequence (5'-3')	Product size (bp)
***Bcl-3*$^{-/-}$**	MRINT3 as	CCA CAG AGC AAC CTG GAA GCA	1250 bp (KO)
	EX32 as	GGC TCC CAA GCT TGA AAA GGC	
	MRNEO as	GCA TCG CCT TCT ATC GCC TTC	
***p50*$^{-/-}$**	WT-50	GCAAACCTGGGAATACTTCATGTGACTAAG	~ 200 bp (KO)
	Bs-7	ATAGGCAAGGTCAGAATGCACCAGAAGTCC	
	HH-Neo	AAATGTGTCAGTTTCATAGCCTGAAGAACG	
***Mdr2*$^{-/-}$**	Neo-forward	CTT GGG TGG AGA GGC TAT TC	279 bp (KO)
	Neo-reverse	AGG TGA GAT GAC AGG AGA TC	
	Mdr2-forward	CAC TTG GAC CTG AGG CTG TG	
	Mdr2-reverse	TCA GGA CTC CGC TAT AAC GG	

2.3.3 RNA isolation

After sacrificing mice, small tissue pieces were taken from each part of the pancreas and liver immediately transferred into RLT lysis buffer containing 1% β-mercaptoethanol, homogenized and frozen in liquid nitrogen. The RNeasy Mini Kit (Qiagen) was used to isolate RNA, according to the manufacturer's instruction. RNA concentration was measured in a NanoDrop 2000 spectrophotometer (Peqlab). To judge the integrity and overall quality of a total RNA preparation, native agarose gel electrophoresis were performed by inspection of the 28s and 18s rRNA bands.

2.3.4 cDNA syntheses

For cDNA synthesis, a 20 µl reaction volume was used for 100 ng-5 µg of total RNA. RNA transcription was performed using the Superscript™ II Reverse Transcriptase Kit (Invitrogen) and Oligo(dt)$_{12-18}$ primer (500 µg/ml, Invitrogen) according to the manufacturer's instruction. The concentration of cDNA was adjusted to 20 ng/µl.

Table 2-4: Quantitative RT-PCR program

Step		Temperature	Time	
Pre-incubation		95 °C	10 min	
	Denaturation	95 °C	10 sec	
Amplification	Annealing	60 °C	20 sec	45 cycles
	Extension	72 °C	10 sec	
		95 °C	1 min	
Melting		55 °C	1 sec	
		98 °C	continuous 0.11 °C / sec	5 acquisitions / sec
Cooling		37 °C	5 min	

Table 2-5: Primers used for RT-PCR

Name	Primer forward (5'-3')	Primer reverse (3'-5')
Cyclophilin	ATG GTC AAC CCC ACC GTG	TTC TGC TGT CTT TGG AAC TTT GTC
Bcl-3	GGA GCC GCG AAG TAG ACG T	TGT GGT GAT GAC AGC CAG GT
IL-6	GAA GTA GGG AAG GCC GTG G	CTC TGC AAG AGA CTT CCA TCC AGT
TNF-α	CAT CTT CTC AAA ATT CGA GTG ACA A	TGG GAG TAG ACA AGG TAC AAC CC
IL-1β	CAA CCA ACA AGT GAT ATT CTC CAT G	GAT CCA CAC TCT CCA GCT GCA
CXCL1	TGG GAT TCA CCT CAA GAA CA	TTT CTG AAC CAA GGG AGC TT
MCP-1	CTT CTG GGC CTG CTG TTC A	CCA GCC TAC TCA TTG GGA TCA
MIP-1α	TGC CCT TGC TGT TCT TCT CT	TTC TTG GAC CCA GGT CTC TTT
p50	CGG GAT AGT GAC AGC GTC TGT	CAG TAA GAG ACT CTG TAA AGC TGA GTT TG

2.3.5 Quantitative RT-PCR

Quantitative RT-PCR was performed on a LightCycler 480 (Roche) using the LightCycler 480 SYBR Green Master Mix I (Roche) according to the protocol (Table 2-4). 100 ng-5 µg cDNA were used as a template. Cyclophilin was used as a housekeeping gene for normalization (Table 2-5). Melting Curve analysis was performed to check real-time PCR reactions or

primer-dimer artifacts and to ensure reaction specificity. Values were calculated using the following equation: Fold difference = $2^{\Delta Ct} = 2^{(Ct\ gene\ of\ interest - Ct\ cyclophilin)}$. *P* values were calculated using the statistical software Prism 5 (GraphPad Software, Inc).

2.3.6 SNP analysis

2.3.6.1 Patients

The respective medical ethical review committees of all participating centres approved the study protocol and all patients gave written informed consent (Approval: 376-11-12122011). AP was diagnosed and categorised according to the revised Atlanta classification.[101] Diagnosis of CP was based on two or more of the following findings: Presence of a history of recurrent pancreatitis or recurrent abdominal pain typical for CP, pancreatic calcifications and/or pancreatic ductal irregularities revealed by endoscopic retrograde pancreaticography or by magnetic resonance imaging of the pancreas and/or pathological sonographic findings. Alcoholic CP (ACP) was defined in patients who had consumed more than 80 g/d alcohol for at least two years in men and more than 60 g/d for women. All other CP patients were summarized in the non-alcohol related CP group (NACP). The controls investigated with the different methods were blood donors from South-West and East Germany. Details of the patients are summarized (Table 2-6).

Table 2-6: Details of patients

Pancreatitis		Number	Males	Age range (years)	Median (years)	AC 1	AC 2	AC 3
AP	**AP (all)**	289	172	9-92	54	108	110	71
	AP-A	56	53	27-76	44.5	9	21	26
	AP-B	137	61	9-92	62	66	43	28
	AP-ERCP	7	3	24-76	57	1	5	1
	AP-HLP	5	4	36-67	50	0	4	1
	AP-IP	71	45	10-89	50	32	30	9
	AP-OP	13	6	42-81	65	1	7	5
CP	**ACP**	293	256	24-79	49	n.a.	n.a.	n.a.
	NACP	248	134	3-77	34	n.a.	n.a.	n.a.
Controls		573	285	60-70	63	n.a.	n.a.	n.a.

Abbreviations: AP = acute pancreatitis, AP-A = alcoholic acute pancreatitis, AP-B = biliary acute pancreatitis, AP-ERCP = post endoscopic-retrograde-cholangiopancreaticography acute pancreatitis, AP-HLP = hyperlipidemia acute pancreatitis, AP-IP = acute pancreatitis in pregnancy, AP-OP = postoperative acute pancreatitis, CP = chronic pancreatitis, ACP = alcoholic chronic pancreatitis, NACP = non-alcohol related chronic pancreatitis. AC1 = Mild acute pancreatitis (according to the revised Atlanta classification), AC2 = moderately severe acute pancreatitis, AC3 = severe acute pancreatitis.

2.3.6.2 Genotyping

Genomic DNA was extracted from peripheral blood leukocytes. A LightSNiP assay to analyse *rs2298428* (NM_001017964.1:c.787G>A; NP_001017964.1:p.Ala263Thr; OMIM*603721, Ubiquitin-conjugating enzyme E2L3, UBE2L3; HGNC: 12488) was designed by TiB-Molbiol (Berlin, Germany). The reaction mix contained 14.4 µl H_2O, 1 µl Reagent mix, 1 µl FastStart DNA Master (LightCycler® FastStart DNA Master HybProbe (Roche Diagnostics, Germany), 1.6 µl $MgCl_2$ (25 mM), and 1 µl DNA (20 ng/µl) in a final reaction mixture of 20 µl. The LightCycler programm included denaturation at 95 °C for 10 sec, 45 quantification cycles with denaturation at 95 °C for 10 sec, primer annealing at 60 °C for 10 sec, and a elongation step at 72 °C for 15 sec. Melting was performed after denaturation at 95 °C for 30 sec and cooling to 40 °C for 120 sec with a final temperature of 75 °C and a ramp rate of 1.5 °C per sec.

2.4 Protein biochemistry

2.4.1 Protein isolation from tissue or cells

The following solutions and buffers were prepared in advance:

MLB-buffer (5×): 50 mM Hepes, pH 7.9 (Sigma-Aldrich); 150 mM NaCl (Sigma-Aldrich); 1 mM EDTA, pH 8.0 (Sigma-Aldrich); 0.5% NP-40 (Sigma-Aldrich); 10% Glycerol (Sigma-Aldrich); 1 mM DTT (Sigma-Aldrich); 0.2% PMSF (Sigma-Aldrich).

MLB working solution (1×): MLB-buffer (5×) was diluted 1:5 with 10% Glycerol (Carl Roth), (e.g. 1ml MLB-buffer (5×) with 4ml 10% Glycerol), 1% Protease inhibitor (Serva) and 1% Phosphatase inhibitor (Serva)) were added afterwards.

Laemmli- buffer (5×): 300 mM Tris-HCl, pH 6.8 (Sigma-Aldrich); 10% SDS (Sigma-Aldrich); 50% Glycerol (Sigma-Aldrich); 0.05% Bromphenol blue (Sigma-Aldrich); 5% β-Mercaptoethanol (Sigma-Aldrich).

For protein isolation, the tissues/cells were homogenized with suitable volume of MLB working solution according to the amount of tissues/cells, and put on ice until foam is gone. After the samples were centrifuged at 4 °C for 10 min full speed, the supernatants, which are the protein lysates, were kept on ice. Protein concentration was measured with the Bio Rad Protein Assay Kit (Bio Rad) and the samples were adjusted to 3 µg/µl with 5× Laemmli buffer.

2.4.2 Immunoblot analysis

Protein lysates were denatured at 95 °C for 5 min and kept on ice afterwards. Protein separation was performed with a SDS-PAGE gel (Gel percentage was depended on the protein size ranging from 7.5% to 15%) in running buffer at 120 V in a Bio Rad Mini Protein Gel System chamber. Discontinuous Gels were consisted of two fractions, which are a Stacking Gel (upper part of the gel, Table 2-7) and a Resolving Gel (lower part of the gel, Table 2-8). Loaded gels were run in running buffer. Separated protein was transferred to a PVDF membrane (Milipore) in a blotting chamber with 1× transfer buffer (Wet Transfer). The

pore size of PVDF membrane (0.2 µm or 0.45 µm), the voltage (300 mA-400 mA) and duration time (1-3 h) of membrane transfer were decided according to the size of target protein.

Table 2-7: Formulations of stacking gel

Stacking gel	**4%**
ddH_2O	3.0 ml
0.5 M Tris-HCl (pH 6.8) (Sigma-Aldrich)	1.3 ml
30% Acrylamide/Bis (Roche)	750 µl
10% SDS (Sigma-Aldrich)	50 µl
10% APS (Sigma-Aldrich)	25 µl
TEMED (Sigma-Aldrich)	10 µl
Total volume	5 ml

Table 2-8: Formulations of resolving gel

Resolving gel	**7.5%**	**10%**	**15%**
ddH_2O	4.9 ml	4.1 ml	2.5 ml
1.5 M Tris-HCl (pH 8.8) (Sigma-Aldrich)	2.6 ml	2.6 ml	2.6 ml
30% Acrylamide/Bis (Roche)	2.5 ml	3.3 ml	5.0 ml
10% SDS (Sigma-Aldrich)	100 µl	100 µl	100 µl
10% APS (Sigma-Aldrich)	50 µl	50 µl	50 µl
TEMED (Sigma-Aldrich)	15 µl	15 µl	15 µl
Total volume	10 ml	10 ml	10 ml

After member transfer, PVDF membrane was incubated with 5% skim milk (or 5%BSA) in TBS-T for 1 h to block any unspecific antibody binding. Afterwards, the membrane was incubated with primary antibody in 5% skim milk (or 5%BSA) in TBS-T overnight at 4 °C (Table 2-9). On the second day, the membrane was washed 3-5 times with TBS-T and incubated with the species-specific HRP-coupled secondary antibody in 5% skim milk (or 5%BSA) in TBS-T for 1 h at room temperature. After washing 3-5 times with TBS-T, the protein band was visualized using the ECL Western Blotting Detection Reagents and Amersham Hyperfilms (GE Healthcare).

2.4.3 Immunoprecipitation and ubiquitination assay

To detect ubiquitination of endogenous p50, mice were pretreated with bortezomib (0.5 mg/kg) intraperitonealy 1h prior to first injection of cerulein for inhibiting the function of proteasomes.

Next, the pancreata of mice were removed, lysed as usual. The concentration of protein lysates were measured and adjusted to 10 µg/µl. 100 µl of them were denatured with 10 µl 1% NP-40 (Sigma-Aldrich), 1 µl 0.5M EDTA (Sigma-Aldrich), 10 µl 10% SDS (Sigma-Aldrich) at 95 °C for 5 min. The samples were cooled down for 3-5 min at RT. While cooking, 100 µl Triton-X was added in 10 ml lysis buffer (final concentration 1%), mixed by vortexing vigorously for 2 min. Then, 900 µl 1% Triton-X was added into 100 µl samples, the mixed solutions were put immediately back on ice to cool down for 5 min. 50 µl "input" aliquots were taken afterwards.

Table 2-9: Primary antibodies for immunoblot analyses

Antibody	Dilution	Species	Company	Product number
Bcl-3	1:1000	rabbit	Santa Cruz	sc-185
ERK1	1:1000	rabbit	Santa Cruz	sc-93
ERK2	1:1000	rabbit	Santa Cruz	sc-154
Phospho-STAT3^{Y705}	1:1000	rabbit	Cell Signaling	# 9131
STAT3	1:1000	rabbit	Cell Signaling	# 9132
Phospho-RelA	1:1000	rabbit	Cell Signaling	# 3033
RelA	1:1000	rabbit	Cell Signaling	# 3034
p50	1:2000	rabbit	Abcam	ab32360
p50	1:1000	rabbit	Cell Signaling	#3035
P52	1:1000	rabbit	Cell Signaling	# 4882
IκBα	1:1000	rabbit	Santa Cruz	sc-371
IκBβ	1:1000	rabbit	Santa Cruz	sc-945
β-actin	1:5000	mouse	Sigma-Aldrich	A5441
COX IV	1:1000	rabbit	Cell Signaling	# 4844
Lamin A/C	1:1000	rabbit	Santa Cruz	sc-20681
MAb to Mono- and Polyubiquitinylated conjugates (FK2)	1:1000	mouse	Enzo Life Sciences	BML-PW8810

Equal amounts of protein were immunoprecipitated with anti-p50 (Santa Cruz) antibody overnight at 4 °C with rotation. On the second day, 30 µl protein G magnetic beads (cell signaling) were incubated with IP samples for 2 h at 4 °C with rotation for combining immunocomplexes of p50. Protein G magnetic beads were pelleted by placing the tubes in a Magnetic Separation Rack, and supernatant was removed carefully after waiting 1 to 2 min for solution to clear. This step was repeated 3 times. The pellets were resuspended with lysis buffer and 5 X Lammli buffer, complexes of p50 were eluted from the magnetic beads for 10

min at 95 °C. Following SDS-PAGE, proteins were transferred to a PVDF membrane and immunoblotted with MAb to Mono- and Polyubiquitinylated Conjugates (FK2), which has been shown to recognize K^{29}-, K^{48}-, and K^{63}-linked polyubiquitinylated and monoubiquitinylated proteins but not free ubiquitin (Table 2-9).

Stock solutions and buffers:

1.5 M Tris-HCl (pH 8.8): 18.17g Tris base (Sigma-Aldrich); 60 ml ddH_2O, adjust to pH 8.8 with HCl, bring total volume to 100 ml with ddH_2O, store at 4 °C.

0.5 M Tris-HCl (pH 6.8): 6g Tris base (Sigma-Aldrich); 60ml ddH_2O, adjust to pH 6.8 with HCl, bring total volume to 100 ml with ddH_2O, store at 4 °C.

10% (w/v) SDS: 10 g SDS (Sigma-Aldrich) was dissolved in 90 ml ddH_2O with gentle stirring and bring to 100 ml with ddH_2O, store at room temperature.

10% (w/v) APS (fresh daily): 100 mg ammonium persulfate (APS, Sigma-Aldrich) was dissolved in 1 ml ddH_2O, aliquoted and store at -20 °C.

10× Running Buffer: 30.3 g Tris base (Sigma-Aldrich); 144.0 g Glycin (Sigma-Aldrich); 10.0 g SDS (Sigma-Aldrich), dissolve and bring total volume to 1 liter with ddH_2O, do not adjust pH with acid or base, store at 4 °C.

10× Transfer Buffer: 30.3 g Tris base (Sigma-Aldrich); 144.0 g Glycin (Sigma-Aldrich), dissolve and bring total volume to 1 liter with ddH_2O, store at 4 °C.

1× Transfer Buffer: Dilute 100 ml 10× Transfer buffer with 200 ml Methanol and 700 ml ddH_2O, prechill the buffer before use.

10× TBS (pH 7.6): 24.2g Tris base (Sigma-Aldrich), 80g NaCl (Sigma-Aldrich), adjust to pH 7.6 with HCl and bring total volume to 1 liter with ddH_2O.

TBS-T: Dilute 100 ml 10× TBS with 900 ml ddH_2O, add 1 ml Tween 20 (0.1%, Sigma-Aldrich).

2.4.4 Electrophoretic mobility shift assay (EMSA)

DNA-protein interactions were evaluated by using Odyssey Infrared EMSA Kit (LI-COR Biosciences) according to the manufacturer. The double stranded oligonucleotides were used as probe (Table 2-10)

Table 2-10: Oligonucleotide probes for EMSA

Name	Probe forward (5'-3')	Probe reverse (3'-5')
NF-κB/Rel	AGTTGAGGGGACTTTCCCAGGC	TCAACTCCCCTGAAAGGGTCCG
NF-κB/p50 homodimers	GATCCACAGGGGGCTTTCCCTCCA	CTAGACCTCCCTTTCGGGGGACAC

2.4.5 Serum analyses

Blood was collected at harvesting and centrifuged at 10000 × g 15 min at 4 °C. Serum was stored at -80 °C until analyses.

2.4.5.1 Amylase (AMY)

Mouse serum was diluted 1:10 with 0.9% NaCl and amylase content was assessed by standard protocol (AMYL2, Cobas 8000)

2.4.5.2 Lipase (LIP)

Mouse serum was diluted 1:10 with 0.9% NaCl and lipase content was assessed by standard protocol (LIPC, Cobas 8000)

2.4.5.3 Alanine aminotransferase (ALT)

Mouse serum was diluted 1:10 with 0.9% NaCl and alanine aminotransferase content was assessed by standard protocol (GPT, Cobas 8000)

2.4.5.4 Alkaline phosphatase (ALP)

Mouse serum was diluted 1:10 with 0.9% NaCl and alkaline phosphatase content was assessed by standard protocol (ALP, Cobas 8000)

2.4.6 Assessment of pulmonary capillary permeability

Lung permeability was determined by injection of Evans blue dye (EBD; 20 ml/kg) in the right femoral artery 30 min before termination of the experiment to assess vascular leakage in the lung. After mice were sacrificed, the lung was flushed with 0.9% saline, removed, weighed, and pooled in a tube of formamide (2 ml/100 mg lung). The tube was incubated at 50 °C for 72 h. EBD was extracted, and relative EBD concentration in the supernatant (compared with the standard curve) was measured at 632 nm.

2.4.7 Lung myeloperoxidase (MPO) assay

Neutrophil sequestration in lung tissue was quantified by measuring tissue MPO activity. To minimize background MPO activity by remaining non-adherent intravascular blood cells, a needle was inserted into the beating right ventricle to perfuse the pulmonary circulation with ice-cold PBS until blanching of the lungs occurred. The entire lung was snap-frozen and stored at -80 °C until being homogenized on the day of assay in 50 mM phosphate buffer (pH 6.0) containing 0.5% hexadecylmethylammonium bromide (Sigma-Aldrich) and sonicated three times for 20 sec each time. The suspension was subjected to three cycles of freezing and thawing and was centrifuged at 4 °C for 10 min at 15,000 × g, and the resulting supernatant was assayed. The reaction mixture consisted of 200 µl of 10 mM PBS (pH 6.0), 100 µl of 0.22% guaiacol (Sigma-Aldrich), and 10 µl of the extracted enzyme. The reaction was started with 6 µl of H_2O_2 (0.1%). The increase in absorbance was monitored spectrophotometrically at 470 nm over 3 min, and the maximum slope of the curve was used to calculate the change in OD per minute (ΔOD/min). This absorbance was corrected for protein content of lung extracts, and results were expressed as activity per unit of protein content (ΔOD/min/mg).

2.4.8 Bronchoalveolar lavage fluid (BALF) analysis

Protein content, total cell counts were analyzed in BALF. Briefly, animals were killed by decerebration. The trachea was then exposed and intubated with a catheter. Between 1 and 3 repeated injections of PBS (0.8 ml) were given to harvest BALF through the catheter. Collected BALF was centrifuged at 300 × g for 10 min at 4 °C, and the supernatant was frozen at -80 °C for subsequent analysis of total protein count (Bio-Rad protein analysis kit) and inflammatory mediators. Cells in the pellet were resuspended in PBS for quantification.

2.5 Cell culture

2.5.1 Isolation of acinar cells

The following solutions were prepared before sacrificing mice:

Solution I: McCoy's Medium 5A (Sigma) with 0.1% BSA (Sigma) (e.g. 49.5 ml McCoy's Medium + 500 µl 10% BSA, sterile filtration)

Solution II: McCoy's Medium 5A (Sigma) with 0.1% BSA (Sigma) and 1.2 mg/ml Collagenase Type VIII (Sigma) (e.g. 10 ml Solution I + 12mg Collagenase, sterile filtration)

Culture Medium: DMEM + Ham's F12 (1:1) (Invitrogen) with 2 mM Glutamine (Invitrogen), 1% Penicillin/Streptomycin (Invitrogen) and 10% FCS (Invitrogen)

The mouse was sacrificed, blood was removed from portal vein and the pancreas was removed into cold sterile cell culture PBS (Invitrogen) in a petri dish. All further steps were performed in a sterile cell culture hood. The pancreas was washed twice with cold PBS, transferred into a new petri dish with 5 ml of Solution II and minced into small pieces with scalpel. The petri dish was kept in a 37 °C incubator for 10 min. The cell suspension was transferred into a 50 ml falcon tube, 10 ml of Solution I then was used to wash the petri dish and added to the cell suspension. Afterwards, the cell suspension was centrifuged at 300 × g for 5 min at room temperature. The pellet was resuspended in 5 ml of Solution II and incubated for 10 min at 37 °C. The cell suspension was filtered with a 70 µm strainer and the petri dish was washed with 10 ml of Solution I and filtered. The filtered cell suspension was resuspended in 20 ml of solution I and centrifuged again. The cell pellet was resuspended in Culture medium and incubated for at least 30 min at 37 °C.

2.5.2 Stimulation of acinar cells

Before isolating acinar cells for stimulation, the KRH working solution was prepared.

10× KRH stock solution: 5.96 g Hepes (Sigma), 6.078 g NaCl (Sigma), 0.14 g KH_2PO_4 (Sigma), 0.296 g $MgSO_4 \cdot 7H_2O$ (Sigma) were dissolved in 100 ml dH_2O.

100mM $CaCl_2$: 0.735 g $CaCl_2$ (Sigma) was dissolved in 50 ml dH_2O.

KRH working solution: 10 ml of the 10× KRH stock solution were mixed with 2 ml 100 mM $CaCl_2$; 1 ml MEM (Invitrogen) and 1ml of L-Glutamine (Invitrogen). The solution was adjusted to pH 7.4 and bring total volume to 100 ml with dH_2O. 45 mg Glucose (Sigma), 200 mg BSA

(Sigma) and 10 mg Trypsin-inhibitor were then added. The KRH working solution was mixed and filtered through a 45 µm sterile filter.

Acinar cells were isolated as previously described (2.5.1) but cells were suspended into KRH working solution instead of Culture medium and rested for at least 30 min at 37 °C before stimulation. Cells were stimulated with Cerulein (Sigma) at different concentrations for various time intervals.

2.5.3 Fluorescence-activated cell sorting (FACS)

FACS buffer was prepared before sacrificing mice.

FACS buffer: 5% FCS (Invitrogen) with 2 mM EDTA (Sigma) in PBS (Intrivogen)

Mouse was sacrificed, the pancreas, lung and spleen of mice were rapidly removed into a petri dish with ice-cold PBS. Single cells were prepared by digestion of different organs with Collagenase D (Roche) or not (Table 2-11). The cell suspension was filtered using a 70 µm cell strainer to eliminate the clumps and debris, and the Collagenase was then inactivated by adding 50 ml of FACS buffer. The cells were centrifuged at 300 × g for 5 min. The supernatant was discarded and the pellet was resuspended in 1 ml of red blood cell lysis buffer (RBC lysis buffer) (Sigma) to lyse erythrocyte. After shaken for 90 sec, the cells were filled up with 20 ml FACS buffer. The cell suspensions were centrifuged at 300 × g for 5 min and the pellet were resuspended in 1-5 ml FACS buffer for further staining.

Table 2-11: Digestion of different organs for FACS

Organ	Digestion solution	Temperature	Time
Pancreas	10 ml PBS + 12 mg collagenase D (Roche) + 1 mg trypsin inhibitor	37 °C	7-8 min
Lung	10 ml PBS + 12 mg collagenase (Roche)	37 °C	40 min
Spleen	Only mince and grind without any digestion	/	/

Single-cell suspensions of pancreatic cells were immunolabeled with fluorochrome-conjugated antibodies in FACS buffer. All antibodies were purchased from eBioscience (Table 2-12). At first, cell suspensions were pre-incubated with purified anti-mouse CD16/CD32 (0.5-1 µl per 100 µl cell suspension) for 20 minutes on ice prior to staining for blocking non-specific Fc-mediated interactions. Fluorochrome-conjugated antibodies were added into the cell suspensions (1 µl per 100 µl cell suspension) and incubated for at least 30 min in the dark on ice or at 4 °C. Cell suspensions were washed with FACS buffer and centrifuged at 300-400 × g for 5 min at 4 °C (twice). Stained cells were resuspended in FACS buffer, and stained with propidium iodide (PI, BD Biosciences) to assess viability. Flow cytometry analysis was performed on a Gallios flow cytometer (Beckman coulter) after gating and excluding dead cells. Data were analyzed using FlowJo software.

Table 2-12: The antibodies for FACS

Antibody	Company	Product number
Anti-Mouse CD16/CD32	eBioscience	14-0161-85
Anti-Mouse CD45 eFluor® 450	eBioscience	48-0451-82
Anti-Mouse CD19 FITC	eBioscience	11-0193-82
Anti-Mouse CD3e PE	eBioscience	12-0031-81
Anti-Mouse CD4 APC	Biolegend	100411
Anti-Mouse CD8 PerCP	Novus Biologicals	1-50069
Anti-Mouse CD11b APC-eFluor® 780	eBioscience	47-0112-82
Anti-Mouse CD11c PerCP	Biolegend	117325
Anti-Mouse F4/80 Antigen APC	eBioscience	17-4801-80
Anti-Mouse Ly-6G and Ly-6C (Gr-1) PE	BD Biosciences	553128

2.5.4 Isolation of bone marrow and differentiation of bone marrow-derived myeloid cells (BMDM)

The mouse was sacrificed and the femur and tibia were separated by cutting at knee joint. All further steps were performed in a sterile cell culture hood. Bone marrow was flushed into a petri dish from bone marrow cavity with ice-cold sterile cell culture PBS (Invitrogen) using syringe and needle. Bone marrow was pipetted up and down to bring the cells into a single-cell suspension. The supernatant was taken and centrifuged at 300-400 × g for 5 min at 4 °C after cell suspension was sit for 5 min. Pellet was washed with 10 ml RPMI medium (Gibco, + 10% FCS + 1% PS), centrifuged at 300-400 × g for 5 min at 4 °C. Pellet was resuspended in 20 ml RPMI medium (Gibco, + 15% FCS + 20% M-CSF + 5% Horse serum + 1% PS). 2 ml cells with 8 ml RPMI medium were distributed into each cell culture dish and cultured for 7 days. The growth and adherence of the cells were checked and the medium was changed at 4th day. The differentiated bone marrow-derived myeloid cells were harvested for further stimulation and experiments 7 days later.

2.5.5 Bone marrow transplantation

6-7 week-old recipient animals were treated with acidified water (pH 2.0) ad libitum containing 100 mg/L neomycin and 10 mg/ml polymyxin B sulfate (Sigma-Aldrich) for 10 days before and until 2 weeks after lethal irradiation. Mice were irradiated (9 Gray) with a cesium γ source, followed by bone marrow transplantation 4 h later. Bone marrow cells were prepared from the bilateral tibia and femur bones of donor mice by flushing the bones with RPMI 1640 medium (Gibco, Grand Island, NY) containing 2% fetal bovine serum, 5 units/ml heparin, penicillin and streptomycin. Cells were filtered through a 40 µm strainer, counted, and resuspended in serum-free RPMI (pH 7.4) containing 20 mM Hepes, penicillin and streptomycin. Recipient

animals received 5×10^6 bone marrow cells in 0.5 ml of bone marrow transplantation medium by tail vein injection. The animals were induced AP and sacrificed 4 weeks after transplantation.

2.6 Statistical analyses

Data are presented as average ± standard deviation (SD). Parameters for the groups were compared by Mann-Whitney test or two-sided Student's t-test as appropriate. For the overall survival analysis, Kaplan-Meier curves were analyzed by log rank test. In all cases, sample sizes were chosen to produce statistically unambiguous results. *P value* less than 0.05 was considered significant.

For SNPs, the significance of the differences between variant frequencies in affected individuals and controls were tested by two-tailed Chi-square test and logistic regression analyses using SPSS (v22.0). A dominant model, defined as CC vs. CT+TT, was utilized for calculations and p-values less than 0.05 was considered to be of statistical significance. In addition, calculations were performed following a recessive model (CC+CT vs. TT). The first allele in the variant description was used as the major allele.

3 Results

3.1 Bcl-3 is upregulated in human and murine AP and determines severity of inflammation

Sterile inflammation typically occurs during the onset of AP and can escalate to the systemic inflammatory response syndrome (SIRS) with high morbidity and mortality. Activation of proinflammatory transcription factors regulating numerous chemokines and cytokines is well established in AP. Particularly, the IKK/NF-κB pathway has been shown to be linked to the course of the disease. Substantial data on the mechanisms driving the excessive stimulation of the immune system are available, whereas little is known about the mechanisms that limit sterile inflammation. Unlike other classical IκB family members, Bcl-3 is believed to play a critical role in counter-regulating inflammatory responses through limiting the transcription of NF-κB-dependent genes. Its role in sterile inflammation remains unclear so far.

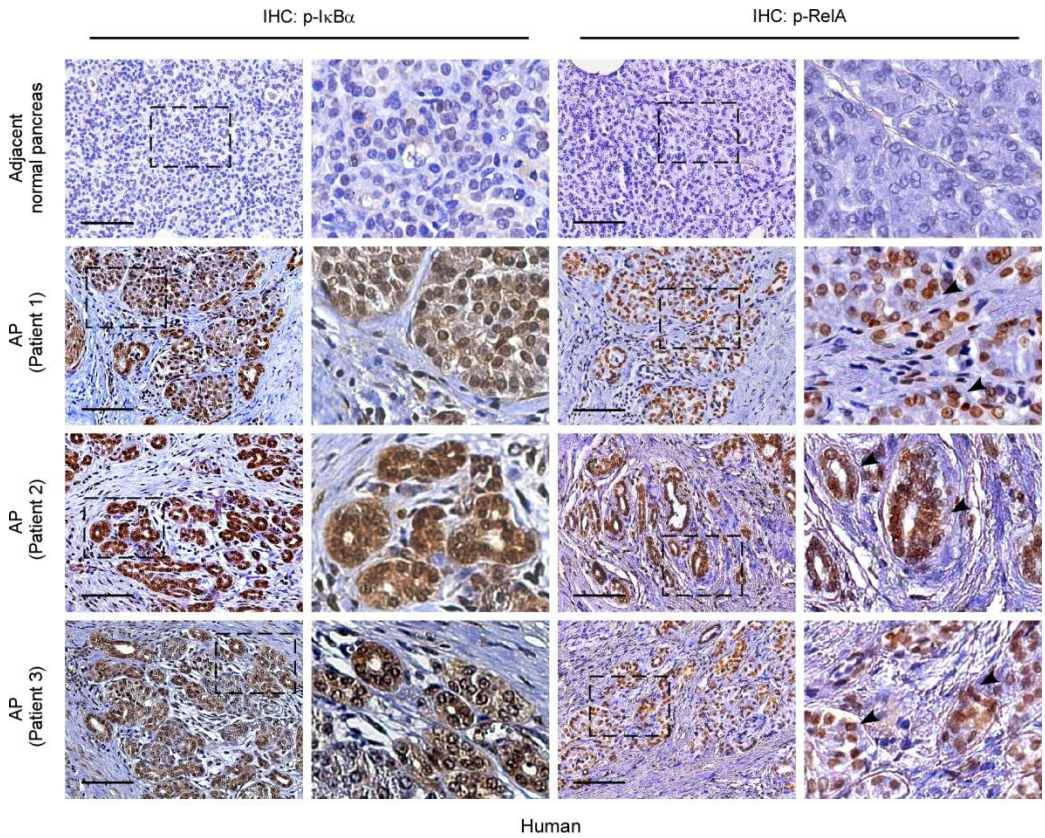

Figure 3-1: NF-κB pathway is activated in human specimens of AP. Immunohistochemical staining of p-IκBα and p-RelA in human paraffin-embedded pancreatic sections from 3 different patients with AP. Note the activation of RelA and IκBα in areas of pancreatic damage. Scale bars equal 50 µm. Boxed regions are shown at higher magnification on the right (enlarged × 3).

We initially analyzed the activation of NF-κB pathway in the pancreas by IHC staining of human specimens in AP, strong phosphorylation of RelA and IκBα were observed in the area of pancreatic damage in contrast to adjacent normal tissue (Figure 3-1) as previously published[102]. All 3 cases of human AP also showed accumulation of Bcl-3-containing aggregates in areas of pancreatic damage (Figure 3-2 A).

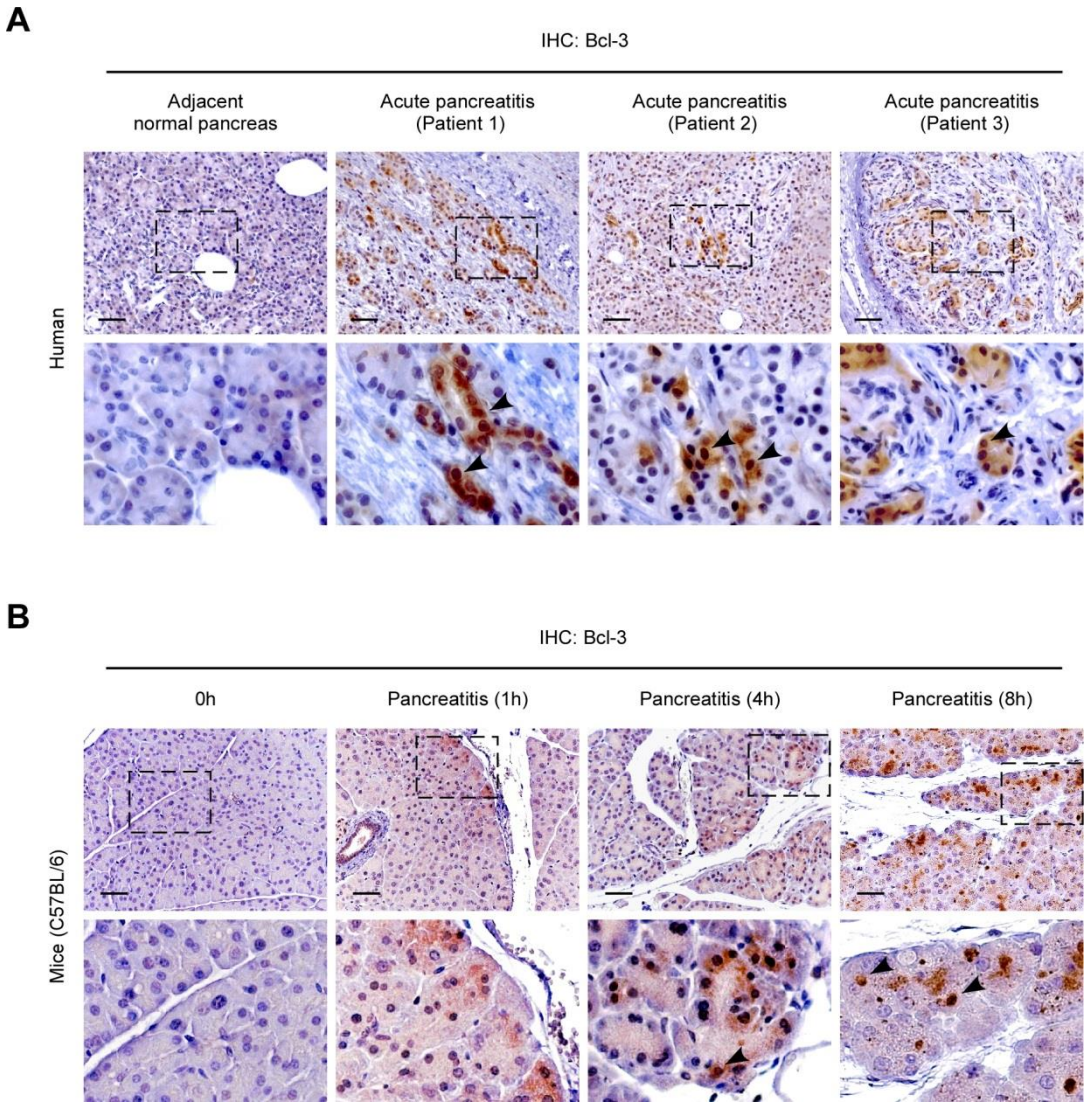

Figure 3-2: Bcl-3 is upregulated in human specimens of AP and cerulein-induced experimental AP in mice. (**A**) Immunohistochemical staining of Bcl-3 in human paraffin-embedded pancreatic sections from 3 different patients with AP. (**B**) Immunohistochemical staining of Bcl-3 in pancreatic tissue of C57BL/6 mice undergoing cerulein-induced AP. Note the upregulation of Bcl-3 (arrowheads) in areas of pancreatic damage. Scale bars equal 50µm. Boxed regions are shown at higher magnification below (enlarged × 3).

These findings were replicated in the cerulein model of AP (Figure 3-2 B). Prior to the injection of cerulein in mice, little Bcl-3 was detected in the pancreas. While administration of cerulein increased Bcl-3 expression after an initial delay, reaching maximal induction by 8h (Figure 3-3 A and B). Furthermore, exocrine pancreatic acini, which consist more than 80% of

gland, were isolated and incubated with 100nM cerulein *in vitro*, Bcl-3 level was shown to increase over a time course after cerulein treatment (Figure 3-3 C).

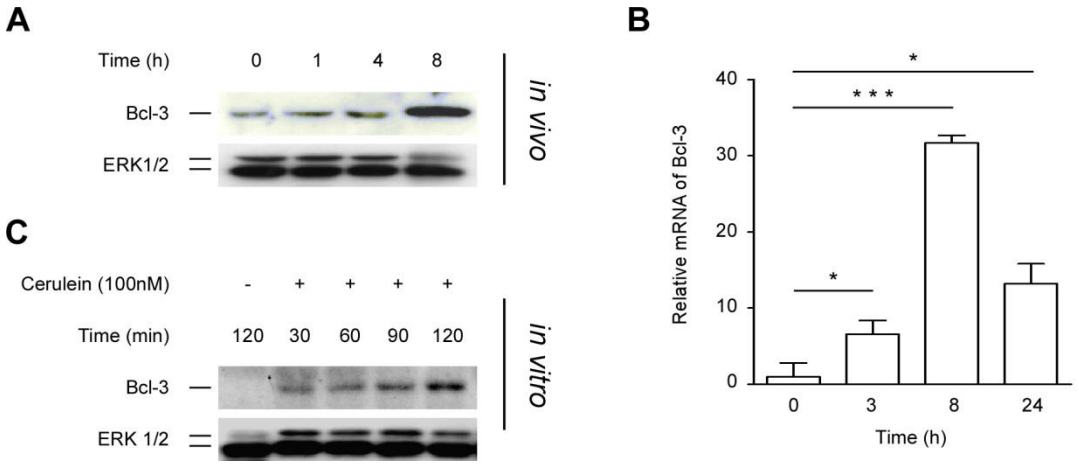

Figure 3-3: (**A**) Pancreata from C57BL/6 mice during AP were harvested and homogenized to detect Bcl-3 by Western blot. Extracellular-signal-regulated kinase (ERK) 1/2 served as loading control (representative blot, n=3). (**B**) mRNA of Bcl-3 was quantified by real-time PCR in pancreatic tissue. Fold change values were normalized to *cyclophilin* mRNA (n=4). (**C**) Isolated primary acinar cells were stimulated with cerulein (100nM), and homogenized at indicated time points to detect Bcl-3 by western blotting. ERK1/2 served as loading control (representative blot, n=3). Values represent mean ± SD. **P* < .05, ***P* < .01, and ****P* < .001.

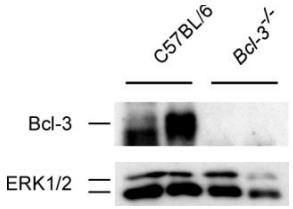

Figure 3-4: Pancreatic tissue from C57BL/6 and *Bcl-3*$^{-/-}$ mice was isolated and homogenized to detect Bcl-3. ERK 1/2 served as a loading control. Note that expression of Bcl-3 is deleted completely in *Bcl-3*$^{-/-}$ offspring (representative blot, n=3 per time point).

To scrutinize the role of Bcl-3 in this setting we utilized the Bcl-3 deficient mouse line (Figure 3-4). At 8 hours after cerulein injection in both C57BL/6 and *Bcl-3*$^{-/-}$ mice, acute inflammatory cells have infiltrated the pancreatic parenchyma, attacking acini, ducts, and islets. Moreover, patchy necrosis and diffuse interstitial edema were emerged typically in pancreatic tissue. Histologic analysis in *Bcl-3*$^{-/-}$ mice revealed a significant more severe form of pancreatic damage compared to C57BL/6 mice, including a significantly increased area of necrosis and edema (Figure 3-5 B and C), as well as higher level of amylase secretion into the serum (Figure 3-5 D). Increased amylase concentration in serum is obtained as a biochemical marker for AP.

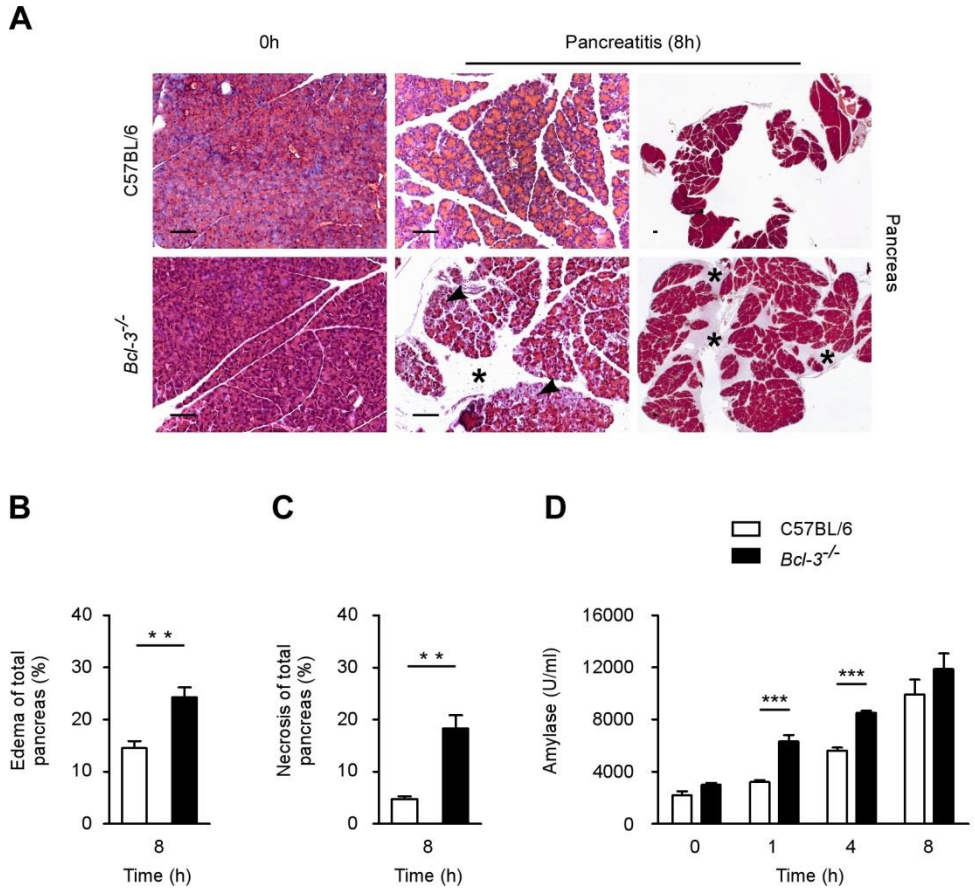

Figure 3-5: Bcl-3 deficiency deteriorates local pancreatic damage. (**A**) Pancreatic tissue of cerulein-injected C57BL/6 and *Bcl-3*$^{-/-}$ mice were analyzed at the indicated time point by H&E staining. Note the increased edema (asterisks) and necrosis (arrowheads) in *Bcl-3*$^{-/-}$ mice. (**B** and **C**) Sections were analyzed to evaluate edema and necrosis in relation to total pancreatic area (n=5). (**D**) Serum amylase levels were measured (n=6). Note the significantly higher release of amylase into the serum of *Bcl-3*$^{-/-}$ mice compare with C57BL/6 mice. Values represent mean ± SD. **P* < .05, ***P* < .01, and ****P* < .001. Scale bars equal 50µm.

In the absence of Bcl-3, acute lung injury seem to be increased as showed more alveolar collapse and wall thickening in the lung, suggesting that Bcl-3 also influences systemic complications in addition to the local damage (Figure 3-6 A). The extent of pulmonary damage was further emphasized by significantly higher degree of MPO activity, which is an index of leukocytes accumulation in the lung, in *Bcl-3*$^{-/-}$ mice 8 and 72 hours after the onset of AP (Figure 3-6 B). Pulmonary damage caused by acute lung injury is also characterized by increased alveolar permeability. Therefore we measured extravasation of evans blue dye from the circulation to the alveoli to evaluate the extent of alveolar permeability. Our data showed that Bcl-3 deficiency led to increased alveolar permeability (Figure 3-6 C). In line with this observation, cellular content in bronchoalveolar lavage fluid of *Bcl-3*$^{-/-}$ mice were also elevated over time (Figure 3-6 D and E). Increased acute lung injury in Bcl-3 deficient mice led to lower survival percentage compared to wild-type mice undergoing severe AP through injecting mice for 5 consecutive days (Figure 3-6 F).

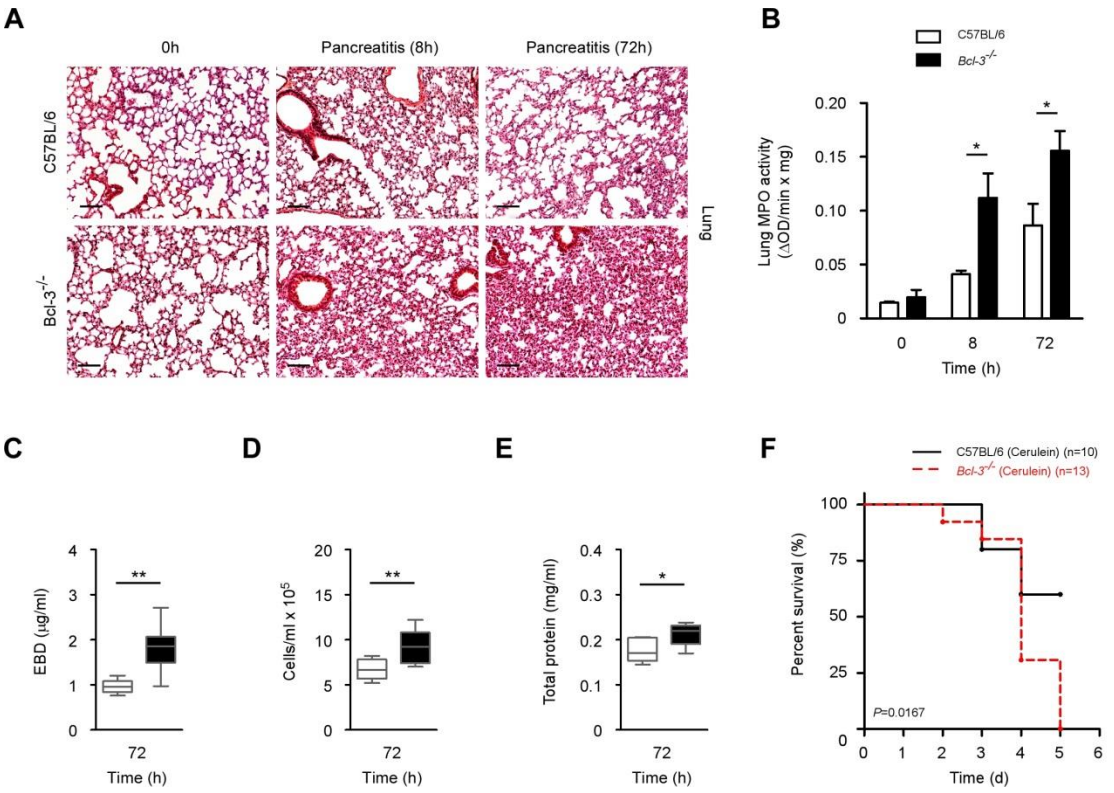

Figure 3-6: (**A**) Morphological analysis of representative H&E staining revealed more alveolar collapse and wall thickening in the lung of *Bcl-3*$^{-/-}$ mice. (**B**) Lung tissues were removed to measure MPO activity (n=6). (**C**) Lung permeability, determined by injection of EBD in the tail vein and measurement of dye concentration in lung tissue at 72 hours (n=4). (**D** and **E**) Total cell count and total protein concentration were measured in bronchoalveolar lavage fluid (BALF) taken from C57BL/6 and *Bcl-3*$^{-/-}$ mice at 72 hours. (**F**) Kaplan-Meier curves of C57BL/6 (black, n=10) and *Bcl-3*$^{-/-}$ (red, n=13) mice during SAP. Values represent mean ± SD. **P* < .05, ***P* < .01, and ****P* < .001. Scale bars equal 50µm.

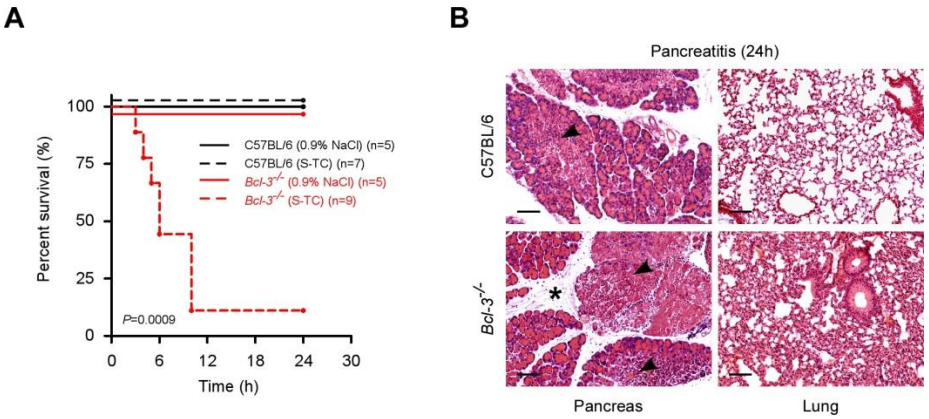

Figure 3-7: (**A**) Kaplan-Meier curves of C57BL/6 (black dashed line, n=7) and *Bcl-3*$^{-/-}$ (red dashed line, n=9) mice during sodium taurocholate (ST-C)-induced pancreatitis. Retrograde pancreatic duct infusion of 0.9% NaCl into C57BL/6 (black line, n=5) and *Bcl-3*$^{-/-}$ (red line, n=5) mice were used as control. (**B**) Alive mice were evaluated 24 hours after operation. Pancreata and lungs were removed for morphological analysis by H&E. Note the appearance of focal necrosis (arrowheads) in the pancreata of both groups. Scale bars equal 50µm.

To rule out model specific effects, we took advantage of a further mouse model of AP. Retrograde infusion of sodium taurocholate via pancreatic duct results in severe necrotizing AP.[51] Even in this model, lethality was dramatically increased in *Bcl-3*$^{-/-}$ mice. 8 out of 9 *Bcl-3*$^{-/-}$ mice died 10 hours after operation, while all C57BL/6 mice survived (Figure 3-7 A). Increased pancreatic necrosis as well as more pulmonary alveolar collapse and wall thickening were displayed in *Bcl-3*$^{-/-}$ mouse compared with C57BL/6 mice at 24h (Figure 3-7 B).
Thus, our data do not only demonstrate an upregulation of Bcl-3 in human and murine AP. Using AP as a model disease, our genetic data place Bcl-3 in a central position during sterile inflammation.

3.2 Bcl-3 restrains the development of PSC in *Mdr2*$^{-/-}$ mice

Disruption of barrier function and toxic injury to liver cells appear to be involved in the pathogenesis of a variety of liver diseases such as PSC. This results in a prolonged sterile inflammation finally leading to liver fibrosis, liver cirrhosis and cholangiocellular carcinoma. Mechanisms driving this sterile inflammation remained unclear so far. To rule out organ- and disease-specific effects of Bcl-3 on sterile inflammation, we took advantage of a further mouse model. Mice lacking the Abcb4 protein encoded by Mdr2 (*Mdr2*$^{-/-}$) develop chronic periductular sterile inflammation and cholestatic liver disease reminiscient of PSC. We used this mouse line to analyze the role of Bcl-3 in this setting generating double-mutant mice (*Bcl-3*$^{-/-}$*/Mdr2*$^{-/-}$).

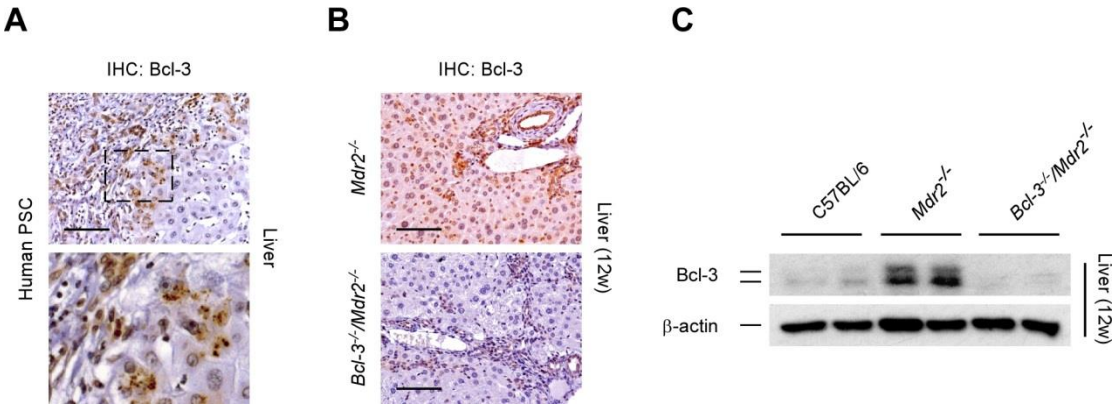

Figure 3-8: (**A**) Immunohistochemical staining of Bcl-3 in human paraffin-embedded liver sections from patients with PSC. Note the Bcl-3 positive cells in liver. Boxed regions are shown at higher magnification below (enlarged × 3). (**B**) Immunohistochemical staining of Bcl-3 in liver tissue of *Mdr2*$^{-/-}$ and *Bcl-3*$^{-/-}$*/Mdr2*$^{-/-}$ mice. (**C**) Immunoblot detection of Bcl-3 in liver tissue. β-actin served as a loading control (representative blot, n=3). Scale bars equal 50µm.

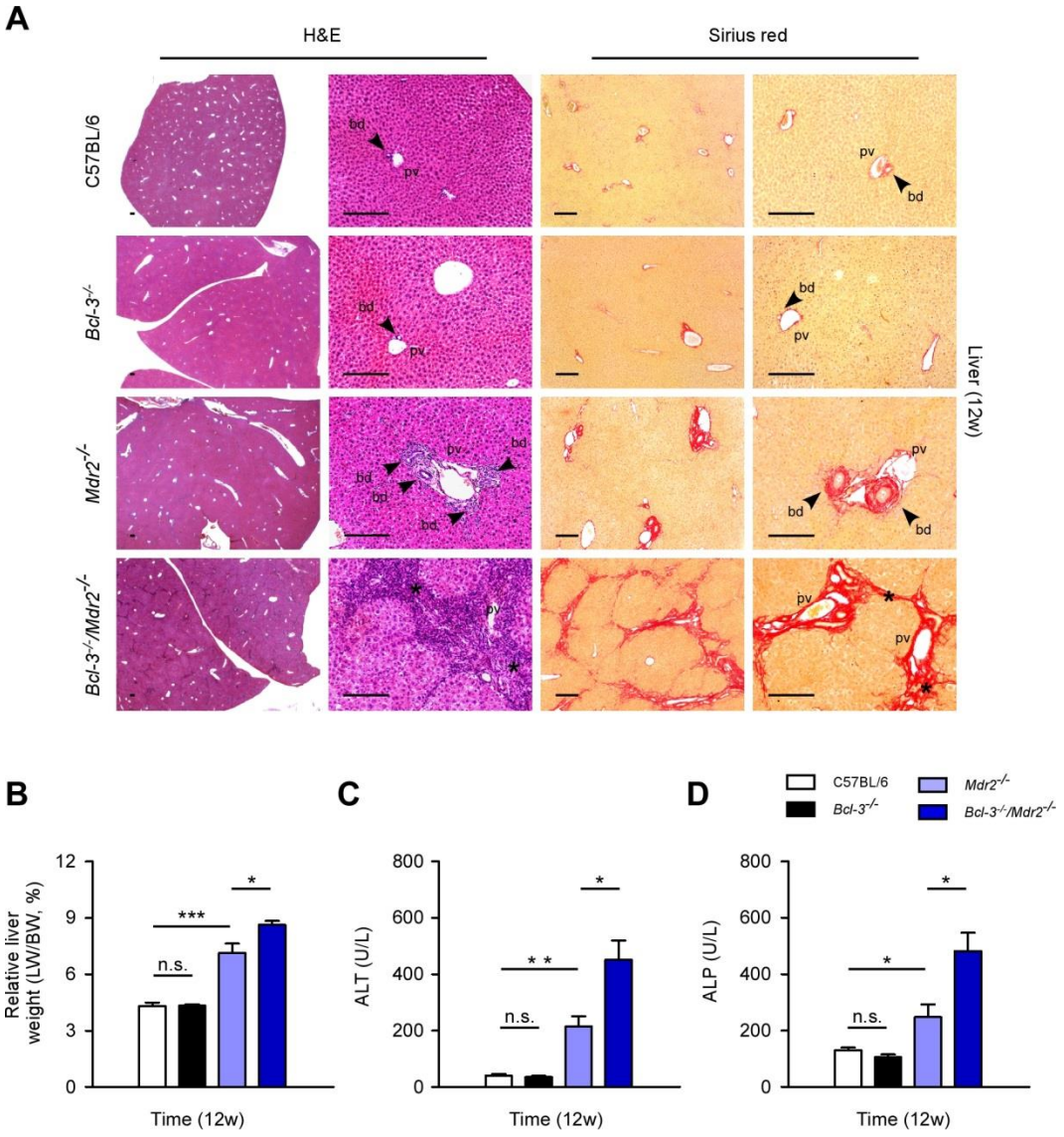

Figure 3-9: Bcl-3 plays beneficial effects on cholestatic phenotype and biliary fibrosis in *Mdr2*$^{-/-}$ mice. (**A**) Histologic sections of H&E- and Sirius red- stained hepatic tissue of 12-week-old C57BL/6, *Bcl-3*$^{-/-}$, *Mdr2*$^{-/-}$ and *Bcl-3*$^{-/-}$*/Mdr2*$^{-/-}$ mice were analyzed. Note the increased proliferation of ductule (arrowheads) in *Mdr2*$^{-/-}$ mice, septal formation and massive matrix deposition (asterisks) in *Bcl-3*$^{-/-}$*/Mdr2*$^{-/-}$ mice. (**B**) Liver weight (LW) to body weight (BW) ratio was calculated (LW/BW). (**C** and **D**) Serum alanine aminotransferase (ALT) (**C**) and alkaline phosphatase (ALP) (**D**) levels were measured in 4 serial groups (n=3). Values represent mean ± SD. **P* < .05, ***P* < .01, and ****P* < .001. Scale bars equal 100µm. bd, bile duct, pv, portal vein.

Human specimens of PSC and *Mdr2*$^{-/-}$ mice reveal high expression levels of Bcl-3 suggesting a role of this protein not only in this model, but also in human specimens of PSC analysis (Figure 3-8 A and B). Loss of Bcl-3 in double mutant mice was confirmed by IHC and Western blot analysis (Figure 3-8 B and C). *Mdr2*$^{-/-}$ mice developed the periportal fibrosis which characterized by the typical onion skin-like matrix formation around the bile ducts compared with wild-type mice,[103] while double mutant mice exhibited increased bile duct damage and periductal fibrosis with septal formation and massive matrix deposition (Figure 3-9 A). In addition, relative liver weight (LW/BW ratio), serum biochemical parameters of liver injury

(alanine aminotransferase, ALT) and cholestasis (alkaline phosphatase, ALP) were more profoundly increased in *Bcl-3*$^{-/-}$*/Mdr2*$^{-/-}$ mice versus the *Mdr2*$^{-/-}$ mice, but not different between *Bcl-3*$^{-/-}$ and control wild-type mice (Figure 3-9 B, C and D).

IHC of cytokeratin 19 (CK19), a marker of bile duct epithelial cells in the liver, revealed the pronounced expansion and hyperproliferation of biliary epithelial cells in *Bcl-3*$^{-/-}$*/Mdr2*$^{-/-}$ mice compared with *Mdr2*$^{-/-}$ mice. Since hepatocellular proliferation is a consequence of liver damage, we next studied hepatocellular proliferation by IHC staining for the proliferation marker Ki67. *Bcl-3*$^{-/-}$*/Mdr2*$^{-/-}$ mice showed increased amount of Ki67-positive hepatocytes compared with *Mdr2*$^{-/-}$ mice (Figure 3-10). These data demonstrated beneficial effects of Bcl-3 on the phenotype of liver damage and cholestasis in *Mdr2*$^{-/-}$ mice suggesting a protective effect of Bcl-3 in sterile inflammation across organs.

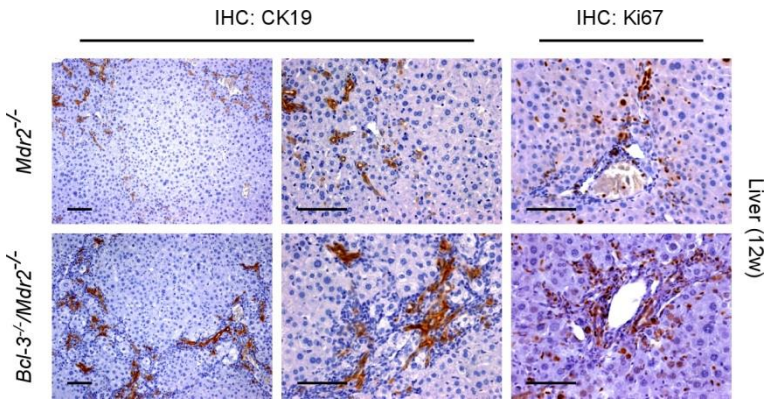

Figure 3-10: Immunohistochemical staining of CK19 and Ki67 in liver tissue of *Mdr2*$^{-/-}$ and *Bcl-3*$^{-/-}$*/Mdr2*$^{-/-}$ mice. Scale bars equal 50µm.

3.3 Bcl-3 in epithelial but not myeloid cells is required to control the inflammatory response during AP

Having established the role of Bcl-3 in sterile inflammation using various models, we next wished to elaborate the underlying mechanisms. In contrast to the *Mdr2*$^{-/-}$ model of chronic sterile inflammation, AP allows time-dependent analysis of inflammation. Therefore, we focused on AP to scrutinize the Bcl-3 dependent effects. To test whether the loss of Bcl-3 affects inflammation and modifies the infiltration of immune cells, we phenotyped the inflammatory pattern during AP *in vivo*. Immunohistochemical analysis confirmed a clear trend toward higher numbers of F4/80+ cells in *Bcl-3*$^{-/-}$ mice compared to control animals, suggesting that more macrophages (MΦ) were infiltrated into the pancreas of Bcl-3-deficient mice during AP (Figure 3-11 A), the degree of which might be an important determinant of severity of the AP. To evaluate the recruitment leukocytes in detail, Fluorescence-activated cell sorting (FACS) were performed between *Bcl-3*$^{-/-}$ and C57BL/6 mice. Not only confirming augmented macrophages infiltration, our data also showed recruitment of CD11b+Gr-1+

myeloid-derived suppressor cells (MDSC), CD11c+ dendritic cells (DC) and Gr-1+ granulocytes were enhanced in *Bcl-3*$^{-/-}$ mice 24 hours after the onset of AP, while the percentage of these leukocyte populations were kept stable in the spleen between C57BL/6 and *Bcl-3*$^{-/-}$ mice (Figure 3-11 B).

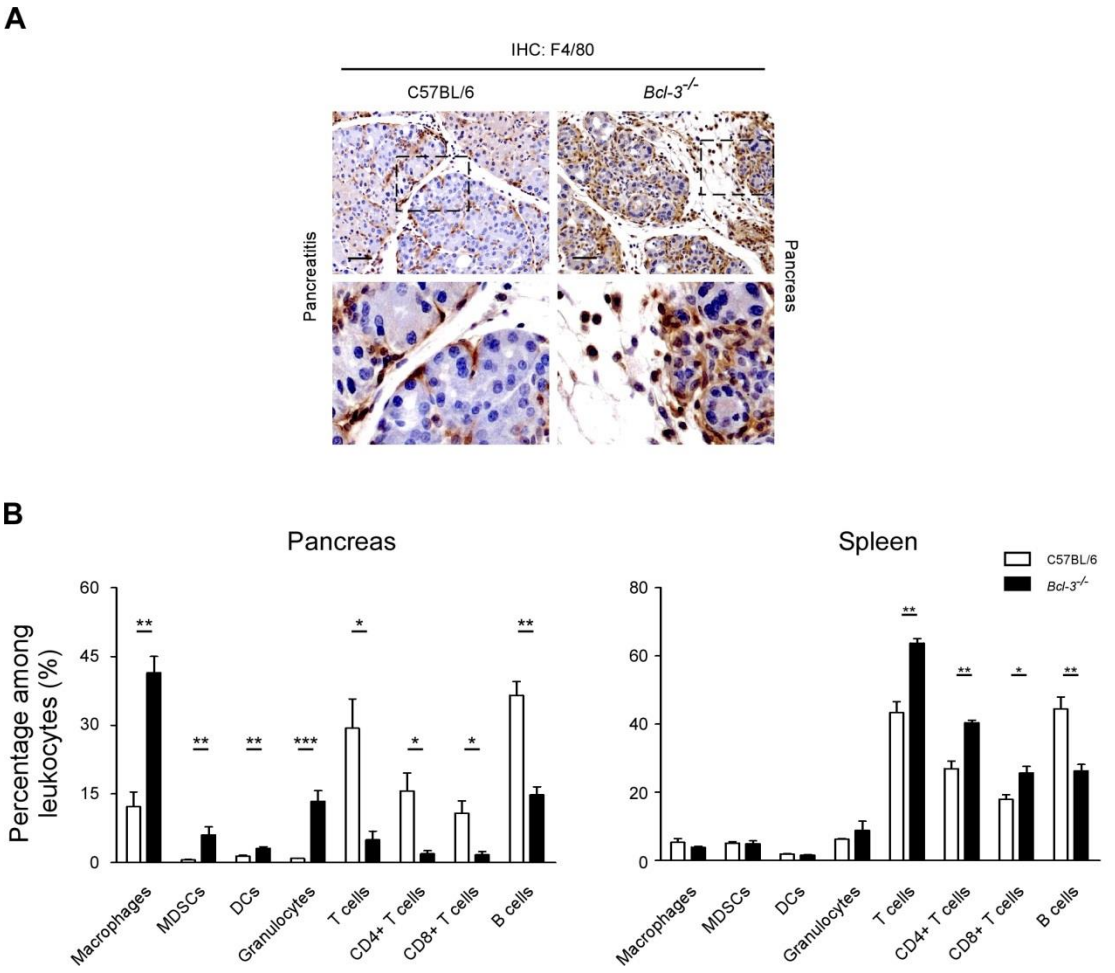

Figure 3-11: (**A**) Immunohistochemical detection of F4/80 during pancreatitis. Note the increase of F4/80 positive cells in *Bcl-3*$^{-/-}$ mice. Boxed regions are shown at higher magnification below (enlarged × 3). (**B**) Pancreatic and splenic leukocytes in C57BL/6 and *Bcl-3*$^{-/-}$ mice were assayed for surface marker expression, including CD45+CD3+ (T cells), CD45+CD3+CD4+ (CD4+ T cells), CD45+CD3+CD8+ (CD8+ T cells), CD45+CD19+ (B cells), CD45+CD11b+F4/80+ (macrophages, MΦ), CD45+CD11b+Gr-1+ (myeloid-derived suppressor cells, MDSC), CD45+CD11c+ (dendritic cells, DC), CD45+Gr-1+ (granulocytes) at 24 hours by fluorescence-activated cell sorting (FACS) (n=3) . Values represent mean ± SD. **P* < .05, ***P* < .01, and ****P* < .001. Scale bars equal 25 µm.

So far, a number of research strongly implied that the release of proinflammatory mediators by acinar cells and the recruitment of leukocytes are crucial events in influencing the ultimate severity of the disease.[39,104–107] To examine the levels of proinflammatory factors, Q-PCR was performed with pancreatic tissues of AP between C57BL/6 and *Bcl-3*$^{-/-}$ mice. Intrapancreatic transcription of cytokines and chemokines involved in AP, such as IL-6, chemokine (C-X-C motif) ligand 1 (CXCL1), monocyte chemoattractant protein-1(MCP-1), macrophage inflammatory protein 1 Alpha (MIP-1α), occurs as soon as 1h after induction of experimental

AP, and the levels of them were higher in mice with Bcl-3 deletion than they were in C57BL/6 mice (Figure 3-12 A). This observation was further confirmed by experiment *in vitro*. Q-PCR analyses showed that the production of these proinflammatory factors was also dramatically elevated in *Bcl-3*$^{-/-}$ acini compared to C57BL/6 acini upon cerulein challenge (Figure 3-12 B).

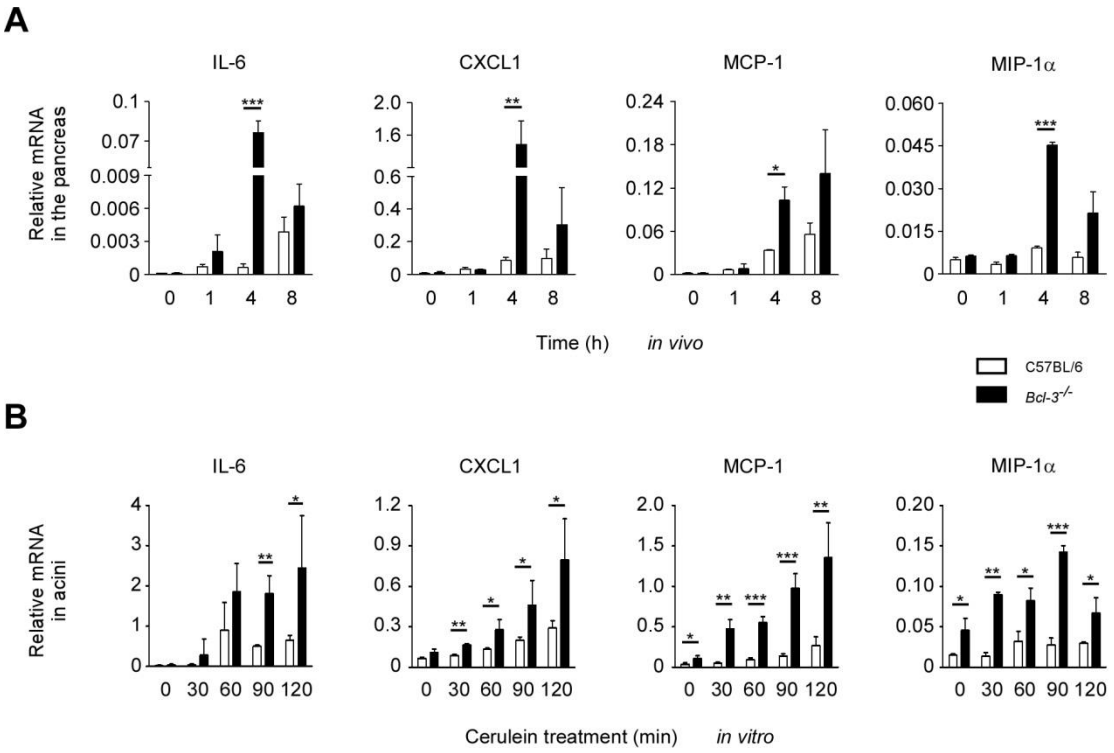

Figure 3-12: (**A**) mRNA of different cytokines and chemokines were quantified by Q-PCR in pancreatic tissues of C57BL/6 and *Bcl-3*$^{-/-}$ mice at indicated time points (n=4). (**B**) Isolated acinar cells were stimulated with cerulein (100nM), and mRNA of different cytokines and chemokines were quantified by Q-PCR. Relative values were normalized to cyclophilin mRNA. (n=4). Values represent mean ± SD. **P* < .05, ***P* < .01, and ****P* < .001.

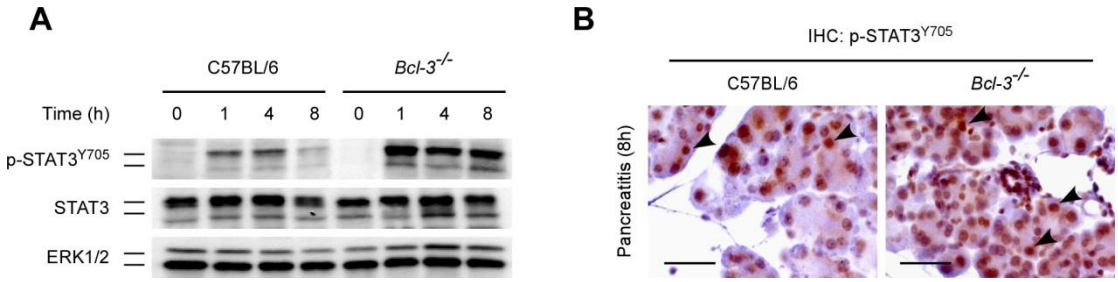

Figure 3-13: (**A**) Pancreatic tissue was isolated at the indicated times and homogenized to detect p-STAT3^{Y705} and STAT3. ERK1/2 served as a loading control (representative blot, n=3 per time point). (**B**) Immunohistochemical detection of p-STAT3^{Y705} during pancreatitis. Note the increase of p-STAT3^{Y705} positive cells in *Bcl-3*$^{-/-}$ mice (arrowheads). Scale bars equal 25 µm.

Because IL-6, as a reliable marker for AP severity, also exerts its proinflammatory effects though the JAK-2/STAT3 pathway activation in AP,[47] we next examined whether STAT3

activation depends on Bcl-3. Activation of STAT3 was clearly enhanced in *Bcl-3*$^{-/-}$ mice compare with C57BL/6 mice, normal STAT3 was not changed between two groups (Figure 3-13 A). These findings were supported by IHC, which demonstrated augment of p-STAT3^{Y705} in acinar cells of *Bcl-3*$^{-/-}$ mice (Figure 3-13 B). Trypsin activity, which is considered a key event in the onset of AP, remained unchanged in both mouse lines (data not shown).

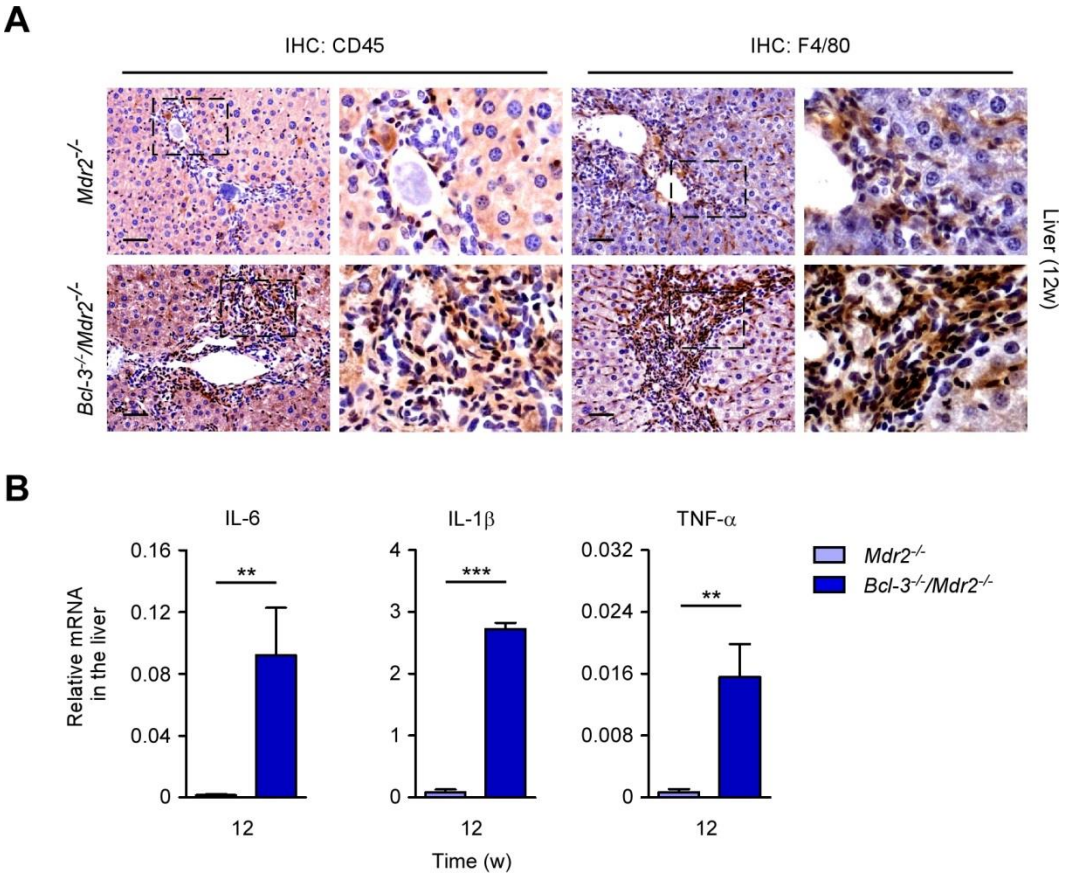

Figure 3-14: Increased recruitment of immune cells in *Bcl-3*$^{-/-}$*/Mdr2*$^{-/-}$ mice. (**A**) Immunohistochemical detection of CD45 and F4/80 in *Mdr2*$^{-/-}$ and *Bcl-3*$^{-/-}$*/Mdr2*$^{-/-}$ mice. Boxed regions are shown at higher magnification on the right (enlarged × 3). (**B**) mRNA of different cytokines were quantified by Q-PCR in hepatic tissues of *Mdr2*$^{-/-}$ and *Bcl-3*$^{-/-}$*/Mdr2*$^{-/-}$ mice. Relative values were normalized to cyclophilin mRNA (n=4). Values represent mean ± SD. **P* < .05, ***P* < .01, and ****P* < .001. Scale bars equal 25µm.

Analysis of liver from *Bcl-3*$^{-/-}$*/Mdr2*$^{-/-}$ mice also showed strong infiltration of leukocytes, particularly macrophages in the portal areas (Figure 3-14 A) and higher expression of cytokines, including IL-6, IL-1β, and TNF-α (Figure 3-14 B) compared with *Mdr2*$^{-/-}$ mice.

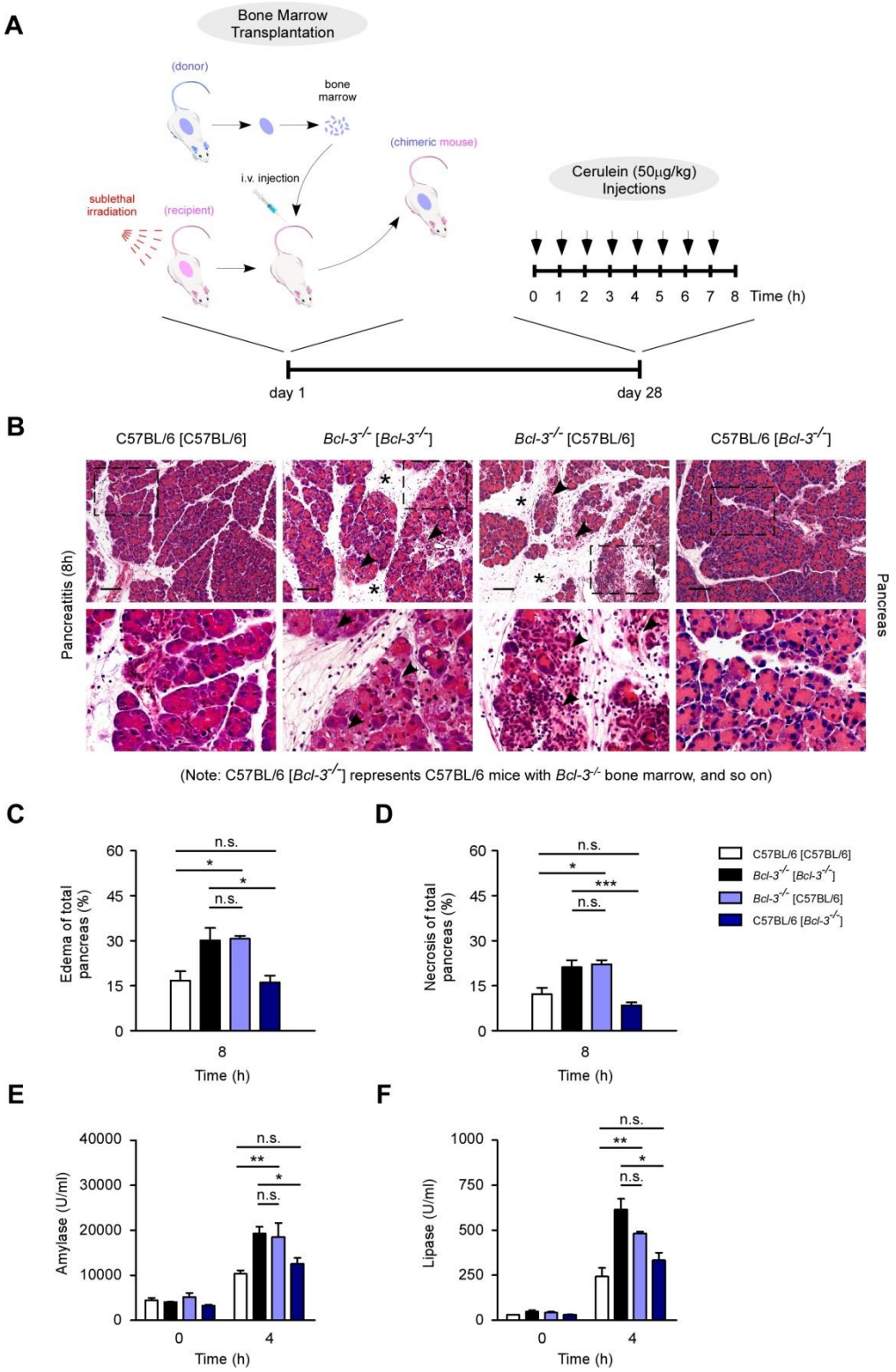

Figure 3-15: (**A**) Schematic diagram of bone marrow transplantation. (**B**) Morphological analysis of representative H&E stains revealed more severe pancreatic damage, including more edema (asterisks), necrosis (black arrowheads) in *Bcl-3*$^{-/-}$ mice in despite of bone marrow. C57BL/6 [*Bcl-3*$^{-/-}$] represents C57BL/6 mice with *Bcl-3*$^{-/-}$ bone marrow, and so on. Boxed regions are shown at higher magnification below (enlarged × 3). (**C** and **D**) Sections were analyzed to evaluate edema (**C**) and necrosis (**D**) in relation to total pancreatic area (n=4). (**E** and **F**) Serum amylase (**E**) and lipase (**F**) levels were measured in control and chimeric animals (n=6). Values represent mean ± SD. **P* < .05, ***P* < .01, and ****P* < .001. Scale bars equal 50μm.

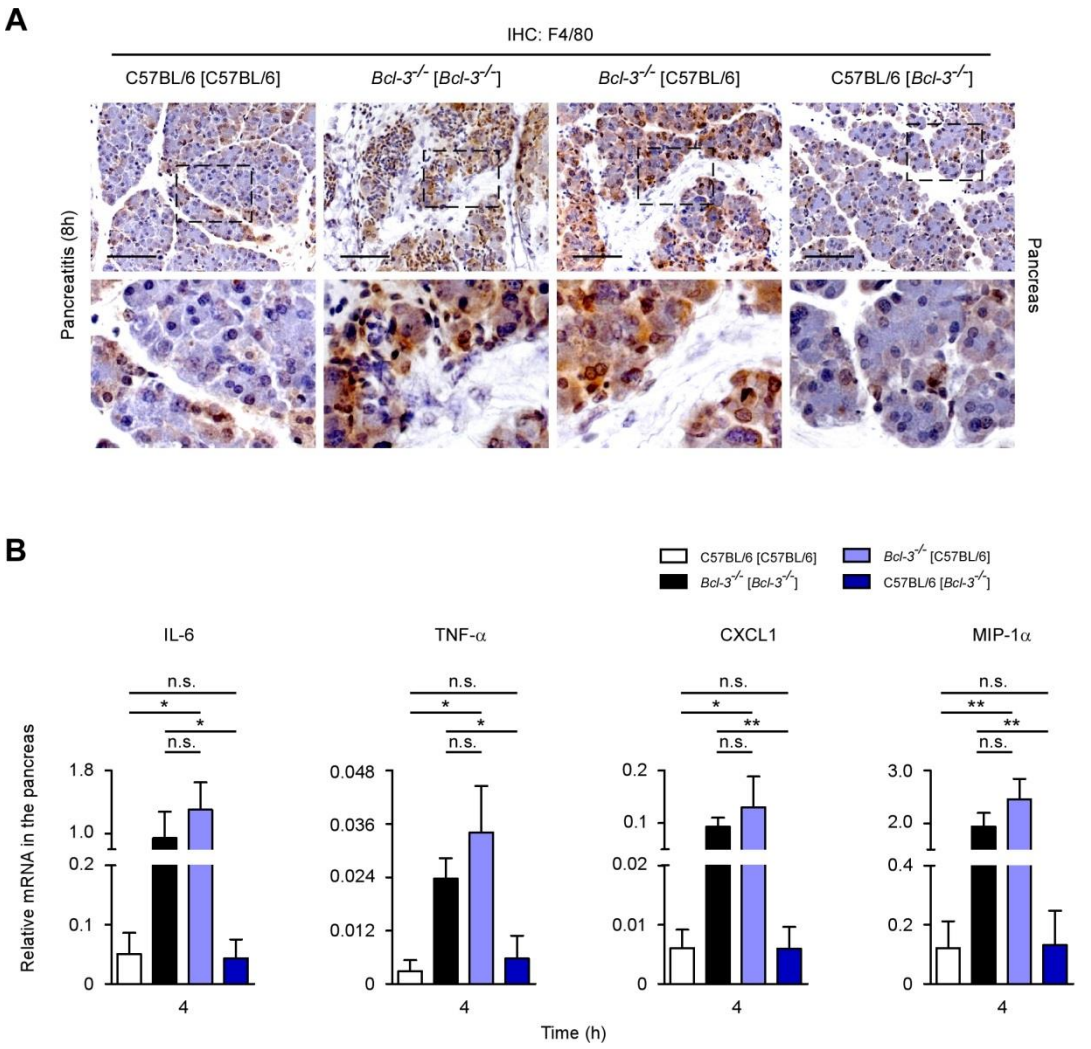

Figure 3-16 (**A**) Immunohistochemical staining of F4/80 in the mice with bone marrow transplantation. Boxed regions are shown at a higher magnification on the right (enlarged x3). (**B**) mRNA of IL-6, TNF-α, CXCL1, and MIP-1α was quantified by Q-PCR in pancreatic tissue of mice with bone marrow transplantation. Relative values were normalized to cyclophilin mRNA (n=4). Values represent mean ± SD. **P* < .05, ***P* < .01, and ****P* < .001. The scale bars equal 50 µm.

Since *Bcl-3*$^{-/-}$ mice are total knockout mice it is unclear whether the observed Bcl-3-mediated protective effects arise from epithelial cells, myeloid cells or others. To further identify the cellular source of Bcl-3 during AP we generated bone marrow chimera (Figure 3-15 A) allowing us to discriminate between the effects of Bcl-3 in epithelial and myeloid cells. Bone marrow chimeras were subjected to AP. It demonstrates that *Bcl-3*$^{-/-}$ mice reconstituted with wild-type bone marrow (*Bcl-3*$^{-/-}$[C57BL/6]) revealed similar extent of inflammation as compared to *Bcl-3*$^{-/-}$ mice reconstituted with *Bcl-3*$^{-/-}$ bone marrow (*Bcl-3*$^{-/-}$[*Bcl-3*$^{-/-}$]). While Bcl-3 deficient bone marrow did not influence severity of AP in wild-type mice (Figure 3-15 B). These changes were further emphasized by quantification of necrotic and edematous areas in sections of pancreatic tissue (Figure 3-15 C and D), higher activities of amylase and lipase in serum (Figure 3-15 E and F), increased infiltration (Figure 3-16 A), and production of proinflammatory factors (Figure 3-16 B). Altogether, these data demonstrate that Bcl-3 in

acinar cells, but not in myeloid cells is required to control the extent of sterile inflammation during AP.

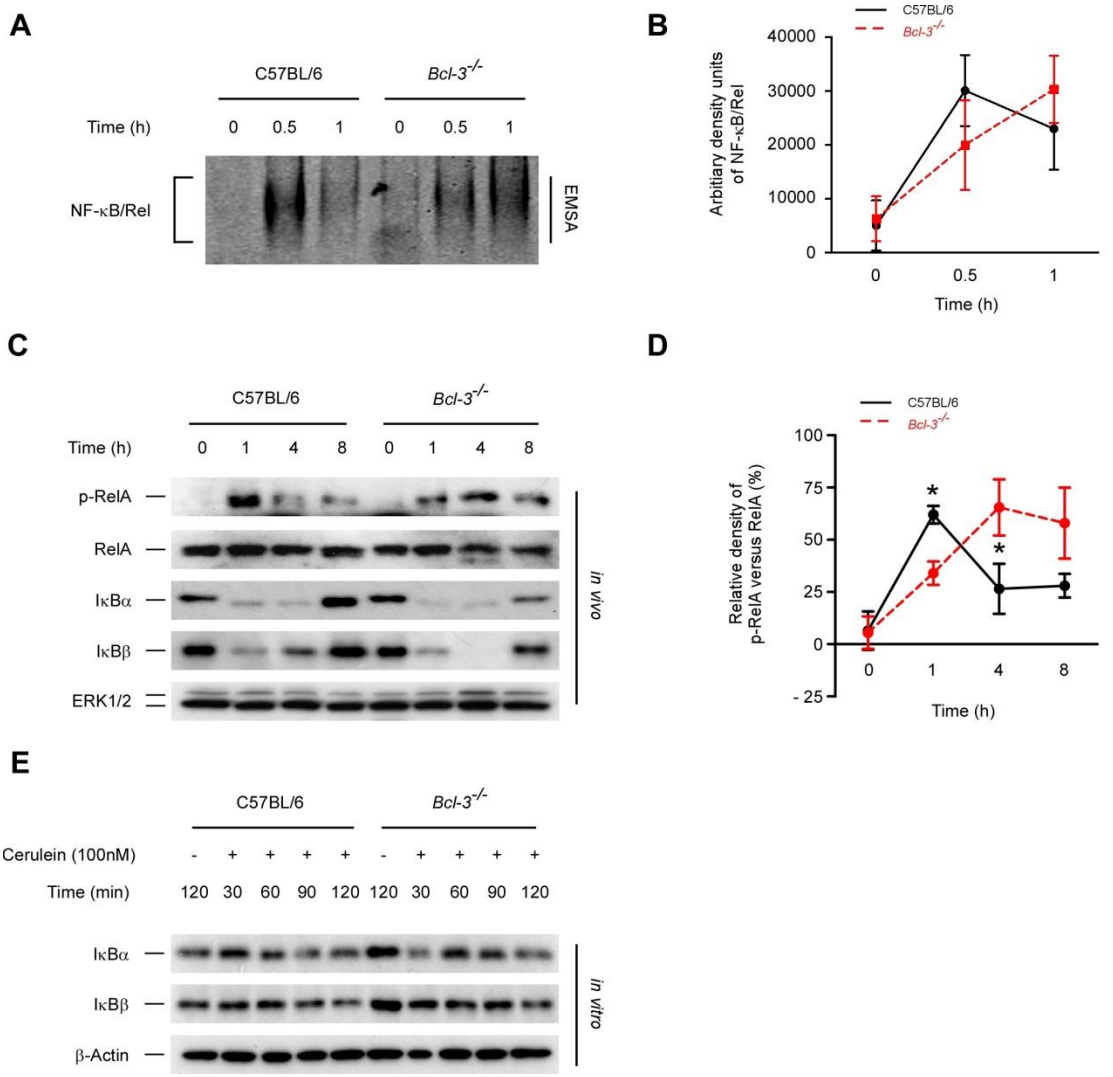

Figure 3-17: Prolonged activation of the canonical NF-κB activation in *Bcl-3*$^{-/-}$ mice. (**A**) Representative EMSA showed NF-κB/Rel binding activity in cerulein-induced AP. (**B**) Graphic representation of densitometry analysis was shown (n=4). (**C**) Immunoblot detection of p-RelA, RelA, IκBα and IκBβ in pancreatic tissue of cerulein-induced AP. ERK1/2 served as a loading control (representative blot, n=3). (**D**) Relative density of pRelA/RelA between C57BL/6 and *Bcl-3*$^{-/-}$ mice. (**E**) Isolated acinar cells were stimulated with cerulein (100nM), and homogenized to detect IκBα and IκBβ by immunoblot. β-actin served as loading control (representative blot, n=3). Values represent mean ± SD. **P* < .05, ***P* < .01, and ****P* < .001 *versus* Bcl-3$^{-/-}$ group.

3.4 Prolonged activation of the canonical NF-κB in *Bcl-3*$^{-/-}$ mice

Next we sought out to seek the underlining mechanisms which account for the Bcl-3-mediated protective effects during AP. As a member of the IκB family Bcl-3 is known to influence activation of the canonical NF-κB pathway. Therefore, we evaluated NF-κB binding activity by electrophoretic mobility shift assays (EMSA) in wild-type and Bcl-3$^{-/-}$ mice. While

early (0.5h and 1h) NF-κB/Rel activation was comparable during AP (Figure 3-17 A and B), loss of Bcl-3 delayed the peak of RelA activation to 4h and lasted until 8h of AP. In wild-type mice NF-κB activation was clearly attenuated at 4 and 8 hours (Figure 3-17 C and D). The degradation of the inhibitor protein IκBα and IκBβ followed the same kinetics of NF-κB/Rel activation in C57BL/6 and *Bcl-3*$^{-/-}$ mice in vivo and in vitro (Figure 3-17 C and E).

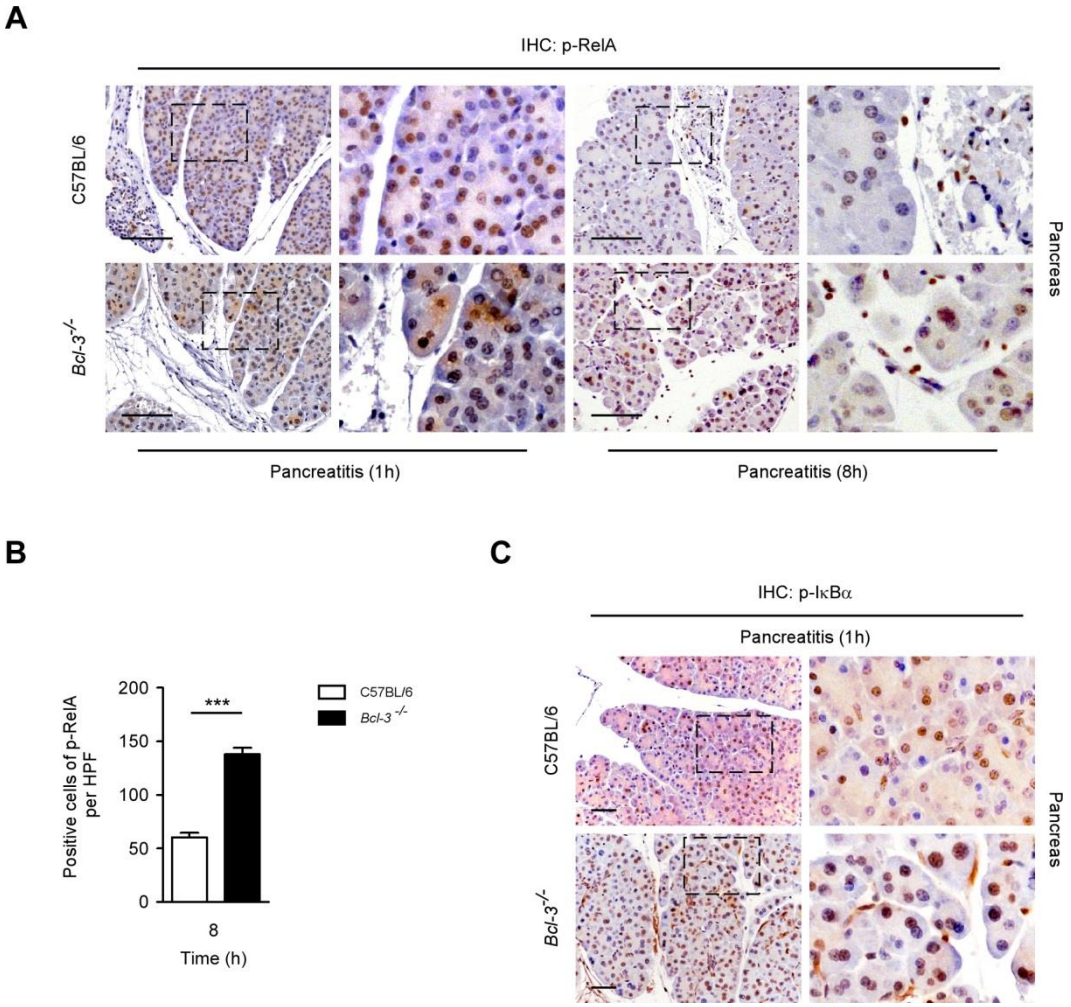

Figure 3-18: (**A**) Immunohistochemical staining of p-RelA in pancreatic tissue of cerulein-induced AP. (**B**) Positive cells of pRel-A per HPF in 8h AP were calculated. (**C**) Immunohistochemical staining of p-IκBα in pancreatic tissue of cerulein-induced AP. Values represent mean ± SD. **P* < .05, ***P* < .01, and ****P* < .001. Scale bars equal 25 µm. Boxed regions are shown at higher magnification on the right (enlarged × 3).

By IHC and calculation of positive cells per high-power field (HPF) we clearly revealed acinar cells as the cellular source of prolonged NF-κB activation, while nuclear RelA in infiltrating myeloid cells was comparable (Figure 3-18 A and B).[47] Moreover, activation of IκBα seemed not to be changed between C57BL/6 and *Bcl-3*$^{-/-}$ mice (Figure 3-18 C). These data demonstrate that Bcl-3 deficiency prolongs activation of the canonical NF-κB pathway and is required to resolve inflammation.

3.5 Bcl-3 stabilizes p50 homodimers to resolve inflammation

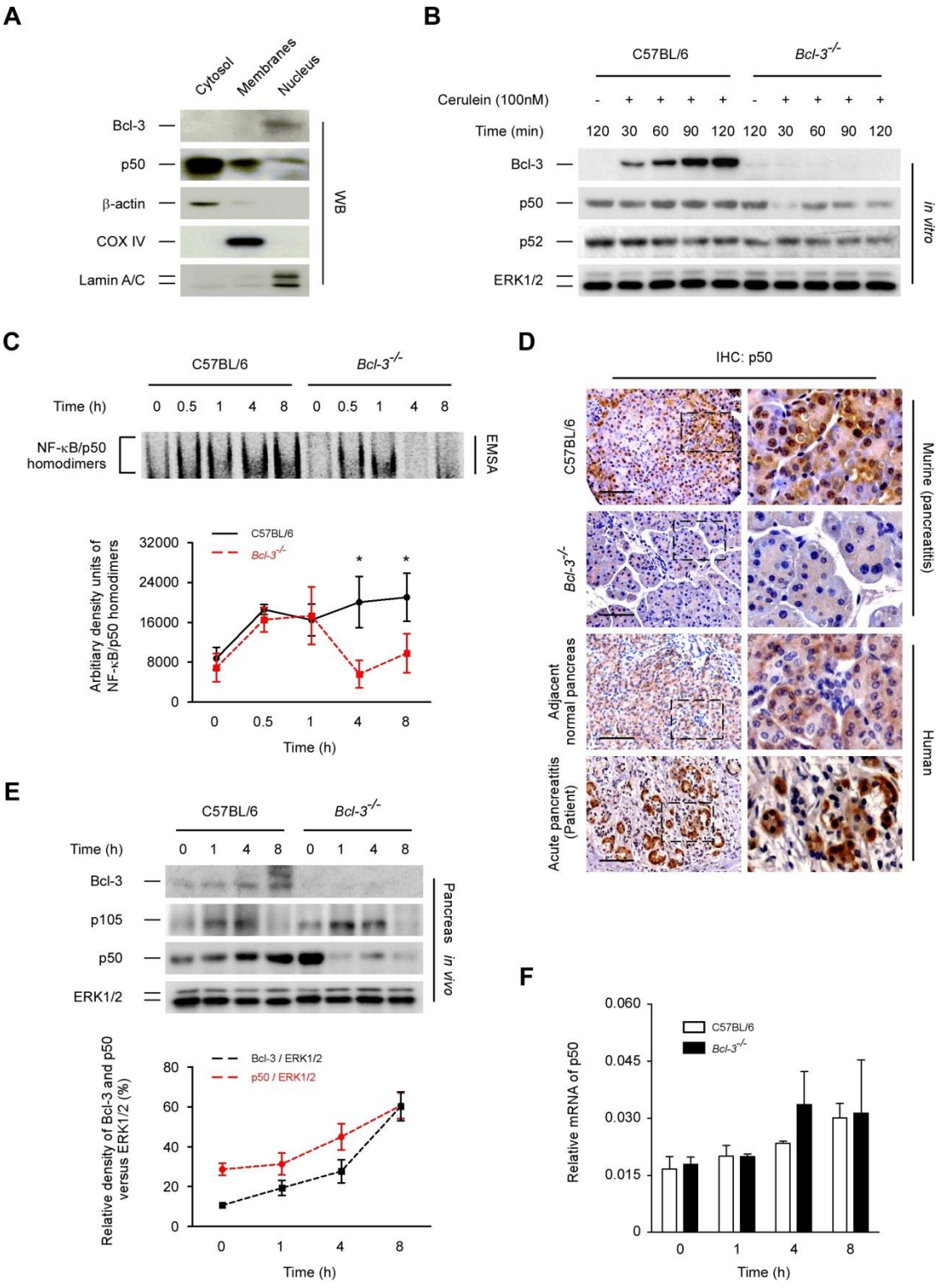

Figure 3-19 Bcl-3 stabilizes p50 homodimers to resolve inflammation. (**A**) Immunoblot detection of Bcl-3 and p50 in fractionated pancreatic tissue of 8h pancreatitis in C57BL/6 mice. Proteins specific to each fraction were confirmed by using β-actin (cytosol), COX IV (mitochondrial membrane), and lamin A/C (nucleus) antibodies (representative blot, n=3). (**B**) Isolated primary acinar cells were stimulated with cerulein (100nM), and homogenized

to detect Bcl-3, p50 and p52 by immunoblot. ERK1/2 served as loading control (representative blot, n=3). (**C**) Representative electrophoretic mobility shift assay (EMSA) showing NF-κB/p50 homodimers binding activity in the pancreas of cerulein-induced AP. Graphic representation of densitometry analysis are shown below (representative blot, n=4). (**D**) Immunohistochemical staining of p50 in pancreatic tissue of cerulein-induced pancreatitis as well as human specimens with AP. (**E**) Immunoblot detection of Bcl-3, p105 and p50 in pancreas of cerulein-induced AP. ERK1/2 served as loading control. Relative density of Bcl-3/ERK1/2 and p50/ERK1/2 in wild-type mice during AP are shown below (representative blot, n=3). **(F)** mRNA of p50 was quantified by Q-PCR in pancreatic tissue of cerulein-induced AP. Relative values were normalized to cyclophilin mRNA (n=4). Values represent mean ± SD. **P* < .05, ***P* < .01, and ****P* < .001. Scale bars equal 50 µm. Boxed regions are shown at higher magnification on the right (enlarged × 3).

Previous research has verified that Bcl-3 mainly interacts with p50 or p52 homodimers in the nucleus for regulation or modulation of NF-κB target genes on DNA level.[91,94] Indeed, subcellular locations of Bcl-3 and p50 confirmed their translocation into the nucleus during the late phase of AP (Figure 3-19 A). We next analyzed the expression of the p50 and p52 subunits during AP using immunoblot analysis. Interestingly, p50 expression in isolated acinar cells diminished in *Bcl-3*$^{-/-}$ cells over time following stimulation with cerulein. Of note, p52 expression was not altered (Figure 3-19 B). These findings were further confirmed by EMSA assays demonstrating the loss of p50 homodimers in *Bcl-3*$^{-/-}$ mice using specific probes. While p50 homodimers were detected in C57BL/6 mice throughout the process of AP, binding of these dimers was lost during inflammation in *Bcl-3*$^{-/-}$ mice (Figure 3-19 C). The weak staining of p50 at the late phase of AP in *Bcl-3*$^{-/-}$ mice using IHC further corroborated these findings (Figure 3-19 D). To replicate the observation of high p50 expression in human AP, we stained specimens from patients with AP using p50 antibody. And indeed, accumulation of p50 contained aggregates, especially in areas of acinar cell vacuolization, were detectable (Figure 3-19 D). Notably, p105, the precursor protein of p50, underwent constitutive processing without differences in both mouse strains. p50 expression seems to increase in line with the upregulaiton of Bcl-3 in wild-type mice during AP (Figure 3-19 E). Likewise, on mRNA levels no significant differences were detectable regarding the transcription of p50 (Figure 3-19 F).

Similar observations were done in Bcl-3 deficient *Mdr2*$^{-/-}$ mice. While the expression of p50 in hepatic tissue of C57BL/6 and *Mdr2*$^{-/-}$ mice were not different, a significant decrease of p50 on protein level was detectable in the double-mutant *Bcl-3*$^{-/-}$*/Mdr2*$^{-/-}$ mice (Figure 3-20 A). IHC staining of p50 in human specimens from patients undergoing PSC further confirmed these findings (Figure 3-20 B). mRNA levels of p50 were higher in *Bcl-3*$^{-/-}$*/Mdr2*$^{-/-}$ mice than those of *Mdr2*$^{-/-}$ mice suggesting compensatory upregulation (Figure 3-20 C). All these data clearly demonstrate an important role for Bcl-3 in sterile inflammation.

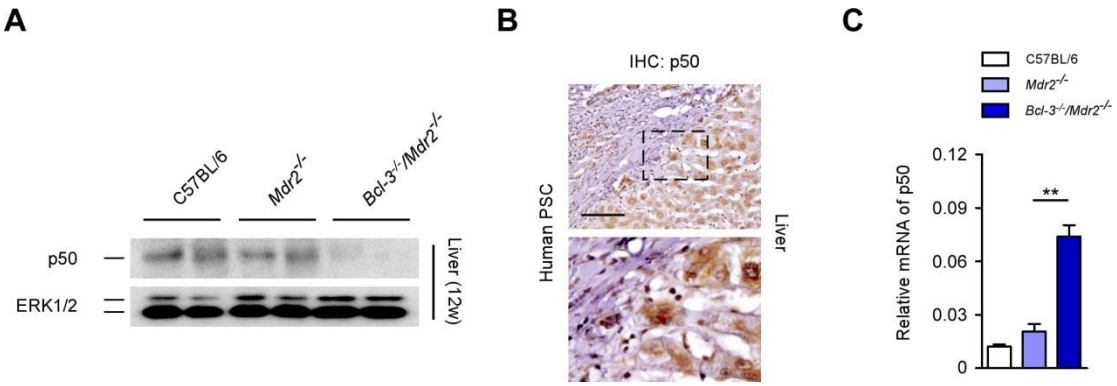

Figure 3-20: (**A**) Immunoblot detection of p50 in liver tissue. ERK1/2 served as a loading control (representative blot, n=3). (**B**) Immunohistochemical staining of p50 in human liver specimens of primary sclerosing cholangitis. Boxed regions are shown at higher magnification below (enlarged x3). (**C**) mRNA of p50 in liver tissue were quantified by Q-PCR. Relative values were normalized to cyclophilin mRNA (n=4). Values represent mean ± SD. **P* < .05, ***P* < .01, and ****P* < .001. Scale bars equal 50µm.

3.6 Bcl-3 inhibits proteasome-dependent degradation of p50

Bcl-3 has previously been shown to stabilize p50 complex by inhibiting ubiquitination of p50 and subsequent degradation in macrophages.[96] To detect whether endogenous p50 is ubiquitinated during AP, C57BL/6 and *Bcl-3*$^{-/-}$ mice were pretreated with the proteasome inhibitor bortezomib 1 hour prior to the induction of AP (Figure 3-21).

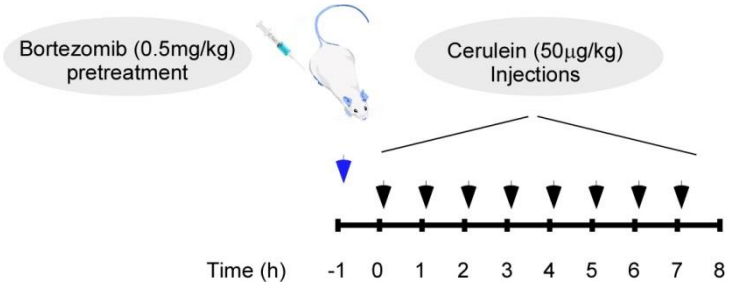

Figure 3-21: Schematic diagram of bortezomib treatment. Mice received an injection of 0.5mg/kg bortezomib 1h before the induction of pancreatitis.

Pretreatment with bortezomib restored p50 expression in *Bcl-3*$^{-/-}$ mice dramatically (Figure 3-22 A). Using further ubiquitination assay, we detected that ubiquitination of endogenous p50 was markedly increased in *Bcl-3*$^{-/-}$ mice compared with that of wild-type mice (Figure 3-22 B). These data clearly suggest that the decrease of p50 in *Bcl-3*$^{-/-}$ mice is due to increased ubiquitination and subsequently proteasome-mediated degradation. Stabilzation of p50 through pretreatment with bortezomib ameliorated edema formation and necrotic area in *Bcl-3*$^{-/-}$ mice undergoing AP (Figure 3-22 C). These findings were further emphasized by decreased relative pancreatic weight (PW/BW ratio) after pretreatment with bortezomib in *Bcl-3*$^{-/-}$ mice (Figure 3-22 D).

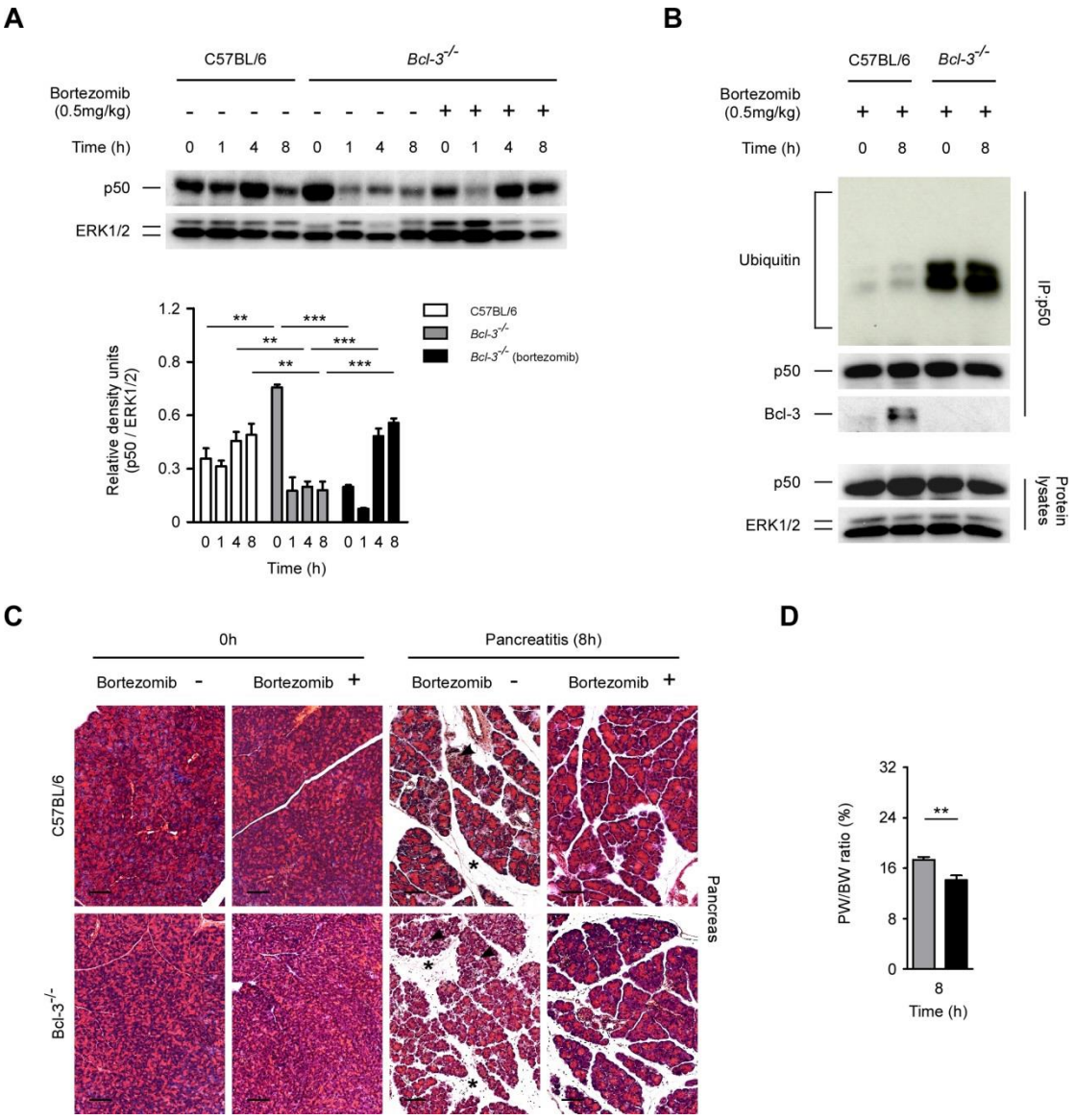

Figure 3-22: Bcl-3 inhibits p50 ubiquitination and proteasome-mediated degradation. (**A**) Western blot analyses showed recovered p50 expression after bortezomib treatment in *Bcl-3*$^{-/-}$ mice. ERK1/2 served as loading control. Graphic representation of densitometry analysis (n=4). (**B**) Ubiquitination assay in the pancreas of mice after bortezomib treatment. Equal amounts of protein were immunoprecipitated with antibody against p50 and immunoblotted with antibody against ubiquitin (representative blot, n=3). (**C**) Morphological analysis of representative H&E-stained pancreatic tissue at the indicated time points. Note the decrease of edema (asterisks) and necrosis (black arrowheads) after bortezomib treatment. (**D**) Pancreas weight to body weight ratio (PW/BW, %) was calculated (n=4). Relative values were normalized to cyclophilin mRNA (n=4). Values represent mean ± SD. **P* < .05, ***P* < .01, and ****P* < .001. Scale bars equal 50µm.

3.7 p50 is required to attenuate AP

To genetically confirm the role of p50 in AP we took advantage of the p50 knockout mouse line. Inactivation of p50 was verified by western blot and EMSA analyses (Figure 3-23 A). No differences were identified in basal levels as well as degradation of IκBα during AP (Figure 3-23 B). Of particular note, the protein-DNA binding activity of NF-κB/Rel seems to be delayed in *p50*$^{-/-}$ mice, which is similar to that of *Bcl-3*$^{-/-}$ mice (Figure 3-23 B).

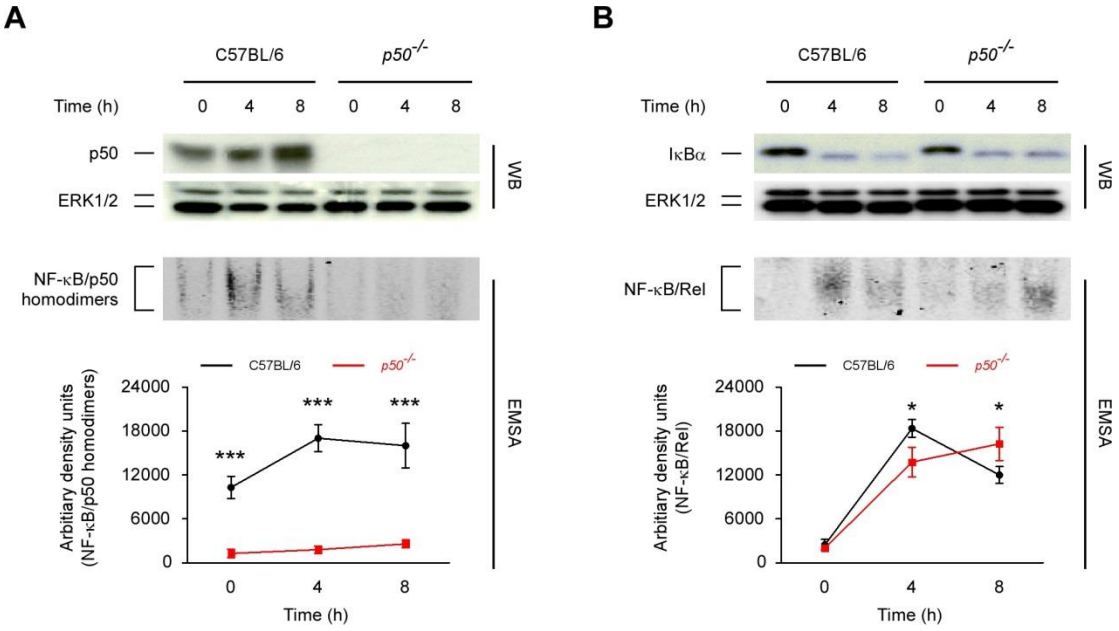

Figure 3-23: (**A**) Immunoblot detection of p50 in the pancreas of cerulein-induced AP. ERK1/2 served as a loading control (representative blot, n=3) (above). Representative EMSA showed NF-κB/p50 homodimers binding activity in pancreas of cerulein-induced AP between C57BL/6 and *p50*$^{-/-}$ mice. Graphic representation of densitometry analyses are shown (representative blot, n=4) (below). (**B**) Immunoblot detection of IκBα in pancreas of cerulein-induced AP. ERK1/2 served as loading control (representative blot, n=3) (above). Representative EMSA showed NF-κB/Rel binding activity in cerulein-induced AP between C57BL/6 and *p50*$^{-/-}$ mice (n=4). Values represent mean ± SD. **P* < .05, ***P* < .01, and ****P* < .001.

On morphological levels *p50*$^{-/-}$ mice displayed severe pancreatic damage with increased edema, infiltration and acinar cell death compared with C57BL/6 mice 8 hours after onset of AP (Figure 3-24 A, B and C). Accordingly, amylase and lipase levels in *p50*$^{-/-}$ mice were dramatically increased 8 hours after the onset of AP (Figure 3-24 D and E). Moreover, inflammatory parameters, including infiltration of macrophages and production of cytokines and chemokines were dramatically increased in *p50*$^{-/-}$ mice (Figure 3-25 A and B).

Taken together, our data provide unambiguous evidence for a central role of Bcl-3 in resolving sterile inflammation through inhibition of p50 ubiquitination. Bcl-3 stabilizes p50 homodimers to block prolonged binding of NF-κB heterodimers to the DNA.

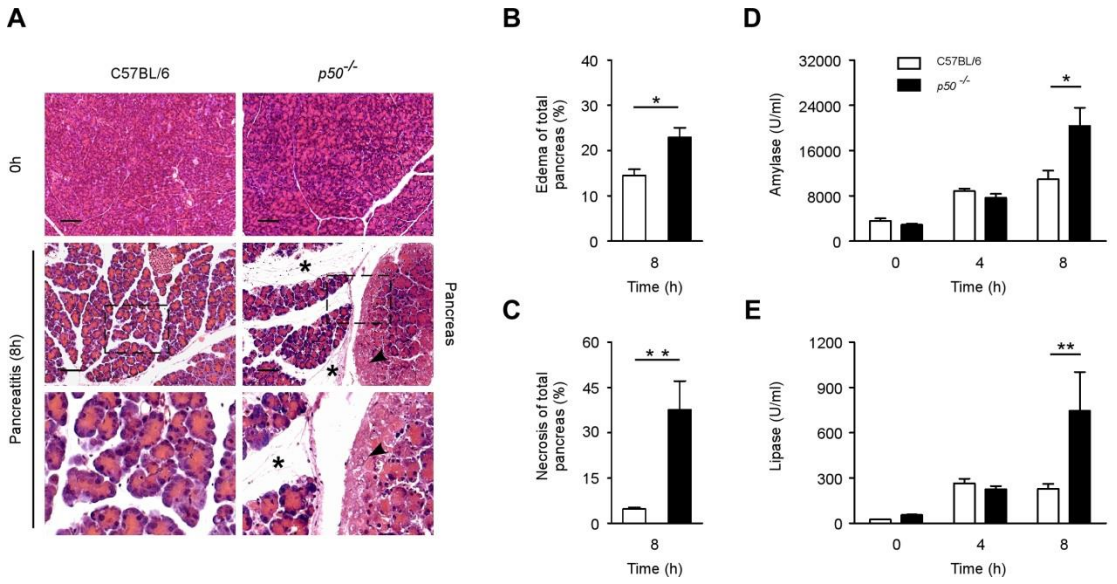

Figure 3-24: p50 deficiency aggravates cerulein-induced AP. (**A**) Morphological analysis of H&E staining in the pancreas of cerulein-induced AP. Note the increased edema (asterisks) and necrosis (arrowheads) in *p50*$^{-/-}$ mice. Scale bars equal 50µm. Boxed regions are shown at higher magnification below (enlarged × 3). (**B** and **C**) Sections were analyzed to quantify edematous (**B**) and necrotic (**C**) area in whole pancreas between C57BL/6 and *p50*$^{-/-}$ mice (n=4). (**D** and **E**) Serum amylase (**D**) and lipase (**E**) levels were measured in C57BL/6 and *p50*$^{-/-}$ animals (n=3). Values represent mean ± SD. **P* < .05, ***P* < .01, and ****P* < .001.

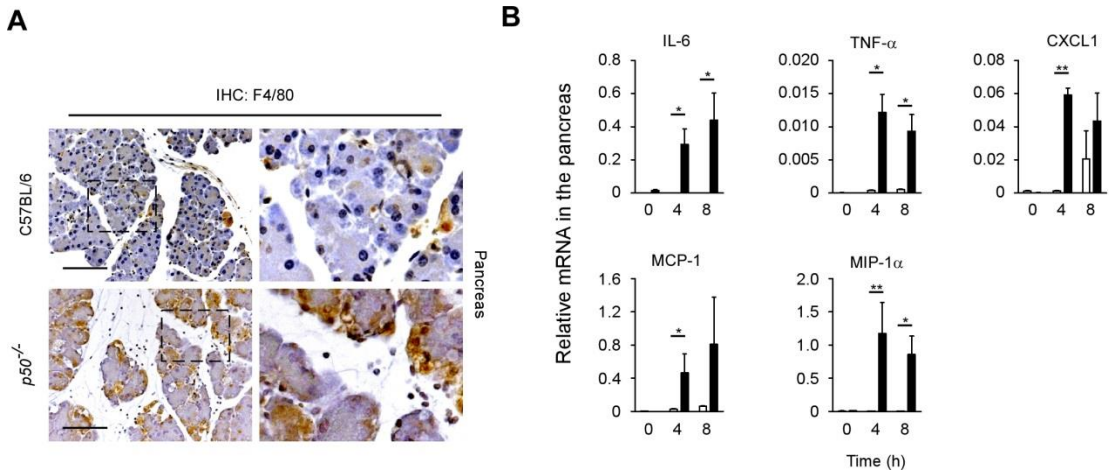

Figure 3-25: (**A**) Immunohistochemical detection of F4/80 in the pancreas of mice undergoing cerulein-induced AP. (**B**) mRNA of IL-6, TNF-α, CXCL1, MCP-1, and MIP-1α in pancreatic tissue of cerulein-induced AP were quantified by quantitative real-time polymerase chain reaction (Q-PCR). Relative values were normalized to cyclophilin mRNA (n=4). Values represent mean ± SD. **P* < .05, ***P* < .01, and ****P* < .001. Scale bars equal 50µm. Boxed regions are shown at higher magnification on the right (enlarged × 3).

3.8 UBE2L3 variant *rs2298428* in acute and chronic pancreatitis

Table 3-1: Details of patients

Pancreatitis		Number	Males	Age range (years)	Median (years)	AC 1	AC 2	AC 3
AP	**AP (all)**	289	172	9-92	54	108	110	71
	AP-A	56	53	27-76	44.5	9	21	26
	AP-B	137	61	9-92	62	66	43	28
	AP-ERCP	7	3	24-76	57	1	5	1
	AP-HLP	5	4	36-67	50	0	4	1
	AP-IP	71	45	10-89	50	32	30	9
	AP-OP	13	6	42-81	65	1	7	5
CP	**ACP**	293	256	24-79	49	n.a.	n.a.	n.a.
	NACP	248	134	3-77	34	n.a.	n.a.	n.a.
Controls		573	285	60-70	63	n.a.	n.a.	n.a.

Abbreviations: AP = acute pancreatitis, AP-A = alcoholic acute pancreatitis, AP-B = biliary acute pancreatitis, AP-ERCP = post endoscopic-retrograde-cholangiopancreaticography acute pancreatitis, AP-HLP = hyperlipidemia acute pancreatitis, AP-IP = acute pancreatitis in pregnancy, AP-OP = postoperative acute pancreatitis, CP = chronic pancreatitis, ACP = alcoholic chronic pancreatitis, NACP = non-alcohol related chronic pancreatitis. AC1 = Mild acute pancreatitis (according to the revised Atlanta classification), AC2 = moderately severe acute pancreatitis, AC3 = severe acute pancreatitis.

Table 3-2: Genotype distribution of *rs2298428* in patients and controls

rs2298428	CC	CT	TT	*P* value	HWE
AP (all) (n=289)	200 (69.2%)	80 (27.7%)	9 (3.1%)	0.5	0.96
ACP (n=293)	192 (65.5%)	92 (31.4%)	9 (3.1%)	0.9	0.88
NACP (n=248)	166 (66.9%)	71 (28.6%)	11 (4.4%)	0.7	0.64
Controls (n=573)	373 (65.1%)	179 (31.2%)	21 (3.7%)	n.a.	0.99

Abbreviations: AP=acute pancreatitis, ACP=alcoholic chronic pancreatitis, NACP=no alcohol related chronic pancreatitis, HWE=Hardy-Weinberg disequilibrium.

Because our data showed that p50 ubiquitination contributes to the severity of AP, we evaluated whether genetic alternation in UBE2L3 (Ubiquitin-conjugating enzyme E2L3) are associated with acute or chronic pancreatitis. Therefore, we screened 289 patients with acute pancreatitis, 541 patients with chronic pancreatitis, and 573 healthy control subjects for variant *rs2298428* in UBE2L3 by direct DNA sequencing (Table 3-1). However, statistical analysis revealed no significant association of genotype distribution of *rs2298428* in AP,

alcoholic chronic pancreatitis (ACP), no alcohol related chronic pancreatitis (NACP) patients and controls (Table 3-2). Insignificant *P*-values were obtained for the recessive and dominant model in addition (Table 3-3). In logistic regression analyses of *rs2298428* in AP, ACP, and NACP patients, cohorts were compared to the control group (Table 3-4). Adjustment for age and sex was performed for all groups. Additionally, stratification for severity categories displayed no significant association (Table 3-5).

Table 3-3: Statistical analyses for genotype distribution of *rs2298428* in two models

	***P* value**	
	dominant model (CC vs. CT+TT)	**recessive model (CC+CT vs. TT)**
AP (all) (n=289)	0.7	0.2
AP-IP (n=71)	0.7	0.2
AP-A (n=56)	0.5	0.8
AP-B (n=137)	0.7	0.6
AC1 (n=108)	0.9	0.9
AC2 (n=110)	0.7	0.08
AC3 (n=71)	0.1	0.6
ACP (n=293)	0.6	0.9
NACP (n=248)	0.6	0.6

Abbreviations: AP = acute pancreatitis, AP-IP = acute pancreatitis in pregnancy, AP-A = alcoholic acute pancreatitis, AP-B = biliary acute pancreatitis, AC1 = Mild acute pancreatitis (according to the revised Atlanta classification), AC2 = moderately severe acute pancreatitis, AC3 = severe acute pancreatitis, ACP = alcoholic chronic pancreatitis, NACP = non-alcohol related chronic pancreatitis. No other subgroups calculated, due to the small numbers in these groups.

Table 3-4: Logistic regression analyses of *rs2298428* in patients compared with controls

rs2298428	**Comparison**	***P* value**	**OR**	**95% CI**
AP (all) (n=289)	vs. controls (n=573)	0.15	1.24	0.93 - 1.66
AC1 (n=108)	vs. controls (n=573)	0.9	1.02	0.68 - 1.56
AC2 (n=110)	vs. controls (n=573)	0.09	1.5	0.94 - 2.37
AC3 (n=71)	vs. controls (n=573)	0.24	1.27	0.81 - 2.34
ACP (n=293)	vs. controls (n=573)	0.85	0.96	0.63 - 1.47
NACP (n=248)	vs. controls (n=573)	0.63	0.89	0.55 - 1.43

Abbreviations: AP = acute pancreatitis, ACP = alcoholic chronic pancreatitis, NACP = no alcohol related chronic pancreatitis, AC1 = Mild acute pancreatitis (according to the revised Atlanta classification), AC2 = moderately severe acute pancreatitis, AC3 = severe acute pancreatitis, ACP = alcoholic chronic pancreatitis, NACP = non-alcohol related chronic pancreatitis.

Table 3-5: Logistic regression analyses of *rs2298428* in the subgroups of AP patients

rs2298428	Comparison	*P* value	OR	95% CI
AP-IP (all) (n=71)	vs. controls (n=573)	0.07	1.79	0.96 - 3.32
AP-IP mild	vs. controls (n=573)	0.28	1.61	0.68 - 3.86
AP-IP moderate	vs. controls (n=573)	0.12	2.26	0.97 - 6.56
AP-IP severe	vs. controls (n=573)	0.60	1.57	0.29 - 8.37
AP-A (n=56)	vs. controls (n=573)	0.45	1.64	0.46 - 5.91
AP-A mild	vs. controls (n=573)	1.00	0.60	n.d
AP-A moderate	vs. controls (n=573)	0.80	1.26	0.22 - 7.19
AP-A severe	vs. controls (n=573)	0.34	2.76	0.35 - 21.94
AP-B (n=137)	vs. controls (n=573)	0.66	1.08	0.76 - 1.54
AP-B mild	vs. controls (n=573)	0.87	0.96	0.58 - 1.58
AP-B moderate	vs. controls (n=573)	0.60	1.17	0.65 - 2.11
AP-B severe	vs. controls (n=573)	0.46	1.34	0.62 - 2.91

Abbreviations: AP-IP = acute pancreatitis in pregnancy, AP-A = alcoholic acute pancreatitis, AP-B = biliary acute pancreatitis. No other subgroups calculated, due to the small numbers in these groups.

4 Discussion

Bcl-3 is an essential negative regulator of NF-κB during TLR and TNF receptor signaling. Its impact on sterile inflammation, however, has not been clarified so far. Using various animal models we demonstrate a central role for Bcl-3 in regulating the extent of inflammatory response during sterile inflammation across organs and species. Lack of Bcl-3 provoked a severe pattern of sterile inflammation characterized by 1) Deteriorated form of morphology, including increased positive proinflammatory signatures, such as edema, necrosis in AP, and more fibrosis around the periportal area of liver lobule; 2) Augmented infiltration of immune cells and production of proinflammatory cytokines. Mechanistically, Bcl-3 stabilizes p50 homodimers, to occupy the NF-κB binding site, thus blocking prolonged binding of NF-κB heterodimers to the DNA, leading to the decrease of inflammatory gene expression (Figure 4-1). Importantly, replication of our findings in human AP and PSC specimens supports our study unveiling an unanticipated role for Bcl-3 in these non-infectious inflammatory diseases.

4.1 Negative regulation of Bcl-3 in sterile inflammation

The role of Bcl-3 in inflammation is still a matter of debate. Several *in vitro* studies support the concept that Bcl-3 acts as a co-activator of NF-κB dependent transcription via its association with p50 and p52 homodimers.[93,108] Other data suggest that Bcl-3 binds to p50 and p52 homodimers, enhancing their occupancy of the DNA binding sites of NF-κB, thus competing with p65/p50 heterodimers.[94,95] And yet, the role of Bcl-3 in models of inflammation *in vivo* has not yet been clarified. Here, we demonstrate that Bcl-3 functions as a negative regulator in *in vivo* models of sterile inflammation. Indeed, Bcl-3 inactivation exacerbated inflammation in the liver and pancreas, as judged by deteriorated form of morphology and augmented infiltration of immune cells. Of note, this anti-inflammatory effect of Bcl-3 seems to be specific to sterile inflammation, as recent studies documented similar conclusions in experimental systems and models in which there is a prominent inflammatory response not triggered by a pathogen, for example, in lung injury caused by transplant-mediated ischemia reperfusion,[109] autoimmune diabetes,[110] or in a contact hypersensitivity mouse model in which keratinocyte-specific Bcl-3 ablation stimulates inflammation.[111] In addition, Bcl-3 showed a proinflammatory effect during dextran-sodium sulphate (DSS)-induced colitis in mice.[112] Colitis either triggered by autoimmune processes or irritant agents is always complicated through bacterial superinfections.[113] It suggests that Bcl-3 is critical for the protection of inflammatory responses not caused by infection.

Ubiquitin-conjugating enzyme E2L3 (UBE2L3) variant *rs2298428* and Bcl-3 variant *rs2927488* have been identified as likely novel genetic risk factors for Crohn´s disease.[114] However, in patients with acute or chronic pancreatitis UBE2L3 variant was not associated with the

severity of either disease corroborating the distinct roles of Bcl-3 during sterile and infectious inflammation.

4.2 Anti-inflammatory effect of Bcl-3 in epithelial cells

Macrophages are an indispensable component of the innate immune system. Activated by recognition of microorganisms through specific receptors, they phagocytose the pathogen and secrete cytokines, chemokines, and other immunologically active molecules to induce and regulate an inflammatory response.[115] Loss of Bcl-3 has been reported to cause an imbalance of cytokine production in response to LPS stimulation or bacterial infection in peritoneal, alveolar, or bone marrow derived macrophages.[100,116,117] Among the cytokines secreted by activated macrophages, TNF-α, IL-12p70, and IL-18 stimulate the production of IFN-γ in NK cells, which enhances microbicidal macrophage functions. However, it is unclear whether the anti-inflammatory effect of Bcl-3 in sterile inflammation arises from infiltrated leukocytes, specifically macrophages. Our experiments with bone marrow chimera place epithelial and not myeloid Bcl-3 in a central role during sterile inflammation although Bcl-3 is activated in myeloid cells. In contrast to infection these findings suggest that Bcl-3 in macrophages is not required for resolution of sterile inflammation.

Previous study demonstrated that Bcl-3 was preferentially recruited to the TNF-α promoter and enhanced inhibition of the TNF-α promoter activity, but not IL-6 promoter in macrophages.[94] However, our data showed that in epithelial cells mRNA level of both IL-6 and TNF-α were increased in Bcl-3 deficient mice, suggesting that Bcl-3 attenuates inflammatory response by reducing the production of IL-6 and TNF-α, which is different with that in macrophages. We also demonstrated that activation of STAT3 was dramatically enhanced in *Bcl-3*$^{-/-}$ mice during AP, indicating that anti-inflammatory effect of Bcl-3 at least partially depends on the inhibition of IL-6/JAK-2/STAT3 pathway. Moreover, increased IL-6 and TNF-α in *Bcl-3*$^{-/-}$ mice might be able to stimulate the production of Bcl-3 through STAT3 and NF-κB signaling pathway respectively as a negative feedback regulation.[118,119]

4.3 Modulation of NF-κB activity by Bcl-3

In contrast to typical members of IκB, Bcl-3 is not generally subject to induced degradation, and instead modulates transcriptional activities of NF-κB complexes in nuclei. Bcl-3 binds to p50 and p52 homodimers to inhibit the transcription of NF-κB dependent target genes such as TNF-α,[94] IL-1β,[116] and IL-10.[100] In fact, we have observed that cytokines and chemokines were dramatically increased along with the recruitment of inflammatory cells upon inactivation of Bcl-3 in AP and *Mdr2*$^{-/-}$ mice. Deficiency of Bcl-3 prolonged canonical NF-κB activation during sterile inflammation. The role of NF-κB in these sterile inflammatory diseases, in particular AP, has been highlighted in several studies.[79,81,82,120,121] While it is generally

accepted that NF-κB is activated during AP, the impact of the pathway on the outcome of this disease is still controversial. One side, overactivation of the NF-κB pathway increases severity of AP,[81,82,120] for example, transgenic overexpression of the IKK2[81] or RelA/p65[82] in mice was sufficient to induce pancreatitis and the level of NF-κB activation correlates with the severity of AP. The other side, total inactivation of NF-κB does not rescue the extent of inflammation-associated damage in the pancreas,[79,121] such as, loss of acinar cell IKK1 triggers spontaneous pancreatitis in mice.[121] Our previous work especially showed the effective protein RelA attenuates the severity of pancreatic damage during AP.[78,79] This conclusion seem to be contradictory with the present findings about Bcl-3 genetic ablation prolongs RelA activation and promotes acinar cell necrosis. However, prolonged RelA activation induced by Bcl-3 deficiency is only the secondary effect following the disinhibition of p50 homodimers. Deteriorated pancreatic damage in *Bcl-3*$^{-/-}$ mice reveals that the inhibitory effects of p50 homodimers are even stronger than those of RelA through transcriptional regulation of the pancreatitis-associated protein (PAP) 1. This clearly suggests that the extent and modulation of NF-κB activation is more important than the on/off mechanism of NF-κB activation pathway on kinase or subunit levels in this setting.

4.4 Effect of Bcl-3 on cell integrity

Modulation of cell death by means of apoptosis inhibition and an increase in proliferation have been described as the main effect of Bcl-3 on oncogenesis.[122,123] However, our data showed that loss of Bcl-3 dramatically increased necrosis, but had no influence on apoptosis (data not shown) during sterile inflammation. It seems that Bcl-3 has different effects on cell integrity in sterile inflammation compared to the role of Bcl-3 as an oncogene. Cell integrity is important for sterile inflammation as necrotic cells release DAMPs, stimulating the TLR system and triggering inflammation and tissue injury.[124] The potential mechanisms about how Bcl-3 affects necrosis during inflammation remains to be elucidated. It is possible that increased inflammation and cell death in *Bcl-3*$^{-/-}$ mice are not directly linked to each other. Rather, increased recruitment of leukocytes destroys acinar cell integrity through neutrophil elastase-mediated dissociation of cell-cell contact,[125] thus evoking cell necrosis.

4.5 Bcl-3 stabilizes p50 via blocking ubiquitination

In addition to interfering with NF-κB activation via binding with p50 or p52 homodimers, Bcl-3 appears to stabilize these homodimers as well.[126] A previous study has demonstrated that Bcl-3 regulates stability of p50 homodimers in LPS-tolerance models,[96] which is a model of sterile inflammation and sepsis. Indeed, we have observed that loss of Bcl-3 was paralleled by degradation of p50 homodimers in the pancreas and liver during sterile inflammation. This degradation is dependent on the proteasome, as proteasome inhibition by bortezomib treatment *in vivo* rescued the reduced p50 homodimers.

The role of ubiquitin as a versatile signaling tag is characteristically illustrated in diverse NF-κB signaling pathways. Ubiquitination not only controls the degradation of IκBs and the processing of NF-κB precursors (p100) by the proteasome, but also regulates the activation of IKK through proteasome-independent mechanisms.[127] We observed prolonged RelA activation and increased p50 ubiquitination in *Bcl-3*$^{-/-}$ mice of AP and cholangitis, suggesting that Bcl-3 blocks ubiquitinaiton of p50 through formation of stable p50 homodimers:Bcl-3 complex,[126] thereby increasing p50 homodimer NF-κB occupancy, indirectly repressing NF-κB target gene transcription. Genetic deletion of Bcl-3 leads to ubiquitination of p50, thereby resulting in aberrant cytokine production involved in sterile inflammation (Figure 4-1).

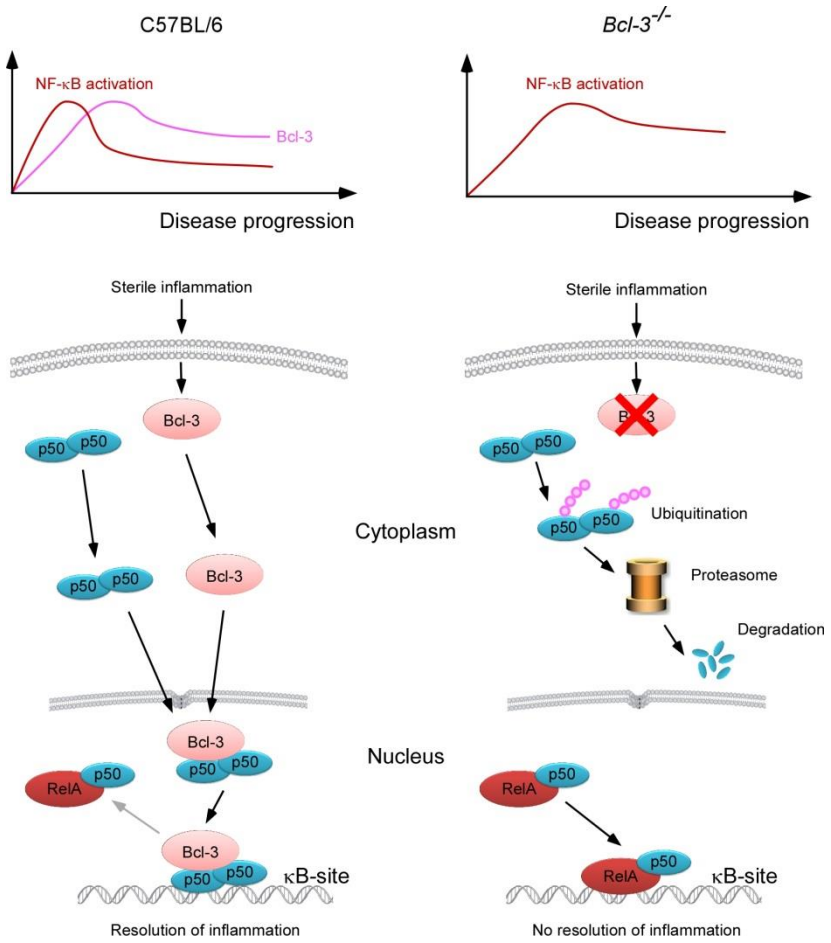

Figure 4-1: Central role of Bcl-3 in sterile inflammation. Upregulated Bcl-3 was transported from cytoplasm to nucleus, where Bcl-3 is able to bind with p50 homodimers and increase NF-κB binding sites occupancy via inhibiting the ubiquitination and subsequently proteasomal mediated degradation of p50 homodimers.

Ubiquitination requires three types of enzymes, which are ubiquitin-activating enzymes (E1s), ubiquitin-conjugating enzymes (E2s) and ubiquitin ligases (E3s), respectively, in three main steps: activation, conjugation and ligation. The addition of ubiquitin can affect proteins in many ways, it can signal for their degradation via the proteasome or lysosome, alter their cellular location, affect their activity and promote or prevent protein interactions.[128–130] It is

unclear so far which ligase complex is associated with p50 ubiquitination although several E3 ligases in the NF-κB pathway have been addressed, such as TRAF6 for IκB kinase (IKK),[131] Skp1, Cul1, Roc1 and βTrCP for IκB proteins,[132] βTrCP for constitutive processing of p100 to p52,[133] and TBLR1 for Bcl-3.[98] Since ubiquitinaiton of p50 plays a crucial role in regulating its function, the nature of the ubiquitin ligase involved needs to be elucidated. We further identified a critical role for p50 homodimers in AP. Inactivation of p50 displayed a severe form during the late phase of AP, which is inconsistent with the time course of Bcl-3 upregulation. This means that kinetics of Bcl-3 expression and p50 stabilization are peaking at a similar time-point during the resolution of AP. This resolution is abrogated in *p50*$^{-/-}$ mice and has not been studied in previous research, which only analyzed developments until 4 hours of inducing pancreatitis.[134] Moreover, we have observed that pretreatment with bortezomib ameliorated the severity of AP, which agrees with a previous report.[135] This suggests that clinical application of bortezomib in this condition would appear to be a rational treatment strategy.

Overall, these findings provide strong evidence for the pivotal role of Bcl-3 in modulating the sterile inflammatory response. Blocking of p50 homodimer ubiquitination and subsequent proteasome-mediated degradation inhibits NF-κB target gene transcription in the nucleus during sterile inflammation. To our knowledge, this is the first study that addresses the role of NF-κB regulation beyond the IKK/IκBα/NF-κB/RelA pathway during sterile inflammation.

5 Summary

The central focus of the present study was to analyze the contribution of Bcl-3 to the control and resolution of sterile inflammation in the pancreas and biliary system.

During sterile inflammation, the binding of DAMPs (released by necrotic cells) to TLRs trigger a signaling cascade, most prominently represented by the activation of IKK/NF-κB pathway. As an atypical member of the IκB family, Bcl-3 plays a central role in the modulation of NF-κB activity. However, the mechanisms through which Bcl-3 controls NF-κB activity during sterile inflammation have remained unexplored so far. To elucidate the importance of Bcl-3 in sterile inflammation, Bcl-3 total knockout mice were characterized in detail using animal models of AP and sterile cholangitis. Moreover, the murine phenotype was compared to pancreata or liver from human patients with AP or PSC respectively.

Bcl-3 was upregulated in the pancreas and biliary system during sterile inflammation in both humans and mice. Genetic inhibition of Bcl-3 resulted in more severe forms of AP and cholangitis, accompanied by increased infiltration of immune cells as well as production of cytokines and chemokines. Also, canonical NF-κB activation was significantly prolonged during sterile inflammation in *Bcl-3*$^{-/-}$ mice. Using various genetic tools we showed that Bcl-3 inhibits ubiquitination and proteasomal mediated degradation of p50 homodimers, thus blocking prolonged binding of NF-κB heterodimers to the DNA. Moreover, generation of bone marrow chimeric mice enabled us to identify the cellular source of Bcl-3 in epithelial but not myeloid cells. SNP analysis of UBE2L3 variant, however, was not associated with the severity of AP and CP.

Thus, the present study addresses the central role of Bcl-3 in controlling the extent of sterile inflammation in various organs and species, therefore opening a new avenue to therapeutically target sterile inflammation.

6 References

1. Medzhitov R. Origin and physiological roles of inflammation. Nature 2008;454:428–435.

2. Akira S, Uematsu S, Takeuchi O. Pathogen recognition and innate immunity. Cell 2006;124:783–801.

3. Rock KL, Latz E, Ontiveros F, et al. The sterile inflammatory response. Annu. Rev. Immunol. 2010;28:321–342.

4. Kishi M, Richard LF, Webster RO, et al. Role of neutrophils in xanthine/xanthine oxidase-induced oxidant injury in isolated rabbit lungs. J. Appl. Physiol. 1999;87:2319–2325.

5. Liu Z-X, Han D, Gunawan B, et al. Neutrophil depletion protects against murine acetaminophen hepatotoxicity. Hepatology 2006;43:1220–1230.

6. Abulafia DP, Rivero Vaccari JP de, Lozano JD, et al. Inhibition of the inflammasome complex reduces the inflammatory response after thromboembolic stroke in mice. J. Cereb. Blood Flow Metab. 2009;29:534–544.

7. Dobschuetz E Von, Hoffmann T, Messmer K. Inhibition of neutrophil proteinases by recombinant serpin Lex032 reduces capillary no-reflow in ischemia/reperfusion-induced acute pancreatitis. J. Pharmacol. Exp. Ther. 1999;290:782–788.

8. Matzinger P. The danger model: a renewed sense of self. Science 2002;296:301–305.

9. Matzinger P. Tolerance, danger, and the extended family. Annu. Rev. Immunol. 1994;12:991–1045.

10. Scaffidi P, Misteli T, Bianchi ME. Release of chromatin protein HMGB1 by necrotic cells triggers inflammation. Nature 2002;418:191–195.

11. Quintana FJ, Cohen IR. Heat shock proteins as endogenous adjuvants in sterile and septic inflammation. J. Immunol. 2005;175:2777–2782.

12. Bours MJL, Swennen ELR, Virgilio F Di, et al. Adenosine 5’-triphosphate and adenosine as endogenous signaling molecules in immunity and inflammation. Pharmacol. Ther. 2006;112:358–404.

13. Kono H, Chen C-J, Ontiveros F, et al. Uric acid promotes an acute inflammatory response to sterile cell death in mice. J. Clin. Invest. 2010;120:1939–1949.

14. Kono H, Kenneth LR. How dying cells alert the immune system to danger. Nat. Rev. Immunol. 2008;8:279–289.

15. Babelova A, Moreth K, Tsalastra-Greul W, et al. Biglycan, a danger signal that activates the NLRP3 inflammasome via toll-like and P2X receptors. J. Biol. Chem. 2009;284:24035–24048.

16. Unterholzner L, Keating SE, Baran M, et al. IFI16 is an innate immune sensor for intracellular DNA. Nat. Immunol. 2011;11:997–1004.

17. Piccinini a M, Midwood KS. DAMPening inflammation by modulating TLR signalling. Mediators Inflamm. 2010;2010:672395.

18. Riva M, Källberg E, Björk P, et al. Induction of nuclear factor-κB responses by the S100A9 protein is Toll-like receptor-4-dependent. Immunology 2012;137:172–182.

19. Gabay C, Lamacchia C, Palmer G. IL-1 pathways in inflammation and human diseases. Nat. Rev. Rheumatol. 2010;6:232–241.

20. Martinon F, Pétrilli V, Mayor A, et al. Gout-associated uric acid crystals activate the NALP3 inflammasome. Nature 2006;440:237–241.

21. Bauernfeind F, Horvath G, Stutz A, et al. NF-kB activating pattern recognition and cytokine receptors license NLRP3 inflammasome activation by regulating NLRP3 expression. J. Immunol. 2010;183:787–791.

22. Fernandes-Alnemri T, Yu J-W, Wu J, et al. AIM2 activates the inflammasome and cell death in response to cytoplasmic DNA. Nature 2012;29:997–1003.

23. Bürckstümmer T, Baumann C, Blüml S, et al. An orthogonal proteomic-genomic screen identifies AIM2 as a cytoplasmic DNA sensor for the inflammasome. Nat. Immunol. 2009;10:266–272.

24. Sakurai T, He G, Matsuzawa A, et al. Hepatocyte necrosis induced by oxidative stress and IL-1a release mediate carcinogen-induced compensatory proliferation and liver tumorigenesis. Cancer Cell 2009;14:156–165.

25. Cohen I, Rider P, Carmi Y, et al. Differential release of chromatin-bound IL-1a discriminates between necrotic and apoptotic cell death by the ability to induce sterile inflammation. Proc. Natl. Acad. Sci. U. S. A. 2010;107:2574–2579.

26. Keller M, Rüegg A, Werner S, et al. Active caspase-1 is a regulator of unconventional protein secretion. Cell 2008;132:818–831.

27. Cayrol C, Girard J-P. The IL-1-like cytokine IL-33 is inactivated after maturation by caspase-1. Proc. Natl. Acad. Sci. U. S. A. 2009;106:9021–9026.

28. Lüthi AU, Cullen SP, McNeela E a., et al. Suppression of interleukin-33 bioactivity through proteolysis by apoptotic caspases. Immunity 2009;31:84–98.

29. Fang F, Lue L-F, Yan S, et al. RAGE-dependent signaling in microglia contributes to neuroinflammation, Abeta accumulation, and impaired learning/memory in a mouse model of Alzheimer's disease. FASEB J. 2010;24:1043–1055.

30. Sims GP, Rowe DC, Rietdijk ST, et al. HMGB1 and RAGE in inflammation and cancer. Annu. Rev. Immunol. 2010;28:367–388.

31. Brett J. The receptor for advanced glycation end products (RAGE) is a cellular binding site for amphoterin. J. Biol. Chem. 1995;270:25752–25761.

32. Hofmann M a., Drury S, Fu C, et al. RAGE mediates a novel proinflammatory axis: A central cell surface receptor for S100/calgranulin polypeptides. Cell 1999;97:889–901.

33. Ariyoshi H, Yoshikawa N, Aono Y, et al. Role of receptor for advanced glycation end-product (RAGE) and the JAK/STAT-signaling pathway in AGE-induced collagen production in NRK-49F cells. J. Cell. Biochem. 2001;81:102–113.

34. Chen G-Y, Tang J, Zheng P, et al. CD24 and Siglec-10 selectively repress tissue damage-induced immune responses. Science 2009;323:1722–1725.

35. Flasar MH, Goldberg E. Acute abdominal pain. Med. Clin. North Am. 2006;90:481–503.

36. Lund H, Tønnesen H, Tønnesen MH, et al. Long-term recurrence and death rates after acute pancreatitis. Scand. J. Gastroenterol. 2006;41:234–238.

37. Gorelick FS. Alcohol and zymogen activation in the pancreatic acinar cell. Pancreas 2003;27:305–310.

38. Frossard J-L, Steer ML, Pastor CM. Acute pancreatitis. Lancet 2008;371:143–152.

39. Bhatia M. Acute pancreatitis as a model of SIRS. Front. Biosci. (landmark Ed. 2009;14:2042–2050.

40. Schütte K, Malfertheiner P. Markers for predicting severity and progression of acute pancreatitis. Best Pract. Res. Clin. Gastroenterol. 2008;22:75–90.

41. Niederau C, Ferrell LD, Grendell JH. Caerulein-induced acute necrotizing pancreatitis in mice: protective effects of proglumide, benzotript, and secretin. Gastroenterology 1985;88:1192–1204.

42. Watanabe O, Baccino FM, Steer ML, et al. Supramaximal caerulein stimulation and ultrastructure of rat pancreatic acinar cell: early morphological changes during development of experimental pancreatitis. Am. J. Physiol. 1984;246:G457–G467.

43. Renner IG, Wisner JR. Ceruletide-induced acute pancreatitis in the dog and its amelioration by exogenous secretin. Int. J. Pancreatol. 1986;1:39–49.

44. Zaninovic V, Gukovskaya a S, Gukovsky I, et al. Cerulein upregulates ICAM-1 in pancreatic acinar cells, which mediates neutrophil adhesion to these cells. Am. J. Physiol. Gastrointest. Liver Physiol. 2000;279:G666–G676.

45. Kim H. Cerulein pancreatitis: oxidative stress, inflammation, and apoptosis. Gut Liver 2008;2:74–80.

46. Guice KS, Oldham KT, Johnson KJ, et al. Pancreatitis-induced acute lung injury. An ARDS model. Ann. Surg. 1988;208:71–7.

47. Zhang H, Neuhöfer P, Song L, et al. IL-6 trans-signaling promotes pancreatitis-associated lung injury and lethality. J. Clin. Invest. 2013;123:1019–1031.

48. Su KH, Cuthbertson C, Christophi C. Review of experimental animal models of acute pancreatitis. HPB (Oxford). 2006;8:264–286.

49. Mizunuma T, Kawamura S, Kishino Y. Effects of injecting excess arginine on rat pancreas. J. Nutr. 1984;114:467–471.

50. Hegyi P, Rakonczay Z, Sári R, et al. L-arginine-induced experimental pancreatitis. World J. Gastroenterol. 2004;10:2003–2009.

51. Laukkarinen JM, Acker GJD Van, Weiss ER, et al. A mouse model of acute biliary pancreatitis induced by retrograde pancreatic duct infusion of Na-taurocholate. Gut 2007;56:1590–1598.

52. Senninger N, Moody FG, Coelho JC, et al. The role of biliary obstruction in the pathogenesis of acute pancreatitis in the opossum. Surgery 1986;99:688–693.

53. Eaton JE, Talwalkar J a., Lazaridis KN, et al. Pathogenesis of primary sclerosing cholangitis and advances in diagnosis and management. Gastroenterology 2013;145:521–536.

54. Guo S, Al-Sadi R, Said HM, et al. Lipopolysaccharide causes an increase in intestinal tight junction permeability in vitro and in vivo by inducing enterocyte membrane expression and localization of TLR-4 and CD14. Am. J. Pathol. 2013;182:375–387.

55. Sheth P, Delos Santos N, Seth a, et al. Lipopolysaccharide disrupts tight junctions in cholangiocyte monolayers by a c-Src-, TLR4-, and LBP-dependent mechanism. Am. J. Physiol. Gastrointest. Liver Physiol. 2007;293:G308–G318.

56. Fickert P, Fuchsbichler A, Wagner M, et al. Regurgitation of bile acids from leaky bile ducts causes sclerosing cholangitis in Mdr2 (Abcb4) knockout mice. Gastroenterology 2004;127:261–274.

57. Mueller T, Beutler C, Picó AH, et al. Enhanced innate immune responsiveness and intolerance to intestinal endotoxins in human biliary epithelial cells contributes to chronic cholangitis. Liver Int. 2011;31:1574–1588.

58. Medvedev AE, Sabroe I, Hasday JD, et al. Tolerance to microbial TLR ligands: molecular mechanisms and relevance to disease. J. Endotoxin Res. 2006;12:133–150.

59. Katt J, Schwinge D, Schoknecht T, et al. Increased T helper type 17 response to pathogen stimulation in patients with primary sclerosing cholangitis. Hepatology 2013;58:1084–1093.

60. Borchers AT, Shimoda S, Bowlus C, et al. Lymphocyte recruitment and homing to the liver in primary biliary cirrhosis and primary sclerosing cholangitis. Semin. Immunopathol. 2009;31:309–322.

61. Hillan KJ, Hagler KE, MacSween RN, et al. Expression of the mucosal vascular addressin, MAdCAM-1, in inflammatory liver disease. Liver 1999;19:509–518.

62. Grant AJ, Lalor PF, Salmi M, et al. Homing of mucosal lymphocytes to the liver in the pathogenesis of hepatic complications of inflammatory bowel disease. Lancet 2002;359:150–157.

63. Smit JJ, Schinkel a H, Mol C a, et al. Tissue distribution of the human MDR3 P-glycoprotein. Lab. Invest. 1994;71:638–649.

64. Oude Elferink RPJ, Paulusma CC. Function and pathophysiological importance of ABCB4 (MDR3 P-glycoprotein). Pflugers Arch. Eur. J. Physiol. 2007;453:601–610.

65. Trauner M, Fickert P, Wagner M. MDR3 (ABCB4) defects: A paradigm for the genetics of adult cholestatic syndromes. Semin. Liver Dis. 2007;27:77–98.

66. Smit JJ, Schinkel a H, Oude Elferink RP, et al. Homozygous disruption of the murine mdr2 P-glycoprotein gene leads to a complete absence of phospholipid from bile and to liver disease. Cell 1993;75:451–462.

67. Mauad TH, Nieuwkerk CM van, Dingemans KP, et al. Mice with homozygous disruption of the mdr2 P-glycoprotein gene. A novel animal model for studies of

nonsuppurative inflammatory cholangitis and hepatocarcinogenesis. Am. J. Pathol. 1994;145:1237–1245.

68. Fickert P, Zollner G, Fuchsbichler A, et al. Ursodeoxycholic acid aggravates bile infarcts in bile duct-ligated and Mdr2 knockout mice via disruption of cholangioles. Gastroenterology 2002;123:1238–1251.

69. Baldwin AS. THE NF- κB AND IκB PROTEINS : New Discoveries and Insights Annual Review of Immunology. Annu. Rev. Immunol. 1996;14:649–681.

70. Chen F, Castranova V, Shi X, et al. New insights into the role of nuclear factor-kappaB, a ubiquitous transcription factor in the initiation of diseases. Clin. Chem. 1999;45:7–17.

71. Hayden, Matthew S. SG. Signaling to NF-kB. 2004:2195–2224.

72. Bollrath J, Greten FR. IKK/NF-kappaB and STAT3 pathways: central signalling hubs in inflammation-mediated tumour promotion and metastasis. EMBO Rep. 2009;10:1314–1319.

73. Steinle AU, Weidenbach H, Wagner M, et al. NF-κB/Rel activation in cerulein pancreatitis. Gastroenterology 1999;116:420–430.

74. Han B, Ji B, Logsdon CD. CCK independently activates intracellular trypsinogen and NF-kappaB in rat pancreatic acinar cells. Am. J. Physiol. Cell Physiol. 2001;280:C465–G472.

75. Vaquero E, Gukovsky I, Zaninovic V, et al. Localized pancreatic NF-kappaB activation and inflammatory response in taurocholate-induced pancreatitis. Am. J. Physiol. Gastrointest. Liver Physiol. 2001;280:G1197–G1208.

76. Rakonczay Z, Hegyi P, Takács T, et al. The role of NF-kappaB activation in the pathogenesis of acute pancreatitis. Gut 2008;57:259–267.

77. Schmid RM. Activation of nuclear factor kappaB in acinar cells does not provoke acute pancreatitis. Gut 2007;56:164–165.

78. Neuhöfer P, Liang S, Einwächter H, et al. Deletion of IκBa activates RelA to reduce acute pancreatitis in mice through up-regulation of Spi2A. Gastroenterology 2013;144:192–201.

79. Algül H, Treiber M, Lesina M, et al. Pancreas-specific RelA / p65 truncation increases susceptibility of acini to inflammation-associated cell death following cerulein pancreatitis. J. Clin. Invest. 2007;117:1490–1501.

80. Aleksic T, Baumann B, Wagner M, et al. Cellular immune reaction in the pancreas is induced by constitutively active IkappaB kinase-2. Gut 2007;56:227–236.

81. Baumann B, Wagner M, Aleksic T, et al. Constitutive IKK2 activation in acinar cells is sufficient to induce pancreatitis in vivo. J. Clin. Invest. 2007;117:1502–1513.

82. Huang H, Liu Y, Daniluk J, et al. Activation of nuclear factor-κB in acinar cells increases the severity of pancreatitis in mice. Gastroenterology 2013;144:202–210.

83. Treiber M, Neuhöfer P, Anetsberger E, et al. Myeloid, but not pancreatic, RelA/p65 is required for fibrosis in a mouse model of chronic pancreatitis. Gastroenterology 2011;141:1473–85, 1485.e1–7.

84. Mankan AK, Lawless MW, Gray SG, et al. NF-kappaB regulation: the nuclear response. J. Cell. Mol. Med. 2009;13:631–643.

85. Schuster M, Annemann M, Plaza-Sirvent C, et al. Atypical IκB proteins - nuclear modulators of NF-κB signaling. Cell Commun. Signal. 2013;11:23.

86. Ohno H, Takimoto G, McKeithan TW. The candidate proto-oncogene bcl-3 is related to genes implicated in cell lineage determination and cell cycle control. Cell 1990;60:991–997.

87. Wulczyn FG, Naumann M, Scheidereit C. Candidate proto-oncogene Bcl-3 encodes a subunit-specific inhibitor of transcription factor NF-kappa B. Nature 1992;358:597–599.

88. Naumann M, Wulczyn FG, Scheidereit C. The NF-kB precusor p105 and the proto-oncogene product Bcl-3 are IkB molecules and control nuclear translocation of NF-kB. EMBO J. 1993;12:213–222.

89. Franzoso G, Bours V, Park S, et al. The candidate oncoprotein Bcl-3 is an antagonist of p50/NF-kappa B-mediated inhibition. Nature 1992;358:339–342.

90. Garry P. Nolan, Tanashi Fujita, Kishor Bhatia, Conrad Huppi, Hsiou-chi Liou, Martin L. Scott and DB. The Bcl-3 proto-oncogene encodes a nuclear IkB-like molecule that preferentially interacts with NF-kB p50 and p52 in a phosphorylation-dependent manner. Mol. Cell. Biol. 1993;13:3557–3566.

91. Franzoso G, Bours V, Azarenko V, et al. The oncoprotein Bcl-3 can facilitate NF-kB mediated transactivation by romoving inhibiting p50 homodimers from select kB sites. EMBO J. 1993;12:3893–3901.

92. Fujita T, Nolan GP, Liou HC, et al. The candidate proto-oncogene bcl-3 encodes a transcriptional coactivator that activates through NF-kappa B p50 homodimers. Genes Dev. 1993;7:1354–1363.

93. Bours V, Franzoso G, Azarenko V, et al. The oncoprotein Bcl-3 directly transactivates through kappa B motifs via association with DNA-binding p50B homodimers. Cell 1993;72:729–739.

94. Kuwata H, Watanabe Y, Miyoshi H, et al. IL-10 – inducible Bcl-3 negatively regulates LPS-induced TNF-a production in macrophages. Blood 2003;102:4123–4129.

95. Mühlbauer M, Chilton PM, Mitchell TC, et al. Impaired Bcl-3 up-regulation leads to enhanced lipopolysaccharide-induced interleukin (IL)-23P19 gene expression in IL-10-/- mice. J. Biol. Chem. 2008;283:14182–14189.

96. Carmody RJ, Ruan Q, Palmer S, et al. Negative regulation of toll-like receptor signaling by NF-κB p50 ubiquitination blockade. Science 2007;317:675–678.

97. Viatour P, Dejardin E, Warnier M, et al. GSK3-mediated Bcl-3 phosphorylation modulates its degradation and its oncogenicity. Mol. Cell 2004;16:35–45.

98. Keutgens A, Shostak K, Close P, et al. The repressing function of the oncoprotein BCL-3 requires CtBP, while its polyubiquitination and degradation involve the E3 ligase TBLR1. Mol. Cell. Biol. 2010;30:4006–4021.

99. Massoumi R, Chmielarska K, Hennecke K, et al. Cyld inhibits tumor cell proliferation by blocking Bcl-3-dependent NF-kappaB signaling. Cell 2006;125:665–677.

100. Riemann M, Endres R, Liptay S, et al. The IkB protein Bcl-3 negatively regulates transcription of the IL-10 gene in macrophages. J. Immunol. 2005;175:3560–3568.

101. Nawaz H, Mounzer R, Yadav D, et al. Revised Atlanta and determinant-based classification: application in a prospective cohort of acute pancreatitis patients. Am. J. Gastroenterol. 2013;108:1911–1917.

102. O'Reilly DA, Roberts JR, Cartmell MT, et al. Heat shock factor-1 and nuclear factor-kappaB are systemically activated in human acute pancreatitis. JOP 2006;7:174–184.

103. Strack I, Schulte S, Varnholt H, et al. β-Adrenoceptor blockade in sclerosing cholangitis of Mdr2 knockout mice: antifibrotic effects in a model of nonsinusoidal fibrosis. Lab. Invest. 2011;91:252–261.

104. Makhija R, Kingsnorth AN. Cytokine storm in acute pancreatitis. J. Hepatobiliary. Pancreat. Surg. 2002;9:401–410.

105. Gukovskaya AS, Vaquero E, Zaninovic V, et al. Neutrophils and NADPH oxidase mediate intrapancreatic trypsin activation in murine experimental acute pancreatitis. Gastroenterology 2002;122:974–984.

106. Demols a, Moine O Le, Desalle F, et al. CD4(+) T cells play an important role in acute experimental pancreatitis in mice. Gastroenterology 2000;118:582–590.

107. Saeki K, Kanai T, Nakano M, et al. CCL2-induced migration and SOCS3-mediated activation of macrophages are involved in cerulein-induced pancreatitis in mice. Gastroenterology 2012;142:1010–1020.e9.

108. Rocha S, Martin a. M, Meek DW, et al. p53 represses cyclin D1 transcription through down regulation of Bcl-3 and inducing increased association of the p52 NF-kB subunit with histone deacetylase 1. Mol. Cell. Biol. 2003;23:4713–4727.

109. Kreisel D, Sugimoto S, Tietjens J, et al. Bcl-3 prevents acute inflammatory lung injury in mice by restraining emergency granulopoiesis. J. Clin. Invest. 2011;121:265–276.

110. Ruan Q, Zheng SJ, Palmer S, et al. Roles of Bcl-3 in the pathogenesis of murine type 1 diabetes. Diabetes 2010;59:2549–2557.

111. Tassi I, Rikhi N, Claudio E, et al. The NF-κB regulator Bcl-3 modulates inflammation during contact hypersensitivity reactions in radioresistant cells. Eur. J. Immunol. 2015:[Epub ahead of print].

112. O'Carroll C, Moloney G, Hurley G, et al. Bcl-3 deficiency protects against dextran-sodium sulphate-induced colitis in the mouse. Clin. Exp. Immunol. 2013;173:332–342.

113. Chassaing B, Darfeuille-Michaud A. The commensal microbiota and enteropathogens in the pathogenesis of inflammatory bowel diseases. Gastroenterology 2011;140:1720–1728.

114. Fransen K, Visschedijk MC, Sommeren S van, et al. Analysis of SNPs with an effect on gene expression identifies UBE2L3 and Bcl-3 as potential new risk genes for Crohn's disease. Hum. Mol. Genet. 2010;19:3482–3488.

115. Zhang G, Ghosh S. Toll-like receptor-mediated NF-κB activation : a phylogenetically conserved paradigm in innate immunity. J. Clin. Invest. 2001;107:13–19.

116. Wessells J, Baer M, Young H a, et al. Bcl-3 and NF-kappaB p50 attenuate lipopolysaccharide-induced inflammatory responses in macrophages. J. Biol. Chem. 2004;279:49995–50003.

117. Pène F, Paun A, Sønder SU, et al. The IκB family member Bcl-3 coordinates the pulmonary defense against Klebsiella pneumoniae infection. J. Immunol. 2011;186:2412–2421.

118. Brocke-Heidrich K, Ge B, Cvijic H, et al. Bcl-3 is induced by IL-6 via STAT3 binding to intronic enhancer HS4 and represses its own transcription. Oncogene 2006;25:7297–7304.

119. Brasier AR, Lu M, Hai T, et al. NF-κB-inducible Bcl-3 expression is an autoregulatory loop controlling nuclear p50/NF-κB1 residence. J. Biol. Chem. 2001;276:32080–32093.

120. Chen X, Ji B, Han B, et al. NF-κB activation in pancreas induces pancreatic and systemic inflammatory response. Gastroenterology 2002;122:448–457.

121. Li N, Wu X, Holzer RG, et al. Loss of acinar cell IKKα triggers spontaneous pancreatitis in mice. J. Clin. Invest. 2013;123:2231–2243.

122. Bauer A, Villunger A, Labi V, et al. The NF-kB regulator Bcl-3 and the BH3-only proteins Bim and Puma control the death of activated T cells. Proc. Natl. Acad. Sci. U. S. A. 2006;103:10979–10984.

123. Maldonado V, Melendez-Zajgla J. Role of Bcl-3 in solid tumors. Mol. Cancer 2011;10:152.

124. Hoque R, Farooq A, Mehal WZ. Sterile inflammation in the liver and pancreas. J. Gastroenterol. Hepatol. 2013;28 Suppl 1:61–67.

125. Mayerle J, Schnekenburger J, Krüger B, et al. Extracellular cleavage of E-cadherin by leukocyte elastase during acute experimental pancreatitis in rats. Gastroenterology 2005;129:1251–1267.

126. Collins PE, Kiely P a, Carmody RJ. Inhibition of Transcription by B Cell Leukemia 3 (Bcl-3) Protein Requires Interaction with Nuclear Factor κB (NF-κB) p50. J. Biol. Chem. 2014;289:7059–7067.

127. Liu S, Chen ZJ. Expanding role of ubiquitination in NF-κB signaling. Cell Res. 2011;21:6–21.

128. Glickman MH, Ciechanover A. The ubiquitin-proteasome proteolytic pathway: destruction for the sake of construction. Physiol. Rev. 2002;82:373–428.

129. Schnell JD, Hicke L. Non-traditional functions of ubiquitin and ubiquitin-binding proteins. J. Biol. Chem. 2003;278:35857–35860.

130. Mukhopadhyay D, Riezman H. Proteasome-independent functions of ubiquitin in endocytosis and signaling. Science 2007;315:201–205.

131. Deng L, Wang C, Spencer E, et al. Activation of the IκB kinase complex by TRAF6 requires a dimeric ubiquitin-conjugating enzyme complex and a unique polyubiquitin chain. Cell 2000;103:351–361.

132. Maniatis T. A ubiquitin ligase complex essential for the NF-kB, Wnt/Wingless, and Hedgehog signaling pathways. Genes Dev. 1999;13:505–510.

133. Amir RE, Haecker H, Karin M, et al. Mechanism of processing of the NF-kappa B2 p100 precursor: identification of the specific polyubiquitin chain-anchoring lysine residue and analysis of the role of NEDD8-modification on the SCF(beta-TrCP) ubiquitin ligase. Oncogene 2004;23:2540–2547.

134. Altavilla D, Famulari C, Passaniti M, et al. Attenuated cerulein-induced pancreatitis in nuclear factor–κB–deficient mice. Lab. Investig. 2003;83:1723–1732.

135. Szabolcs A, Biczó G, Rakonczay Z, et al. Simultaneous proteosome inhibition and heat shock protein induction by bortezomib is beneficial in experimental pancreatitis. Eur. J. Pharmacol. 2009;616:270–274.

7 Abbreviations

ABC	ATP-binding cassette
AGe	advanced glycation end-product
AIM2	absence in melanoma 2
ALP	alkaline phosphatase
ALT	alanine aminotransferase
ANCA	anti-neutrophil-cytoplasmatic-antibodies
AP	acute pancreatitis
Arg	L-arginine
BAFFR	B-cell activating factor receptor
BALF	bronchoalveolar lavage fluid
Bcl-3	B cell leukemia 3
BMDM	bone marrow derived macrophages
CCK	cholecystokinin
CLR	C-type lectin receptor
CXCL1	chemokine (C-X-C motif) ligand 1
DAMPs	termed damage associated molecular patterns
DC	dendritic cells
DSS	dextran-sodium sulphate
E1	ubiquitin-activating enzyme
E2	ubiquitin-conjugating enzyme
E3	ubiquitin ligase
EBD	evans blue dye
ECM	extracellular matrix
EMSA	electrophoretic mobility shift assays
FACS	fluorescence-activated cell sorting
HLA	human leukocytes antigen
HMGB1	high-mobility group box 1
HPF	High-power field
HSP	heat shock protein
IBD	inflammatory bowel disease
ICAM-1	Intercellular adhension molecule 1
IFN-γ	interferon-γ
IL	interleukin
IκB	inhibitor of NF-κB
IKK	IκB kinase
LPS	lipopolysaccharide
LTA	lipoteichoic acid

LTβR	lymphotoxin-β receptor
MCP-1	monocyte chemoattractant protein-1
Mdr2	multidrug resistance protein 2
MDR3	multidrug resistance protein 3
MDSC	myeloid-derived suppressor cells
MIP-1α	macrophage inflammatory protein 1 Alpha
MPO	myeloperoxidase
MyD88	myeloid differentiation primary response gene 88
NEMO	NF-κB essential modifier
NF-κB	nuclear factor κB
NIK	NF-κB inducing kinase
NLR	NOD-like receptor
NLRP3	NOD-, LRR- and pyrin domain-containing 3
NLS	nuclear translocation signals
NO	nitric oxide
PAMP	pathogen-associated molecular patthern
PAP	pancreatitis-associated protein
PC	phosphatidylcholine
PRR	pattern recognition receptor
PSC	primary sclerosing cholangitis
Q-PCR	quantitative real-time polymerase chain reaction
RAGe	receptor for AGes
RLR	RIG-I-like receptor
ROS	reactive oxygen species
SIRS	systemic inflammatory response syndrome
Spi2A	serine protease inhibitor 2A
SPINK1	serine protease inhibitor Kazal type 1
TAD	transactivation domain
TLR	Toll-like receptor
TGF-β1	transforming growth factor β1
TNF	tumor necrosis factor
TRIF	TIR domain–containing adaptor-inducing IFNβ
UBE2L3	Ubiquitin-conjugating enzyme E2L3
VCAM	vascular cell adhesion molecule

8 Acknowledgements

First of all, I would like to thank PD Dr. med. Hana Algül for accepting me as a graduate student. I am deeply grateful for the opportunity he gave me to perform research, highly relevant for human diseases in one of the most renowned hospitals of Munich. Dr. Algül provided me with excellent supervision, continuous support, and helpful discussions. Most importantly however, he enabled me to develop my own ideas and research plans, a trait critically required in the repertoire of every graduate student. Moreover, I thank Univ.-Prof. Dr. med. Roland M. Schmid, who along with Dr. Algül opened the doors for my doctoral studies at the TUM.

Continuing, I want to express my gratitude to all the members of my laboratory including Marina, Patrick, Jiaoyu, Nina, Sonja, Angelika, Matthias, Magda, Karen, Chantal, and Viktoria. I thank you for the friendly, creative atmosphere, the helpful discussions, and the great support. Additionally, I want to express my gratitude to Thomas Wartmann and Bianca-Sabrina Targosz for providing the assistance in animal model and ubiquitination assay.

Finally, I want to thank my family and friends. I am especially grateful to my beloved parents and wife who have always been helping me out of difficulties, supporting without a word of complain, and giving me great confidence all these years. Thank you for enriching my background and creating an environment where new ideas can always be fostered and realized.